Transport, Deposition and Release Kinetics of Nano-TiO_2 in Saturated Porous Media

BY

ITZEL GUADALUPE GODINEZ
B.S., University of Illinois at Chicago, USA, 2006
M.S., University of Illinois at Chicago, USA, 2008

THESIS

Submitted in partial fulfillment for the requirement of the degree of Doctorate of Philosophy in Civil Engineering in the Graduate College at the University of Illinois at Chicago, 2013

Chicago, Illinois

Defense Committee:

Dr. Christophe J. G. Darnault, Chair and Advisor
Dr. Karl J. Rockne
Dr. Krishna R. Reddy
Dr. Amid P. Khodadoust
Dr. G. Ali Mansoori, Bioengineering/Chemical Engineering

This thesis is dedicated to my parents Jose Luis Godinez Gonzalez and Elena Chavez de Godinez as well as my siblings Oswaldo, Maritza, Nereyda, Jose and Armando. I am forever grateful for your support and advice during my studies.

ACKNOWLEDGEMENTS

I would like to take this opportunity to thank some of the individuals who have been extremely helpful and supportive during this exciting journey called Graduate School.

To my advisor Dr. Christophe J. G. Darnault I would like to give sincere thanks for his assistance and support. This dissertation would not have been possible without his guidance.

I thank my thesis committee members Professors Karl J. Rockne, Krishna R. Reddy, Amid P. Khodadoust and G. Ali Mansoori from the University of Illinois at Chicago (UIC) for their willingness to serve on the committee as well as their constructive advice and support. To Professor J. Ernesto Indacochea, Director of Graduate Studies in the Department of Civil and Materials Engineering at UIC, and Florencio Dias, Director of Advising and Outreach Programs in the Department of Mathematics, Statistics and Computer Science at UIC, I extend my gratitude for your continuous advice, help and support.

I would like to acknowledge my fellow lab colleagues Burcu Uyusur and Emre Köken for their assistance, moral support and above all friendship. Deep thanks are also given to my colleagues and friends Raja Kaliappan, Dorin Bogdan, Kamel Babaeivelni, Azivy Che Azis, Kelly Granberg, Solidea Bonina and Priscilla Viana. To Sara Arevalo and Edgar Chino I extend my most sincere thanks for being there for me when I needed it most; their kind words and constructive criticism will be forever appreciated.

ACKNOWLEDGEMENTS (continued)

I am grateful to the National Science Foundation (NSF) – University of Illinois at Chicago Bridge to the Doctorate Fellowship, the UIC Abraham Lincoln Fellowship and the UIC Department of Civil and Materials Engineering for providing me with financial support during my PhD.

I would like to thank my parents, my siblings, my brother-in-law Gerardo and above all my nephews Noel, Marco, Gerardo, Samuel, Christopher, Diego and Aaron as well as my nieces Winifred and Vanessa for continuously reminding me that the journey to attain my PhD was indeed worth it. I wish that you kids strive to achieve all of your dreams. Last but not least, I would like to thank Andres Felipe Hernandez for his unconditional support and love.

TABLE OF CONTENTS

CHAPTER I. LITERATURE REVIEW……..... 1

1.1. Nanotechnology……. 1

1.2. Fate and transport of engineered nanoparticles……. 5

1.3. Favorable, unfavorable and reversible deposition……. 7

CHAPTER II. INTRODUCTION……... 9

CHAPTER III. AGGREGATION AND TRANSPORT OF NANO-TIO_2 IN SATURED POROUS MEDIA: EFFECTS OF PH, SURFACTANTS AND FLOW VELOCITY…... 15

3.1. Abstract…….. 15

3.2. Introduction…… 16

3.3. Materials and Methods……... 17

3.3.1. Colum system……..... 17

3.3.2. Nano-TiO_2 dispersions…….. 18

3.3.3. Characterization of nano-TiO_2…….. 20

3.3.4. Nano-TiO_2 transport column experiments……..... 21

3.3.5. Tracer breakthrough experiments……..... 24

3.3.6. Sedimentation experiments……... 24

3.3.7. Colloid transport theory…… 25

3.4. Results…… 27

3.4.1. Nano-TiO_2 characterization, porous medium permeability coefficient and tracer BTCs……... 27

3.4.2. Sedimentation analysis…….. 29

3.4.3. Effect of surfactants vs. no surfactant in the transport of nano-TiO_2…… 30

3.4.4. Influence of pH, flow velocity and non-ionic surfactant concentration on transport of nano-TiO_2…… 36

3.4.5. Influence of pH, flow velocity and anionic surfactant on transport nano-TiO_2 ……. 41

3.4.6. Influence of non-ionic vs. anionic surfactant in the transport of nano-TiO_2. 42

3.5. Discussion……... 42

3.5.1. Nano-TiO_2 aggregation…….. 43

3.5.2. Nano-TiO_2 mobility and transport……. 45

3.5.3. Nano-TiO_2 deposition and secondary energy minimum……... 46

CHAPTER IV. DEPOSITION AND RELEASE KINECTICS OF NANO-TIO_2 IN SATURED POSOUS MEDIA: EFFECTS OF SOLUTION IONIC STRENGTH AND SURFACTANTS ……. 48

4.1. Abstract……... 48

4.2. Introduction……. 48

4.3. Materials and Methods…… 49

4.3.1. Preparation of nano-TiO_2 suspensions and characterization of nano-TiO_2.. 49

4.3.2. Group one column experiments…… 52

4.3.3. Group two column experiments…… 54

4.3.4. Batch experiments…… 55

4.3.5. Dynamic Light Scattering……. 55

4.3.6. Sedimentation…… 56

4.3.7. Zeta potential measurements……. 56

4.3.8. Interaction energy profiles…… 57

4.3.9. Transport Theory……... 59

4.3.10. Nano-TiO_2 aggregation kinetics…….. 62

4.4. Results and discussion…… 62

4.4.1. Stability of nano-TiO_2 in suspension…… 62

4.4.2. Zeta potential of nano-TiO_2 and sand…… 68

4.4.3. Influence of ionic strength and surfactants on nano-TiO_2 transport…….. 70

4.4.4. Release of previously deposited nano-TiO_2…….. 82

CHAPTER V. CONCLUSION……... 88

CITED LITERATURE……..... 90

VITA…… 103

APPENDIX A…….. 107

APPENDIX B…….. 113

LIST OF TABLES

CHAPTER I. LITERATURE REVIEW

Table 1. Engineered nanomaterials and nanoparticles…… 2

CHAPTER III: AGGREGATION AND TRANSPORT OF NANO-TiO_2 IN SATURATED POROUS MEDIA: EFFECTS OF PH, SURFACTANTS AND FLOW VELOCITY

Table 1. Experiment conditions and column properties……. 22

Table 2. Zeta potential measurements of dispersion systems……..... 28

Table 3. Experimental parameters from BTC experiments calculated with filtration theory for a flow velocity of 0.0483 cm/s……..... 39

Table 4. Experimental parameters from BTC experiments calculated with filtration theory for a flow velocity of 0.0967 cm/s……... 39

Table 5. Nano-TiO_2 transport recovery: total transport recovery and transport recovery from secondary energy minimum…….. 40

CHAPTER IV: DEPOSITION AND RELEASE KINETICS OF NANO-TiO_2 IN SATURATED POROUS MEDIA: EFFECTS OF SOLUTION IONIC STRENGTH AND SURFACTNATS

Table 1. Group one column experiments: Transport and deposition behavior of the nano-TiO_2 suspensions that adhere to the regulations of the physicochemical filtration theory (Tufenkji and Elimelech, 2004)……. 61

Table 2. Experimental parameters from group one column experiments for suspension systems that maintained kinetic stability during the injection of nano-TiO_2: Attachment efficiency between nano-TiO_2–nano-TiO_2 and nano-TiO_2–sand, maximum transport distance (L_{max}) and energy barriers estimated from total interaction energy profiles (flow velocity 9.42 x 10^{-4} m/s, Hamaker constant for nano-TiO_2-water-nano-TiO_2 3.5 x 10^{-20} J (Gomez-Merino et al., 2007) and nano-TiO_2-water-sand 1.4 x 10^{-20} J (Jribi et al., 2009))…….. 65

Table 3. Group one column experiments: Nano-TiO_2 transport recovery as a function of pore volume……. 87

Table 4. Group two column experiments: Nano-TiO_2 transport recovery as a function of pore volume……. 87

LIST OF FIGURES

CHAPTER III: AGGREGATION AND TRANSPORT OF NANO-TIO_2 IN SATURATED POROUS MEDIA: EFFECTS OF PH, SURFACTANTS AND FLOW VELOCITY

Fig. 1. Experimental set-up……. 23

Fig. 2. Sedimentation of nano-TiO_2 in Dispersion 1 and Dispersion 2 systems……. 30

Fig. 3. Nano-TiO_2 BTCs without surfactant and with non-ionic surfactant (Triton X-100) and anionic surfactant (SDBS) at pH 7 and flow velocity of 0.0483 cm/s. BTC for a Br^- tracer is also included. Left y-axis is for nano- TiO_2 C/C_0, right y-axis is for tracer (Br^-) C/C_0…..……. 33

Fig. 4. Nano-TiO_2 BTCs without surfactant and with non-ionic surfactant (Triton X-100) and anionic surfactant (SDBS) at pH 7 and flow velocity of 0.0967 cm/s. BTC for a Br^- tracer is also included. Left y-axis is for nano- TiO_2 C/C_0, right y-axis is for tracer (Br^-) C/C_0……. 34

Fig. 5. Nano-TiO_2 BTCs without surfactant and with non-ionic surfactant (Triton X-100) and anionic surfactant (SDBS) at pH 9 and flow velocity of 0.0483 cm/s. BTC for a Br^- tracer is also included…….. 35

Fig. 6. Nano-TiO_2 BTCs without surfactant and with non-ionic surfactant (Triton X-100) and anionic surfactant (SDBS) at pH 9 and flow velocity of 0.0967 cm/s. BTC for a Br^- tracer is also included……... 36

CHAPTER IV: DEPOSITION AND RELEASE KINETICS OF NANO-TIO_2 IN SATURATED POROUS MEDIA: EFFECTS OF SOLUTION IONIC STRENGTH AND SURFACTNATS

Fig. 1. Aggregation kinetics of nano-TiO_2 at pH 9 in suspension systems at 0.0011 M, 0.011 M and 0.11 M……... 64

Fig. 2. Sedimentation of nano-TiO_2 at pH 9 in suspension systems at 0.0011 M, 0.011 M and 0.11 M…….. 67

Fig. 3. Zeta potential of nano-TiO_2 at pH 9 in suspension systems at 0.0011 M, 0.011 M and 0.11 M…….. 69

Fig. 4. Zeta potential of silica sand at pH 9 in suspension systems at 0.0011 M, 0.011 M and 0.11 M…….. 70

Fig. 5. Group one nano-TiO_2 breakthrough curve experiments at pH 9 and 0.0011 M..... 73

Fig. 6. Group one nano-TiO_2 breakthrough curve experiments at pH 9 and 0.011 M…… 74

Fig. 7. Group one nano-TiO_2 breakthrough curve experiments at pH 9 and 0.11 M…….. 75

Fig. 8. Percentage of nano-TiO_2 adsorbed to the sand in batch experiments as a function of ionic strength and the presence of surfactants…….. 78

Fig. 9. Computed nano-TiO_2–nano-TiO_2 interaction energy profiles for suspension systems at ionic strengths 0.0011 M and 0.011 M and pH 9; (a) interaction energy barriers and (b) secondary energy minimum wells. Interaction energies were calculated by use of the starting zeta potentials and mean nanoaggregate diameters displayed in Fig. 3 and Table 1, respectively. ……. 80

Fig. 10. Computed nano-TiO_2–Sand interaction energy profiles for suspension systems at ionic strengths 0.0011 M and 0.011 M and pH 9; (a) interaction energy barriers and (b) secondary energy minimum wells. Interaction energies were calculated by use of the starting zeta potentials and mean nanoaggregate diameters displayed in Fig. 3 – 4 and Table 1, respectively…... 81

Fig. 11. Group two nano-TiO_2 breakthrough curve experiments at pH 9 and 0.011 M…. 85

Fig. 12. Group two nano-TiO_2 breakthrough curve experiments at pH 9 and 0.11 M…... 86

LIST OF ABBREVIATIONS

$1/W$	Inverse stability ratio
ASTM	American Society for Testing and Materials
BTCs	Breakthrough curves
C60	Fullerenes
CCC	Critical coagulation concentration
CMC	Critical micelle concentration
CNT	Carbon nanotubes
DI	Deionized
DLS	Dynamic light scattering
DLVO	Derjaguin–Landau–Verwey–Overbeek
EDL	Electrostatic double layer
ER	Electrorheological effect
FWHM	Full width at half-maximum
IARC	International Agency for Research on Cancer
IC	Ion Chromatography
M	Molarity
mM	Milli-molar
mV	Milli-volts
NaBr	Sodium bromide
Nano-TiO_2	Titanium dioxide nanoparticles
NaOH	Sodium hydroxide
Nm	Nanometer
NOM	Natural organic matter
NPs	Nanoparticles
NZVI	Nanozero-valent iron
OATs	Advanced oxidation technologies
pH_{pzc}	pH point of zero charge
PVs	Pore volumes
QCM-D	Quartz crystal microbalance with energy dissipation monitoring
S/V	Surface area to volume ratio
SDBS	Sodium dodecylbenzene sulfonate
SDS	Sodium dodecyl sulfate
SRHA	Suwannee River humic acid
Ti	Titania
TiO_2	Titanium dioxide
TOP	Trioctylphosphine
TOPO	Trioctylphosphine oxide
USEPA	United States Environmental Protection Agency
UV/Vis	Ultraviolet-visible
VDW	van der Waals
XRD	X-ray diffraction

CHAPTER I. LITERATURE REVIEW

1.1. Nanotechnology

The basics, realm and invariable nature of nanotechnology rest in the capability to work at the molecular level. Nanotechnology is most commonly defined as the branch of science and engineering that concerns with things that have at least one dimension in the 1–100 nanometer (nm) range; one nanometer is equivalent to one-billionth (i.e. 10^{-9}) of a meter (Mansoori, 2005). Nanomaterials can be engineered to attain the form of nanofilms, nanowires/nanotubes and nanoparticles which consist of one, two and three dimensional nanostructures, respectively (Mansoori, 2005; USEPA, 2007). The unique physico-chemical properties of nanomaterials and nanoparticles (e.g. magnetic, optical, thermal, electrical and mechanical) can be ascribed to three characteristics associated to size effect. These characteristics include quantum size confinement which results in the overlapping of grain size with physical length (e.g. electron mean-free path and electron wavelength), the spontaneous increase of interfacial defects (e.g. grain boundaries and triple junctions) and distortion of elastic layers (Zhang, 1997; Andrievski and Glezer, 2001; Campbell et al., 2002; Puzder et al., 2003). Another key feature of nanomaterials and nanoparticles is their large surface area-to-volume ratio (S/V). Because of this condition, nanomaterials and nanoparticles have a much greater proportion of atoms on their surface than their interior as compared to their bulk counterparts. This provides the engineered nanosized structures with great adsorption and/or catalytic properties (Obare and Meyer, 2004; Nurmi et al., 2005; Li et al., 2006).

Engineered nanomaterials and nanoparticles can be categorized into four groups: carbon-based, metal-based, dendrimers and nanocomposites (USEPA, 2007). Nanoparticles are generally synthesized through two methodologies. The first approach is referred to as "top-down" and consists in dividing a large portion of solid into smaller parts by chemical methods (i.e. mecano-synthesis) that break apart the bonds that keep the elements of the bulk solid together (Jolivet and Barron, 2007). The second approach is known as "bottom-up" and requires the "assembling" of atoms or molecular entities via condensation in a gas phase or in solution (Jolivet and Barron, 2007). Table 1 provides a detailed description of the properties, applications and frequent synthesis methods of several nanomaterials and nanoparticles.

Table 1. Engineered nanomaterials and nanoparticles.

Category Group	Nanomaterial or Nanoparticle	Common Synthesis Methodologies	Properties	Applications	References
Carbon-Based	Fullerenes	➢ Electric-arc process ➢ Laser ablation	Hydrophobic surface; surface may be subjected to modifications; hollow cage structures; carbon atoms are chemically equivalent.	Lubricants; Diagnostic and therapeutic pharmaceuticals.	Arbogast et al., 1991; Feuston et al., 1991; Dorn and Duchamp, 2004; Fowler and Manolopoulos, 2006.
	Carbon Nanotubes (CNT)	➢ Arc discharge ➢ Laser ablation ➢ Catalyzed decomposition ➢ Chemical vapor deposition	Hydrophobic surface, hollow tubes; surface can be functionalized; excellent thermal stability; mechanical and electrical properties; high modulus of elasticity.	Energy storage devices; nanoprobes and sensors; electronic devices; biomedical application.	Dai, 2002; Smith and Luzzi, 2004; Ramirez, 2005; Zhou et al., 2009.

Table 1. Engineered nanomaterials and nanoparticles (continued).

Category Group	Nanomaterial or Nanoparticle	Common Synthesis Methodologies	Properties	Applications	References
Metal-Based	Quantum Dots	➢ Bottom-up colloidal synthesis ➢ Pyrolysis of organometallic precursors (e.g. Cd and Se) in a coordinating solvent composed of TOP and TOPO	Photoluminescence; exhibit strong size dependent optical and electrical properties.	Biology; bio-imaging; photovoltaic devices; light emitting devices; computing.	Murray et al., 1993; Denison et al., 2004; Michalet et al., 2005; Biju et al., 2008; Xu et al., 2008.
	Nanozero-Valent Iron (nZVI)	➢ Reduction of ferric (Fe(III)) or ferrous (Fe(II)) salts with sodium borohydride	High S/V ratio; great density of reactive surface sites as well as great intrinsic reactivity of surface sites.	Environmental remediation (e.g. porous media and groundwater).	Nurmi et al., 2005; Kanel et al., 2006; Li et al., 2006; Comba et al., 2011.
	Bimetallic Iron Nanoparticles	➢ Chemical preparation method in liquid phase ➢ Coupling of nZVI with a second catalytic metal (e.g. Pd, Ni, Pt or Ag)	High S/V ratio; high level of stepped surface; high surface energy; bimetallic layer increases the rate of dechlorination reaction and curtails production of chlorinated byproducts.	Environmental remediation of chlorinated organic pollutants.	Zhang et al., 1997; Schrick et al., 2002; Wang et al., 2009; Luo et al., 2010.
	Titanium Dioxide Nanoparticles (Nano-TiO_2)	➢ Sol-gel process ➢ Microemulsion ➢ Wet impregnation ➢ Liquid phase deposition ➢ Hydrothermal method	Photocatalyst; wide-bandgap semiconductor; high S/V ratio; porosity; ion exchange properties.	Paints; pigments; cosmetic additives; photocatalyst for environmental remediation purposes.	Bavykin et al., 2006; Stewart et al., 2006; Chen and Mao, 2007; Wang et al., 2010; Liu et al., 2011.

Table 1. Engineered nanomaterials and nanoparticles (continued).

Category Group	Nanomaterial or Nanoparticle	Common Synthesis Methodologies	Properties	Applications	References
Metal-Based (continued)	Gold Nanoparticles	➢ Reduction of metal salts followed by nucleation and growth in the presence of a stabilizing agent	High S/V ratio; surfaces permit the construction of biocompatible monolayers for drug delivery purposes; low cytotoxicity.	Spanning electronics; optics; catalysis; drug delivery.	Hutchings, 2005; Hong et al., 2006; Shan and Tenhu, 2007; Jeong et al., 2009.
Dendrimer	Dendrimer	➢ Convergent process ➢ Divergent process	Well-defined and highly-branched structures; high densities of peripheral functionalities; symmetrical shapes; chemical versatility.	Drug delivery vehicles; catalysis.	Bosman et al., 1999; Boiko et al., 2001; Fuchs et al., 2004; Scott et al., 2005.

In the dawn of the second developmental stage of nanotechnology—associated with the engineering of active nanostructures—there is a rising debate that urges to evaluate the possible risks derived from this new technology (USEPA, 2007). The intentional and controlled generation of nanomaterials and nanoparticles could modify their behavior in the environment as compared to natural and air-borne nanoparticles. Understanding the fate and transport of engineered nanostructures in natural environmental systems is crucial to assess the possible routes of exposure to humans and the ecosystems. Currently, there is limited information concerning the environmental chemistry, transport and ecotoxicology of engineered nanomaterials and nanoparticles. Nonetheless, the list of commercially available products containing materials manufactured through nanotechnology is expanding at an extremely fast pace.

1.2. Fate and transport of engineered nanoparticles

Comprehending the mechanisms of physicochemical filtration of colloids and engineered nanoparticles in saturated subsurface environments is critical for several natural and engineering processes. Transport and deposition behavior of colloids and nanoparticles are of interest to determine the conditions that govern the mobility of particles in the subsurface environment and to provide insight in the role these particles play in enhancing/facilitating the transport of pollutants in groundwater (Jegatheesan and Vigneswaran, 1997; Jegatheesan and Vigneswaran, 2000; Cheng et al., 2004).

By elucidating the mechanisms responsible for the fate and transport of particles, scientists and engineers can develop more comprehensive methodologies to establish proper risk assessments and effective subsurface remediation. In the last two decades the manufacturing and commercialization of nanoparticles has increased tremendously and their release into the environment is inevitable. In an effort to generate knowledge and data to delineate the mobility behavior particular to engineered nanoparticles, researchers have conducted several transport studies utilizing distinct nano-sized particles in well-controlled settings that mimic different types of subsurface environments. The size of nanoparticles and nanoaggregates is within submicron range which permits to characterize them as miniature colloidal particles. The following provides a summary of important findings with respect to research studies regarding engineered nanoparticles. Espinasse et al. (2007) found that deposition of fullerenes increases with increasing ionic strength, low flow velocity and the presence of polysaccharide-like natural

organic matter. In the presence of divalent cations such as Ca^{2+}, polysaccharides might initiate gel formation thus destabilizing fullerenes and inducing deposition onto porous media (Jermann et al., 2007; Espinasse et al., 2007). Saleh et al. (2008) modified the surfaces of NZVI with distinct polymers and surfactants. The electrosteric stabilization of these nanoparticles yields exceptional resistance to varying electrolyte conditions. Transport theory predicts that electrosteric stabilized NZVI may travel tens to hundreds of meters in sandy groundwater aquifers under proper in situ injection flow velocities. Fang et al. (2009) studied the stability of nano-TiO_2 in soil suspensions and their mobility through saturated homogenous soil columns. Retention of nano-TiO_2 was significant in porous media containing high clay content and under high soil salinity conditions. Conversely, a considerable portion of nano-TiO_2 passed through porous media having large collector diameters and at low ionic strength. The morphology and rate of formation of nano-TiO_2 aggregates in aqueous suspension as a function of ionic strength and type of electrolyte solution were investigated by French et al. (2009). An increase in ionic strength and valence of the ions (i.e. going from monovalent (Na^+) to divalent (Ca^{2+}) cations) in the electrolyte solution induced a size increase of nano-TiO_2 aggregates. The increase in ion valence proved to be a more dominant factor in altering the morphology of the nano-TiO_2 aggregates in a shorter period of time compared to the increase in ionic strength.

The stability of nanoparticles in aquatic and subsurface environments is also impacted by the presence of natural organic matter (NOM). Previous studies revealed similar interaction characteristics between NOM and fullerenes, carbon nanotubes or quantum dots as compared to NOM and colloids in the submicron range, an indication of the effects of NOM on the stability and mobility of nanoparticles in porous media (Chen and Elimelech, 2007; Espinasse et al.,

2007; Navarro et al., 2008). In the case of colloids, the NOM adsorbed at their surface may modify the physico-chemical properties of the underlying solid and impact the stability and behavior of colloids (Franchi and O'Melia, 2003; Mylon et al., 2004; Chen et al., 2006; Pelley and Tufenkji, 2008). NOM stabilizes colloids by means of electrostatic and steric repulsions in the presence of monovalent electrolytes (Mylon et al., 2004). Nevertheless, divalent electrolytes at high concentrations do not contribute to colloid stability because of cation complexation with NOM (Amirbahman and Olson, 1995; Kretzschmar and Sticher, 1997; Mylon et al., 2004). The adsorbed NOM surface coatings have shown to enhance the transport of natural (Akbour et al., 2002) and synthetic colloids (Deshiikan et al., 1998; Franchi and O'Melia, 2003), along with biocolloids (Johnson and Logan, 1996) in saturated porous media.

1.3. Favorable, unfavorable and reversible deposition

In the last several years authors have pointed out that the existing filtration theory does not adequately predict the deposition of colloids because it assumes that particle deposition rate is constant (Redman et al., 2004; Tufenkji and Elimelech, 2005; Kuznar et al., 2007). After conducting a controlled-laboratory column deposition study, Tufenkji and Elimelech (2004a) concluded that in the presence of repulsive Derjaguin–Landau–Verwey–Overbeek (DLVO) interactions there are favorable (i.e. absence of repulsive colloidal interaction energies) and unfavorable (i.e. presence of repulsive colloidal interaction energies) deposition interplays. A fraction of the colloids deposit at a slow rate onto the collectors; these colloids possess enough energy to surpass the repulsive energy barrier and are able to reach the primary energy minimum. A second fraction of the colloids deposit at a fast rate; the latter is due to the presence of deep

secondary energy minima (Tufenkji and Elimelech, 2004a; Litton and Olson, 1993). Hahn and O'Melia (2004) developed a Brownian Dynamic/Monte Carlo (MC/BD) simulation model in combination with Maxwell calculations to support a different position on particle deposition and reentrainment/release of colloids under unfavorable chemical conditions. The simulation model provides more accurate results on particle deposition rates than classical models that assume irreversible deposition of particles in the primary energy minimum. Other studies have demonstrated that deposition in the secondary energy minimum can be reversed when the energy barrier is eliminated following a decrease in the ionic strength of the electrolyte solution (Franchi and O'Melia, 2003; Hahn et al., 2004; Hahn and O'Melia, 2004). In the case of manufactured nanoparticles, deposition of nano-TiO_2 onto chemically-treated-silica grains due to secondary energy minimum was reported by Godinez and Darnault (2011). The nano-TiO_2 aggregates deposited in the secondary energy well were released from the saturated porous media during the flushing period of the experimental trials due to changes in solution chemistry induced by injection of de-ionized (DI) water. The reentrainment/release of nano-TiO_2 was depicted in the breakthrough curves by a flushing peak. In saturated subsurface environments, reversible deposition in secondary energy minimum has direct implications in predicting the correct transport behavior of particles. Nonetheless, there is limited documentation of this phenomenon with respect to engineered nanoparticles.

CHAPTER II. INTRODUCTION

Nanotechnology represents a fast growing economic sector that is constantly evolving with changes in technology, markets as well as product quality and demand (Fiorino, 2010). Novel nano-sized materials and particles are revolutionizing science and engineering due to their enhanced physico-chemical properties compared with their bulk counterparts. By manufacturing nano-size materials and particles of specific size, shape and crystalline configuration, nanotechnology possesses the capacity to transform the inherent characteristics of the majority of man-made objects and activities. Nanotechnology's uttermost societal impact is anticipated to be as drastic as that of the first industrial revolution (Mansoori, 2005). By the year 2015, this industry is projected to reach a market value of approximately $1 trillion (Robichaud et al., 2005).

Among the engineered nanoparticles (NPs) derived from this industry, titanium dioxide is one of the most popular (USEPA, 2007; Wiesner et al., 2006). TiO_2 nanoparticles have been implemented as a pigment in inks, paints, paper, plastics, cosmetics and nano-fibers (USEPA, 2007). They have also proven to be a superior photocatalyst characterized by large photo-stability, porosity, ion exchange capability and high specific surface area-to-volume ratio (Hoffmann et al., 1995). These physico-chemical properties lead to the application of TiO_2 nanoparticles in advanced oxidation technologies (AOTs) to treat toxins such as organic and inorganic compounds that may not be easily eradicated by conventional technologies in water treatment plants (Antoniou et al., 2009) and subsurface environments (Quan et al., 2005).

In the U.S. the current annual production of nanosized TiO_2 is of 40000 metric tons; it is estimated that by the year 2025 this figure will increase to ~2.5 million metric tons (i.e. an upper bound calculation) (Robichaud et. al., 2009). This presents a complex challenge for the scientific and public organizations responsible for assessing possible environmental hazards and health risks since the proliferation of applications and products containing titanium dioxide will inherently result in sources of these nanoparticles to the environment with the potential to pollute the air, surface and groundwater as well as the soil. (Wiesner et al., 2006). In municipal wastewater treatment plants, the presence of Ti-based particles has been reported in effluents at concentrations of 10 – 100 μg/L (Kiser et al., 2009). These effluents are eventually discharged into surface waters which is a concern because the International Agency for Research on Cancer has categorized TiO_2 in Group 2B of possibly carcinogenic materials (IARC 2006, volume 93). Conversely, TiO_2 nanoparticles have demonstrated to be toxic to bacteria (Adams, et al., 2006), algae (Aruoja et al, 2009), mice (Liu et al, 2009) and rats (Warheit et al., 2007). Research and development studies have not determined whether the toxicity derived from these nanoparticles is the result of their size, structure, concentration or their innate physico-chemical properties (Warheit, et al., 2007; Aruoja et al., 2009).

The extent of the threat of TiO_2 nanoparticles (nano-TiO_2) to the environment and public health is correlated to their ability to remain dispersed (i.e. stable) in the environment or to form submicron aggregates, and consequently their mobility. The aggregation of nano-TiO_2 and the electrostatic interaction between nano-TiO_2 and the surfaces of porous media are impacted by the solution ionic strength and pH (Guzman et al., 2006; Fang et al., 2009; French et al., 2009). As the pH of nano-TiO_2 dispersions approaches the point of zero charge (pH_{pzc}) of nano-TiO_2, their

aggregates size increases while their mobility decreases (Guzman et al., 2006). At or near the pH_{pzc}, the surface ionization of nanoparticles is suppressed or reduced to zero, thereby diminishing the repulsive forces between nanoparticles and allowing the formation of nanoaggregates. The morphology and aggregation rate of nano-TiO_2 is a function of the ionic strength and electrolyte solution characteristics (French et al., 2009). An increase of the ionic strength and/or the valence charge of the cations diminish the magnitude of the electrostatic repulsion resulting in an intensification of the aggregation phenomena (Saleh et al., 2008; French et al., 2009)

Research suggests that the mobility and retention of engineered TiO_2 NPs in well-defined porous media packed in columns is controlled by the complexity of the porous media matrix (e.g. grain and pore size distribution), the physicochemical parameters of solution chemistry (e.g. ionic strength, pH and the presence of natural organic matter (NOM) or surfactants), the surface properties of TiO_2 and the fluid dynamics characteristic of the column system (Chen et al., 2012; Chen et al., 2011; Thio et al., 2011; Godinez and Darnault, 2011). For example, transport experimental data have demonstrated temporal and spatial variations of TiO_2 deposition in columns. In particular, breakthrough curves have showed a transition from blocking to ripening shapes whereas the retention profiles in column experiments have revealed a change of the maximum TiO_2 retention from the end towards the entrance point of the column as the ionic strength increases and the pH of the suspension approaches the point of zero charge of TiO_2 (Chen et al., 2012; Chen et al., 2011; Solovitch et al., 2010). Conversely, it has been reported that when the prepared TiO_2 suspensions are not stable under the conditions tested, the influence of NPs aggregation is coupled to that of deposition in the column (Chen et al., 2011; Solovitch et

al., 2010). At near the pH_{pzc} of TiO_2 the surface ionization of NPs is suppressed causing a reduction in the repulsive forces between NPs thus allowing the formation of nanoaggregates; whereas, at alkaline conditions TiO_2 in suspension develops a noticeable negative charge density as a result of deprotonation of its surface hydroxyl groups (Svecova et al., 2008). As consequence, the mobility and stability of TiO_2 are enhanced when the pH of its suspension is several units away from its pH_{pzc} (Godinez and Darnault, 2011). In the presence of natural organic matter (NOM) the amount of Suwannee River humic acid (SRHA) adsorbed to TiO_2 was shown to increase with increasing ionic strength and a greater starting SRHA concentration at moderate acidic conditions (Chen et al., 2012). This enhanced the stability and transport of TiO_2 as a result of increased electrostatic and steric interactions between NPs and NPs-sand. On the contrary, at alkaline condition and ionic strengths lower than 60 mM the adsorption of SRHA to TiO_2 demonstrated to be negligible. As the ionic strength surpassed 60 mM a minimum amount of SRHA adsorbed to TiO_2 suggesting that at alkaline conditions the presence of SRHA hardly influenced the stability and transport of the NPs (Chen et al., 2012). Surfactants may also adsorb to nanoparticles and affect their solubility and transport in porous media by modifying their electrostatic, hydrophobic and steric interactions (Tiraferri and Sethi, 2009; Lin et al., 2010; Tian et al., 2010). Surfactant may also sorb onto the surfaces of porous media and affect its hydraulic properties as well as interactions forces (Brown and Jaffe, 2001; Abu-Zreig et al., 2003; Wiel-Shafran et al., 2006; Mingorance et al., 2007). For example, the use of an anionic surfactant, sodium dodecylbenzene sulfonate (SDBS), to disperse and stabilize engineered nanoparticles (i.e. silver nanoparticles and carbon nanotubes) led to surfactant-solubilized nanoparticles that were highly mobile in saturated sandy porous media. Nonionic and ionic surfactants are

commonly used to coat nano-TiO_2 to remain dispersed (i.e. stable) during the fabrication of paints and cosmetics (Tkachenko et al., 2006).

TiO_2 aggregates may be though of as porous fractals with a lower packing density and a much higher surface area than a solid particle with a similar hydrodynamic diameter (Guzman et al., 2006). Nonetheless, a model laboratory system using a quartz crystal microbalance with energy dissipation monitoring (QCM-D) revealed that the deposition behavior of TiO_2 onto silica was in qualitative agreement with the Derjaguin-Landau-Verwey-Overbeek (DLVO) theory that is applied to predict colloidal stability (Fatisson et al., 2009).

In order to evaluate the environmental consequences of the release and accumulation of engineered nanosized TiO_2 in subsurface and estuarine environments it is critical to comprehend the mechanisms controlling the deposition, mobility and stability of these NPs in porous media because their bioavailability, reactivity and ecotoxicology will certainly be governed by their transport behavior (Botta et al., 2011; Zhu et al., 2011; Labille et al., 2010). Thus, the overall objective of this study is to contribute to the state of science of the transport, deposition and release kinetics of nano-TiO_2 in saturated porous media. The specific goals of the study include:

(A) To explore the effects of physico-chemical parameters such as pH, presence of non-ionic (Triton X-100) and anionic (SDBS) surfactants as well as flow velocity on the aggregation and transport mechanisms of nano-TiO_2 in saturated porous media.

(B) To investigate the effects of ionic strength in the aggregation and deposition of nano-TiO_2 in saturated porous media.

(C) To examine the impact that the abrupt and gradual reduction in ionic strength possesses in the release of nano-TiO_2 previously deposited onto sand grains.

(D) To characterize and predict through implementation of experimental data nanoparticle deposition coefficients, maximum transport distance and total interaction energy between nano-TiO_2 and nano-TiO_2 and collectors.

CHAPTER III. AGGREGATION AND TRANSPORT OF NANO-TIO_2 IN SATURATED POROUS MEDIA: EFFECTS OF PH, SURFACTANTS AND FLOW VELOCITY

The chapter is a first-author manuscript published in the Water Research Journal in 2011.

3.1. Abstract

Transport of manufactured nano-TiO_2 in saturated porous media was investigated as a function of morphology characteristics, pH of solutions, flow velocity, and the presence of anionic and nonionic surfactants in different concentrations. Surfactants enhanced the transport of nano-TiO_2 in saturated porous media while a pH approaching the point of zero charge of nano-TiO_2 limited their transport. The deposition process, a retention mechanism of nano-TiO_2 in saturated porous media was impacted by surfactant and pH. In Dispersion 1 systems (pH 7), the size of the nano-TiO_2 aggregates was directly related to the presence of surfactants. The presence of non-ionic surfactant (Triton X-100) induced a size reduction of nano-TiO_2 aggregates that was dependent on the critical micelle concentration. In Dispersion 2 systems (pH 9), the stability provided by the pH had a significant effect on the size of nano-TiO_2 aggregates; the addition of surfactants did impact the size of the nano-TiO_2 aggregates but in less significance as compared to Dispersion 1 systems. The electrostatic and steric repulsion forces in connection with the size of nano-TiO_2 aggregates and flow velocity impacted the single-collector efficiency and attachment efficiency which dictated the maximum transport distance of nano-TiO_2 for the Dispersion 1 and

Dispersion 2 systems. By doubling the flow velocity at pH 9, the No Surfactant, 50% CMC Triton X-100, 100% CMC Triton X-100 and 100% CMC SDBS dispersion systems allowed nano-TiO_2 to attain maximum transport distances of 0.898, 2.17, 2.29 and 1.12 m, respectively. Secondary energy minima played a critical role in the deposition mechanisms of nano-TiO_2. Nano-TiO_2 deposited in the secondary energy wells may be released because of changes in solution chemistry. The deposition of nano-TiO_2 in primary and secondary energy minima, the reversibility of their deposition should be characterized to analyze the transport of nanoparticles in porous media. This is necessary to assess the risk of nanoparticles to the environment and public health

3.2. Introduction

The stability and transport of nano-TiO_2 may be influenced not only by the intentional and controlled generation of nano-TiO_2 with specific surface coating that may modify their behavior in environmental systems compared to natural and air-borne nanoparticles (Nowack and Bucheli, 2007; Navarro, et al., 2008), but also to the presence of surfactant and/or humic substances in subsurface environments. Information regarding the transport of nano-TiO_2 through porous media is essential to create a coherent notion of their mobility through soil matrices as well as to assess the potential threats to groundwater pollution. The objective of this chapter is to explore the effects of environmental physico-chemical parameters on nano-TiO_2 aggregation and transport mechanisms in saturated porous media. Laboratory scale column experiments were performed to investigate and characterize the effects of pH, anionic and nonionic surfactants and flow velocity on the aggregation and transport of nano-TiO_2 in saturated porous media. The

single-collector efficiency for physico-chemical filtration in saturated porous media was also applied to characterize the particle deposition and maximum transport distance of the nano-TiO_2 under favorable and non-favorable physical and chemical transport conditions. The parameters selected for these experiments fall within the ranges found in natural subsurface environments. Techniques of UV/Vis Spectrophotometer, Dynamic Light Scattering (DLS) and Zeta-Potential were implemented to determine nanoparticle concentration, changes in particle size and surface charge, respectively.

3.3. Materials and Methods

3.3.1. Column system

The porous medium used in these experiments consisted of ASTM 20/30 unground quartz silica sand from U.S. Silica Company, Ottawa, Illinois. The sand was sieved through a stainless steel U.S. 30 mesh to achieve a collector diameter d_c of 0.600 mm. The coating of the sand by metal oxides (e.g. Fe, Al, Ti, Ca, Mg, Na, K) may affect the surface charge of the porous media and induce colloid deposition at its surface (Litton and Olson, 1996). Therefore, to eliminate the metal oxides coating, the sand was chemically treated according to a procedure developed by Lenhart and Saiers, (2002) that included a series of acid and base washes.

For each experimental trial, 18.2 g of cleaned sand was packed into a Spectra/Chrom® Aqueous column (Cole-Parmer Inc., Vernon Hills, Illinois) with an inner diameter and length of 0.9 cm and 15 cm, respectively. The sand was supported on a Polypropylene Spectra/Mesh screen with

pore size of less than 0.500 mm. The sand was introduced into the column in 1 cm intervals. After each addition of sand, the sides of the column were tapped continuously to achieve uniform packing and avoid settling during the experiments. The sand column was saturated by applying DI water to the column from the bottom utilizing an L/S ® brushless digital drive (Cole-Parmer Vernon Hills, Illinois) connected to an L/S ® multi-channel pump head (Cole-Parmer Vernon Hills, Illinois) and Tygon® Autoanalysis Tubing (Cole-Parmer Vernon Hills, Illinois). To assure a homogenous compaction of the sand grains, at least 25 pore volumes (PVs) of DI water were passed through the column. The average porosity of the sand equaled 0.271. The permeability coefficient of the sand was determined according to the ASTM D 2434 – 68 (2006) method.

3.3.2. Nano-TiO_2 dispersions

Aeroxide® TiO_2 P 25 was obtained from Evonik Degussa Corporation (Parsippany, NJ). Aeroxide® TiO_2 P 25 is a mixture of two crystalline phases, anatase (80%) and rutile (20%), and its purity is in excess of 99.5%. According to the manufacturer, the density at 20° C, specific surface area (BET) and average particle size of TiO_2 are 3.8 g/cm^3, 50±15 m^2/g and 21 nm, respectively.

Two sets of nanoparticle dispersions were compounded for the study. The chemical characteristics of the electrolyte solution in both dispersions consisted of 0.01 M NaBr (Sigma-Aldrich Co.) and 0.001 M NaOH (Sigma-Aldrich Co.) with a final ionic strength of approximately 0.011 M. The concentration of nano-TiO_2 in both dispersions was 25 mg/L. Dispersions 1 and 2 were prepared through sonication of nano-TiO_2 in an ultrasonic bath for a

period of 1 hour in electrolyte solution with adjusted pH values of 7.0 and 9.0, respectively. The 0.001 M NaOH was used to target the desired pH. The pH values and ionic strength of the dispersion systems were based on the typical characteristics of most fresh groundwater aquifers (Davis and de Wiest, 1966).

Upon sonication, the dispersions were cooled to room temperature (21-22°C) and each was separated into four-100 mL volume parts. A nonionic surfactant, Triton X-100 (Sigma-Aldrich Co.) and an anionic surfactant, sodium dodecyl benzene sulfonate (SDBS) (Sigma-Aldrich Co.) were incorporated at 50% (e.g. only Triton X-100) and 100% (e.g. both surfactants) critical micelle concentrations (CMC) in some of the dispersions. If additional pH adjusting was required to maintain the dispersions at the specific pH, 0.001 M NaOH was utilized. Adsorption of surfactants and the role of surfactants in stabilizing colloidal dispersions have been studied extensively, as these phenomena are relevant to a range of industrial and environmental applications such as processing of minerals, personal care applications and soil remediation (Romero-Cano et al., 2002; Shao et al., 2010). Triton X-100 and SDBS are effective surfactants capable of adsorbing to the surface of colloids providing them with higher capacity to disperse in aqueous environments. We have selected these two surfactants to facilitate the dispersion of TiO_2 in the electrolyte solutions. Dispersion 1 (pH 7) and dispersion 2 (pH 9) each consisted of the following four systems: No Surfactant, 50% CMC Triton X-100, 100% CMC Triton X-100 and 100% CMC SDBS. These systems became the feeding solutions for the different experiments conducted in this study. All feeding dispersions were prepared before conducting the experiments to diminish spontaneous aggregation of nano-TiO_2 and its unstable behavior in the aqueous dispersions. Prior to performing an experiment, the corresponding 100 mL feed

dispersion was further sonicated for 45 min in the ultrasonic bath, cooled to room temperature and stirred.

3.3.3. Characterization of nano-TiO_2

All characterization techniques of nano-TiO_2 were conducted at room temperature. To corroborate the average primary particle size provided by the manufacturer, an X-ray diffraction (XRD) analysis of Aeroxide® TiO_2 P 25 was conducted. An X-ray Diffractometer, D5000 (Siemens), with monochromatic Cu Kα radiation (λ = 1.5418 Å) operated at 40 kV and 30 mA was utilized. Diffraction patterns were recorded in the 2θ angular range of 24.5˚ to 26˚ with step sizes of 0.01˚ and dwell time of 1 second. The average zeta potential of the different nano-TiO_2 solution dispersions was determined by a Zeta-Meter System 3.0+ (Zeta Meter, Inc., Staunton, VA) apparatus. Dispersion systems were prepared, sonicated for 1 hour, cooled to room temperature and stirred prior to taking the zeta potential measurements. The zeta potential value of a dispersion system was obtained by averaging ten zeta potential measurements. The average radius of the nano-TiO_2 aggregates in the various dispersion systems was measured using a DynaPro Titan Dynamic Light Scattering (DLS) probe from Wyatt Technology Corporation. The solution dispersions were prepared as indicated for the zeta-potential measurements with one additional step: dilution after the sonicating/cooling process to avoid multiple scattering of the DLS instrument. To not disturb the aggregate dimension, the dilutions were conducted with the same chemical characteristics of its corresponding solution minus the TiO_2. To ensure a representative sample of the aggregates subjected to the DLS analysis, the solution dispersions were agitated vigorously for 2 minutes utilizing a vortex mixer prior to creating the dilutions.

Before taking the DLS readings, the dilutions were again agitated for 30 seconds. Two DLS scattering analyses were taken per dispersion system; each run consisted of 20 DLS readings. The radius of the nano-TiO_2 aggregates in each dispersion system was determined by taking the mean value of the measurements.

3.3.4. Nano-TiO_2 transport column experiments

Table 1 provides a list of parameters utilized in the nano-TiO_2 transport experiments. Once the soil matrix was homogenously compacted and completely saturated, the corresponding nano-TiO_2 dispersion (i.e., 10 PVs) was loaded into the supply tank (i.e. a Pyrex beaker with cover) of the experimental set-up. A steady and almost pulse-free flow of dispersion was maintained through the soil matrix at a flow velocity (i.e. Darcy velocity) of $4.83x10^{-4}$ m/s (flow rate of 0.5 mL/min) or $9.67x10^{-4}$ m/s (flow rate of 1 mL/min) with the L/S ® brushless digital drive-pump system. Tygon® Autoanalysis Tubing was used to deliver the dispersion into the column. The dispersion was introduced from the bottom of the column as described in Figure 1. The moment the feed dispersion entered the column system, effluent samples were taken for nano-TiO_2 concentration measurements. Samples were hand-collected in 5 mL BD Falcon round-bottom disposable polypropylene tubes (Fisher Scientific, Pittsburg, PA). Ten additional PVs of DI water were added to the supply tank immediately after the initial feed dispersion was depleted, to flush out any remaining nano-TiO_2 or nano-TiO_2 aggregates from the porous media. The pump was turned off after the flushing period was concluded. A total of 45 effluent samples were collected for each of the experiments conducted.

Table 1. Experiment conditions and column properties.

Parameter Description	Unit	Value
Inner diameter of column	cm	0.9
Length of column	cm	15
Pore volume of column	mL	2.54
Collector diameter	mm	0.600
Porosity of filter media		0.271
Ionic strength (0.01 M NaBr & 0.001 M NaOH)	M	0.011
Initial concentration of TiO_2	mg/L	25
Flow Velocity 1	m/s	4.83×10^{-4}
Flow Velocity 2	m/s	9.67×10^{-4}
Temperature	˚C	22

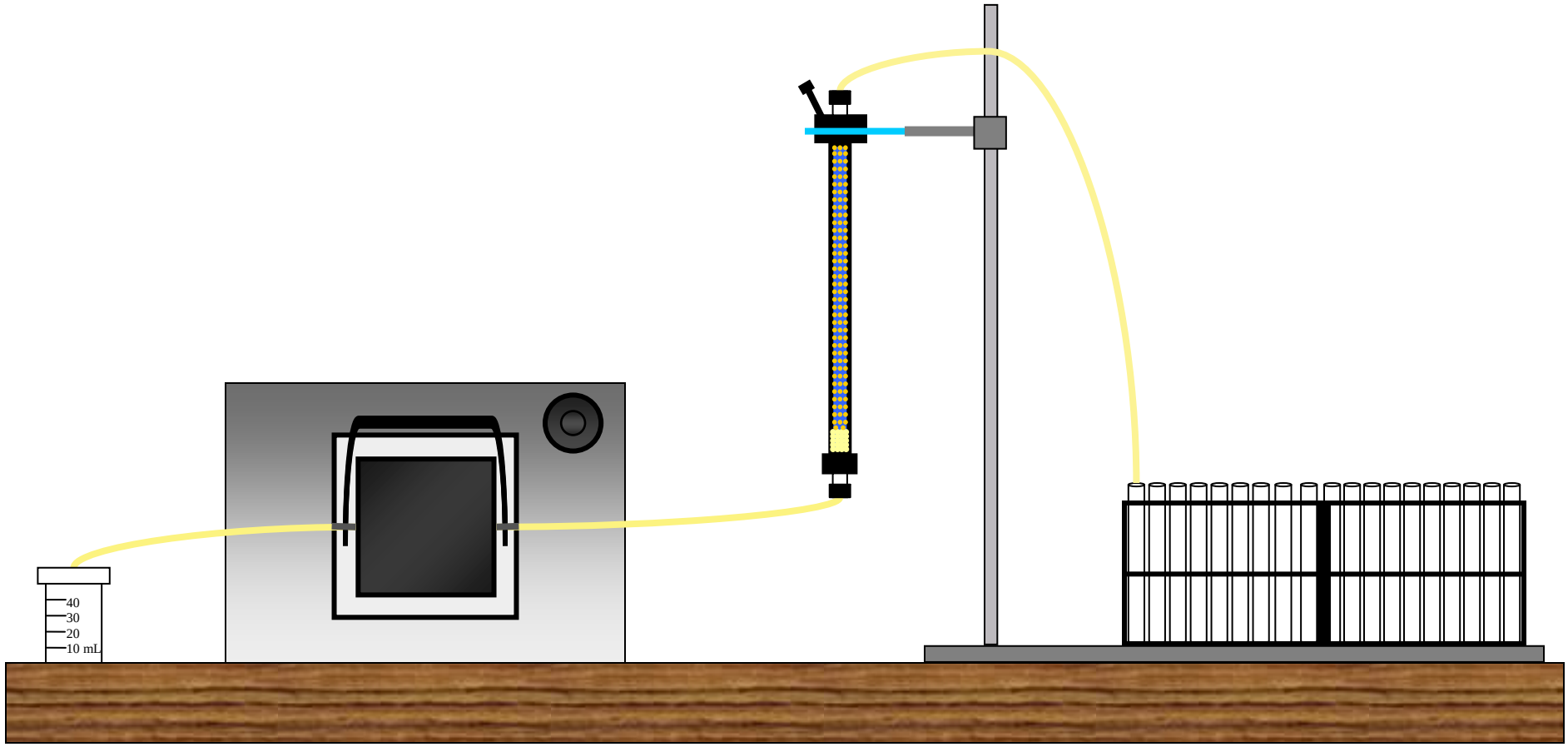

Fig. 1. Experimental set-up.

The influent and effluent concentrations of nano-TiO_2 were analyzed using a Cary 300 Bio UV/Vis Spectrophotometer (Varian, Inc., Walnut Creek, CA). The absorbance of the samples was measured for the wavelength range of 220 – 420 nm. The scanning control parameters of the spectrophotometer were set for data intervals corresponding to 1.000 nm, with average scanning time of 0.100 second and a scanning rate of 600.0 nm/min. The absorbance of nano-TiO_2 was correlated to the feed dispersion characteristics. For each system, a "most relevant" wavelength value for absorbance was selected. The later turned out to be at 330 nm wavelength. The concentration of nano-TiO_2 dispersions entering the column, C_0, and in the effluent, C, were used to generate breakthrough curves (BTCs) of C/C_0 as a function of PVs passing through the soil matrix. To create the nano-TiO_2 BTCs, only the odd-numbered effluent-collected samples were utilized.

3.3.5. Tracer breakthrough experiments

The hydraulic properties of the porous media within the column systems were evaluated through tracer tests. The even-numbered effluent samples collected in each experimental trial were used to determine the bromide (Br^-) concentration. An IC25 and AS 50 Ion Chromatograph System (Dionex Corporation) were used to perform the different isocratic Br^- ion-trace analyses via conductivity detection. The concentration of Br^- ions entering the column, C_0, and in the effluent, C, were used to produce BTCs of C/C_0 as a function of PVs.

3.3.6. Sedimentation experiments

The stability of nano-TiO_2 in the different dispersion systems was evaluated through sedimentation experiments. The different dispersion systems were prepared following procedures described in section 2.2. The dynamic aggregation process was monitored utilizing a Cary 300 Bio UV/Vis Spectrophotometer, measuring the sedimentation process of nano-TiO_2 via time-resolved optical absorbance. The absorbance of the samples was measured at a wavelength of 300 nm. Optical absorbency was recorded every 6 min for 180 min. For each dispersion system, the experiments were carried out in duplicates and the results presented are the average of the runs.

3.3.7. Colloids transport theory

The theoretical framework originally developed to analyze colloidal transport in porous media was utilized to investigate the transport of nano-TiO_2 through saturated soil. The mean particle sizes of the nanoaggregates in this study are within the submicron range. Therefore, we can characterize nano-TiO_2 as miniature colloids, as also suggested in the case of various nanoparticle aggregates (Lecoanet et al., 2004, Lecoanet and Weisner, 2004; Brant et al., 2007; Guzman et al., 2006; Phenrat et al., 2007; French et al., 2009).

Tufenkji and Elimelech (2004a) formulated a correlation equation to prognosticate the single-collector contact efficiency for physico-chemical filtration in saturated porous media. The theoretical approach takes into account colloid deposition on soil grains as a result of colloid transport to the non-mobile surface collector (i.e. soil grain) followed by attachment (Tufenkji and Elimelech, 2004a). The three mechanisms responsible for colloids transport are Brownian

diffusion, interception, and gravitational sedimentation (Yao et al., 1971). The general expression for the single-collector contact efficiency (η_0) is given by Tufenkji and Elimelech (2004a) as:

$$\eta_0 = \eta_D + \eta_I + \eta_G \quad (1)$$

where η_D represents the transport by diffusion, η_I is the transport by interception and η_G is the transport by gravitational sedimentation.

The actual single-collector removal efficiency (η) is defined as the product between attachment-collision efficiency (α) and η_0 (Equation 1). Note that α can be calculated in terms of the physico-chemical parameters of the systems as (Tufenkji and Elimelech, 2004a):

$$\alpha = -\frac{2}{3}\frac{d_c}{(1-f)L\eta_0}\ln\left(C/C_0\right) \quad (2)$$

where L represents the length of the filtering porous media, and C/C_0 is the ratio between the colloid effluent concentration and the colloid influent concentration, d_c is the diameter of the spherical collector and f is the porosity of the porous medium. The maximum distance (L_{max}) that colloids may be transported in saturated porous media can be estimated as the distance where 99.9% colloids removal from the pore solution occurred, L_{max} is expressed as (Fang et al., 2009; He et al., 2009):

$$L_{\max} = -\frac{2}{3}\frac{d_c}{(1-f)\alpha\eta_0}\ln\left(C/C_0\right) \quad (3)$$

where C/C_0 is 0.01.

3.4. Results

3.4.1. Nano-TiO_2 characterization, porous medium permeability coefficient and tracer BTCs

The size distribution of Aeroxide® TiO_2 P 25 was calculated based on X-ray diffraction analysis and Scherrer's formula (Cullity and Stock, 2001):

$$d_{hkl} = \frac{0.9\lambda}{B\cos\theta_B} \quad (4)$$

where d_{hkl} represents the mean size particle distribution (nm), λ is the wavelength of Cu Kα radiation (λ = 0.15418 nm), B (radians) constitutes the full width at half-maximum (FWHM) of the broadened diffraction line observed on the 2θ angular range, and θ_B is the Bragg angle of diffraction. The computed mean particle size distribution of the nanoparticles was 18.9 nm. This crystallite size differs by 2.1 nm from the one provided by the manufacturer. The average zeta potential of nano-TiO_2 in Dispersion 1 and 2 systems are presented in Table 2. The DLS tests provided hydrodynamic size of nano-TiO_2 in Dispersion 1 and 2 systems (Tables 3 and 4). Since the hydraulic particle size is greater than the average particle size of TiO_2, it can be concluded

that the nanoparticles aggregated in the different dispersion solutions. Less aggregation was observed in the dispersion systems at pH 9 compared to those at pH 7. As the pH of the dispersion system approaches the pH_{pzc} of nano-TiO_2 which is reported in literature to be between 6.7 and 7.0 (Leong and Ong, 2003; Pelton et al., 2006; Liu et al., 2008; Boncagni et al., 2009), the aggregation phenomena of nano-TiO_2 occurred. The size of nano-TiO_2 aggregates in the dispersions containing surfactants was smaller than the one without surfactant regardless of the pH, demonstrating that surfactants allow nano-TiO_2 to remain dispersed or stable. Note that surfactants adsorb to the surface of nano-TiO_2 creating steric repulsion between nanoaggregates thus inhibiting interactions and preventing more aggregation which can cause an increase in particle size.

Table 2. Zeta potential measurements of dispersion systems.

pH	Dispersion System	Zeta Potential (mV)
7	No Surfactant	20.0
	50% CMC Triton X-100	13.6
	100% CMC Triton X-100	21.2
	100% CMC SDBS	-11.6
9	No Surfactant	-16.8
	50% CMC Triton X-100	-17.9
	100% CMC Triton X-100	17.6
	100% CMC SDBS	-19.2

The ASTM D 2434-68 (2006) method for permeability of granular soils at constant head was utilized to determine the coefficient of permeability of the column system. The permeability coefficient *k* was calculated as 3.86×10^{-4} m/s, indicating a significant flow of water through the

porous media which is characteristic of clean sand (Holtz and Kovacs, 1981). The Br^- BTCs in all experiments included a monotonic increase with a C/C_0 value greater than 0.5 attained at 1.5 PVs and a plateau value of passage through the sand column of 1. A monotonic trend was also observed in the Br^- BTC descent. The BTCs of the dispersion systems under the same pH and flow velocity turned out to be extremely close in appearance. Thus, the Br^- BTCs displayed in Figures 3 – 6 represent the mean tracer curve of the dispersion systems presented in the figure.

3.4.2. Sedimentation analysis

The sedimentation experiments demonstrated that there is no significant sedimentation taking place in the inlet reservoir during the feeding of nano-TiO_2 into the column. According to the optical absorbency results (Figure 2), sedimentation is irrelevant for all the different dispersion systems for the first 60 minutes of the experiments. Considering that the feeding of nano-TiO_2 into the column at 4.83×10^{-4} m/s and 9.67×10^{-4} m/s took 52 and 26 minutes, respectively, we can attest that the application of the transport theory for steady-state systems is correct and the results supported.

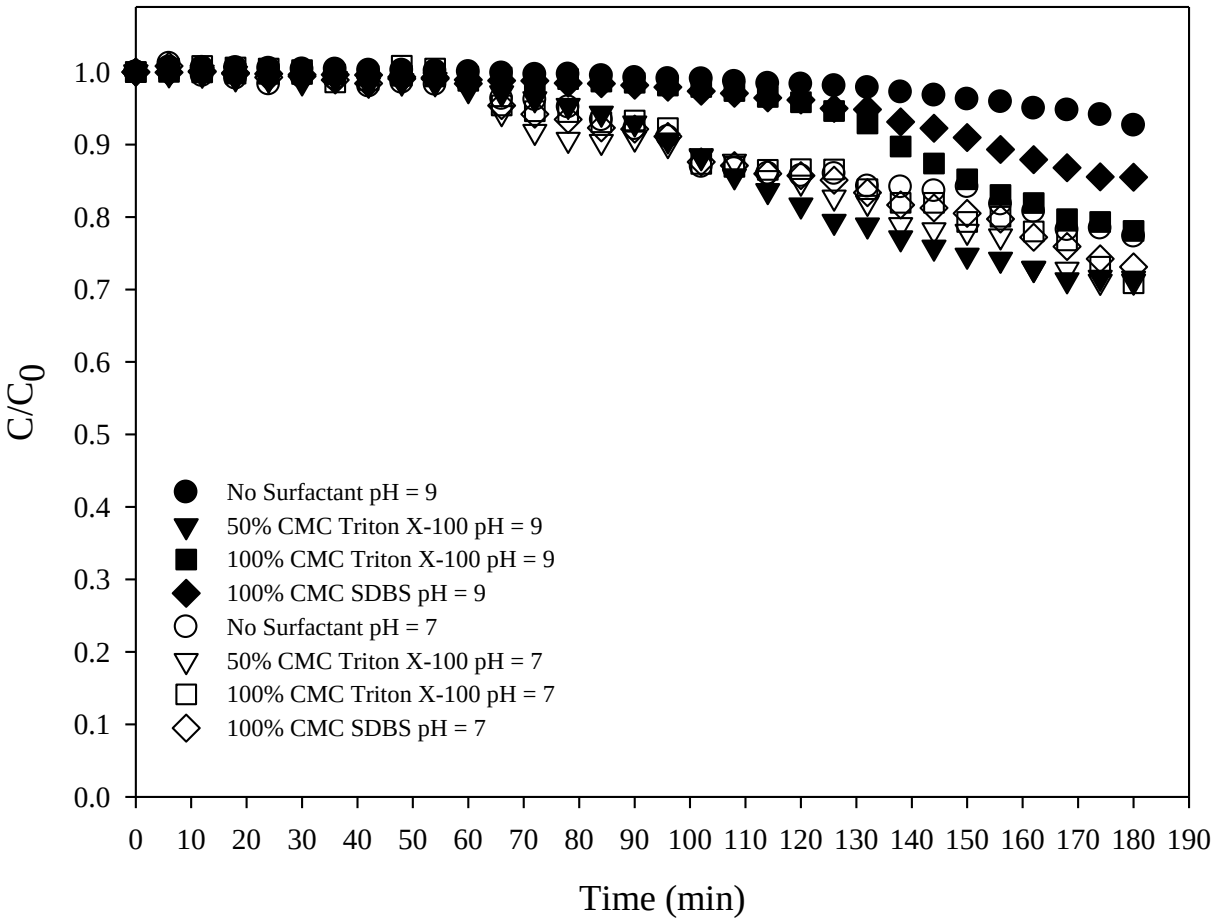

Fig. 2. Sedimentation of nano-TiO_2 in Dispersion 1 and Dispersion 2 systems.

3.4.3. Effect of surfactants vs. no surfactant in the transport of nano-TiO_2

The presence of Triton X-100, a non-ionic surfactant, and SDBS, an anionic surfactant, enhanced the transport of nano-TiO_2 in saturated porous media for Dispersion 1 (pH 7) systems. Figure 3 describes the nano-TiO_2 BTCs for the No Surfactant, 50% and 100% CMC Triton X-100, and 100% CMC SDBS systems at 4.83×10^{-4} m/s. The C/C_0 effluent fraction concentration of nano-TiO_2 increased with the presence of surfactant and percent CMC. During the flushing period of

the experiment, a sudden increase in C/C_0 was registered in the nano-TiO_2 BTCs. The increase in C/C_0 registered during the flushing period of the experiments will be referred from now on as the flushing peak of the BTCs. To determine the quantity of nano-TiO_2 that exited through the column, the percentage transport recovery for each experiment was computed (Table 5). The percentage transport recovery of nano-TiO_2 for dispersion systems with no Surfactant, 50% and 100% CMC Triton X-100, and 100% CMC SDBS at $4.83x10^{-4}$ m/s and pH 7 were 3.80%, 5.92%, 8.59% and 7.72%, respectively. Figure 4 shows the nano-TiO_2 BTCs of these same dispersion systems under a varied flow velocity of $9.67x10^{-4}$ m/s. The increase in flow velocity translated to an augmentation in nano-TiO_2 C/C_0 effluent fraction concentration. At a flow velocity of $9.67x10^{-4}$ m/s, the percentage transport recovery of nano-TiO_2 for dispersion systems with No Surfactant, 50% and 100% CMC Triton X-100, and 100% CMC SDBS were 4.98%, 11.6%, 21.2% and 29.6%, respectively. The concentration of nano-TiO_2 in the effluent was once more correlated to the presence of surfactant and percent CMC. The BTCs in Figure 4 also registered an increase in the flushing peak.

To determine the effect that pH had on the transport of nano-TiO_2 through the saturated porous medium, the experiments were also conducted at pH 9. Figure 5 corresponds to the nano-TiO_2 BTCs of No Surfactant, 50% and 100% CMC Triton X-100, and 100% CMC SDBS at pH 9 and $4.83x10^{-4}$ m/s. Based on the C/C_0 fraction concentration of nano-TiO_2 measured in the effluent, it was observed that the increase in pH induced better transport conditions for the nanoaggregates of all dispersions. At pH 9, the nanoaggregates in the dispersions are approximately two pH units apart from the pHpzc of nano-TiO_2. At $4.83x10^{-4}$ m/s, the addition of non-ionic and anionic surfactant did not necessarily improve the transport behavior of nano-TiO_2 compared to the No

Surfactant dispersion. No particular dispersion system dominated the transport of nano-TiO_2 under the present conditions. During the flushing period, similarly to the case at pH 7, the dispersion systems presented a well-established flushing peak. The presence and concentration of surfactant seemed to control the flushing peak maximum. The percentage transport recovery of nano-TiO_2 for dispersion systems with No Surfactant, 50% and 100% CMC Triton X-100, and 100% CMC SDBS at $4.83x10^{-4}$ m/s and pH 9 were 42.5%, 45.9%, 41.1% and 45.4%, respectively (Table 5). Figure 6 shows the nano-TiO_2 BTCs of the dispersion systems described above under $9.67x10^{-4}$ m/s flow velocity. The increase in flow velocity and presence of non-ionic and anionic surfactant enhanced the transport of nano-TiO_2 and the patterns of the nano-TiO_2 BTCs were much more well-defined. The flushing peaks in Figure 6 were not as pronounced as those in Figure 5, which may be the result of much greater transport of nano-TiO_2 during the first ten PVs. At pH 9 and $9.67x10^{-4}$ m/s the four dispersion systems registered their greatest transport of nano-TiO_2 the column. The percentage transport recovery of No Surfactant, 50% and 100% CMC Triton X-100, and 100% CMC SDBS were 48.2%, 76.2%, 75.5.% and 63.4%, respectively.

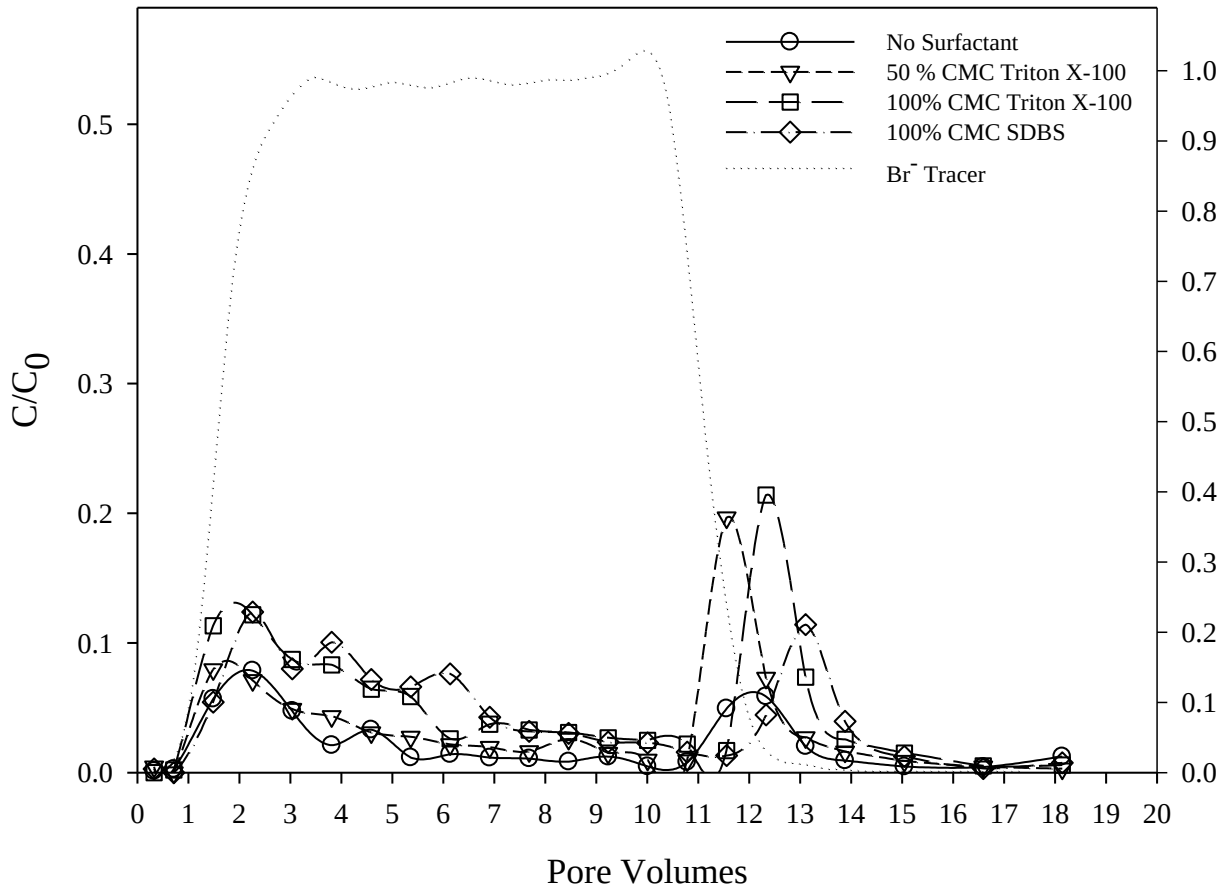

Fig. 3. Nano-TiO_2 BTCs without surfactant and with non-ionic surfactant (Triton X-100) and anionic surfactant (SDBS) at pH 7 and flow velocity of 0.0483 cm/s. BTC for a Br^- tracer is also included. Left y-axis is for nano-TiO_2 C/C_0, right y-axis is for tracer (Br^-) C/C_0.

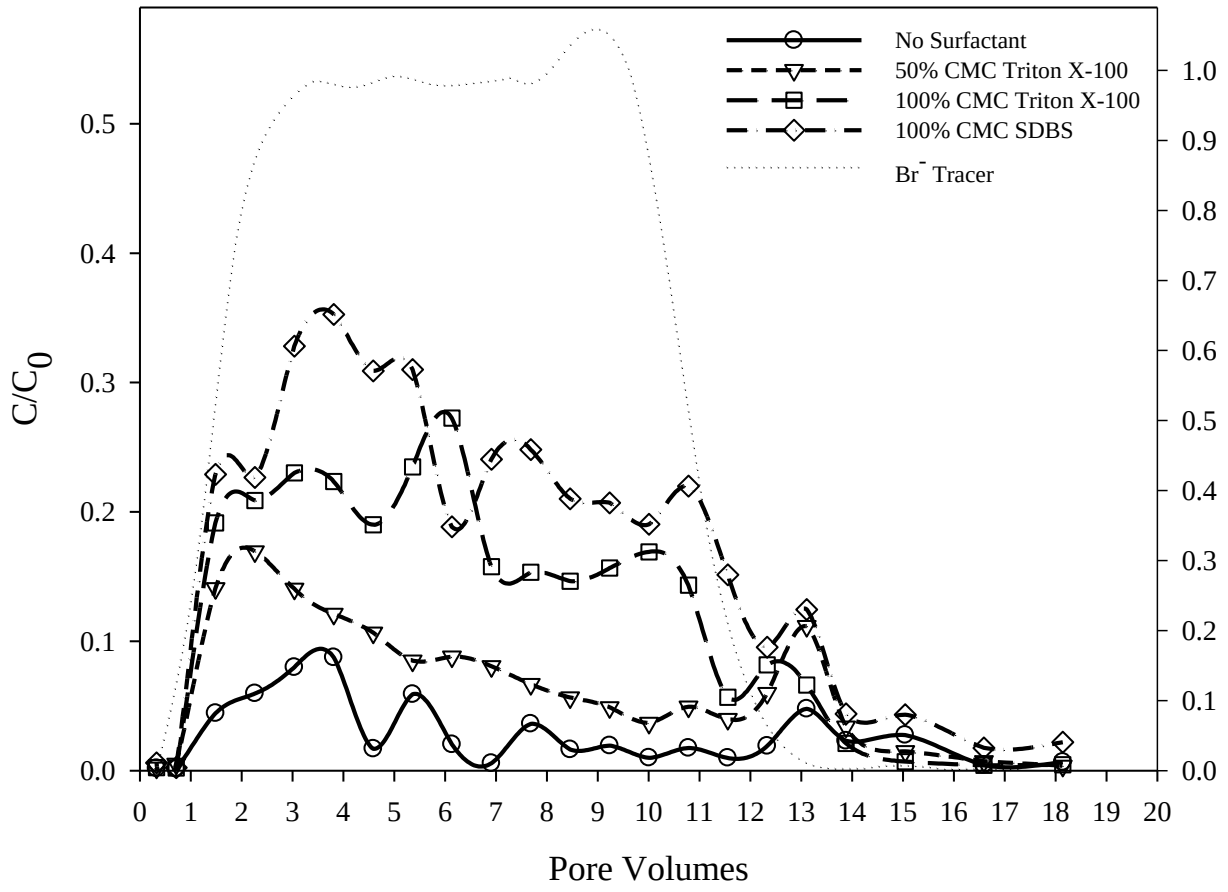

Fig. 4. Nano-TiO_2 BTCs without surfactant and with non-ionic surfactant (Triton X-100) and anionic surfactant (SDBS) at pH 7 and flow velocity of 0.0967 cm/s. BTC for a Br^- tracer is also included. Left y-axis is for nano-TiO_2 C/C_0, right y-axis is for tracer (Br^-) C/C_0.

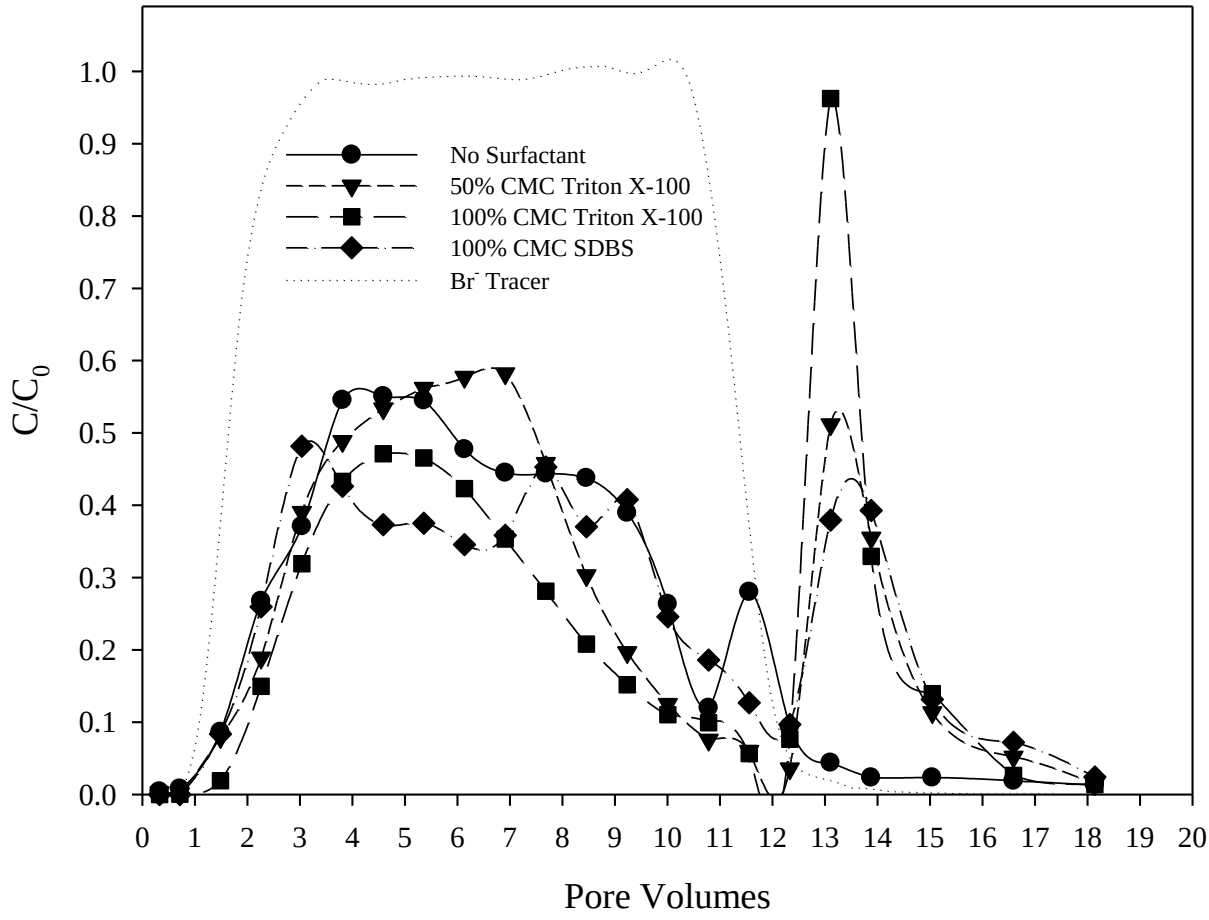

Fig. 5. Nano-TiO_2 BTCs without surfactant and with non-ionic surfactant (Triton X-100) and anionic surfactant (SDBS) at pH 9 and flow velocity of 0.0483 cm/s. BTC for a Br^- tracer is also included.

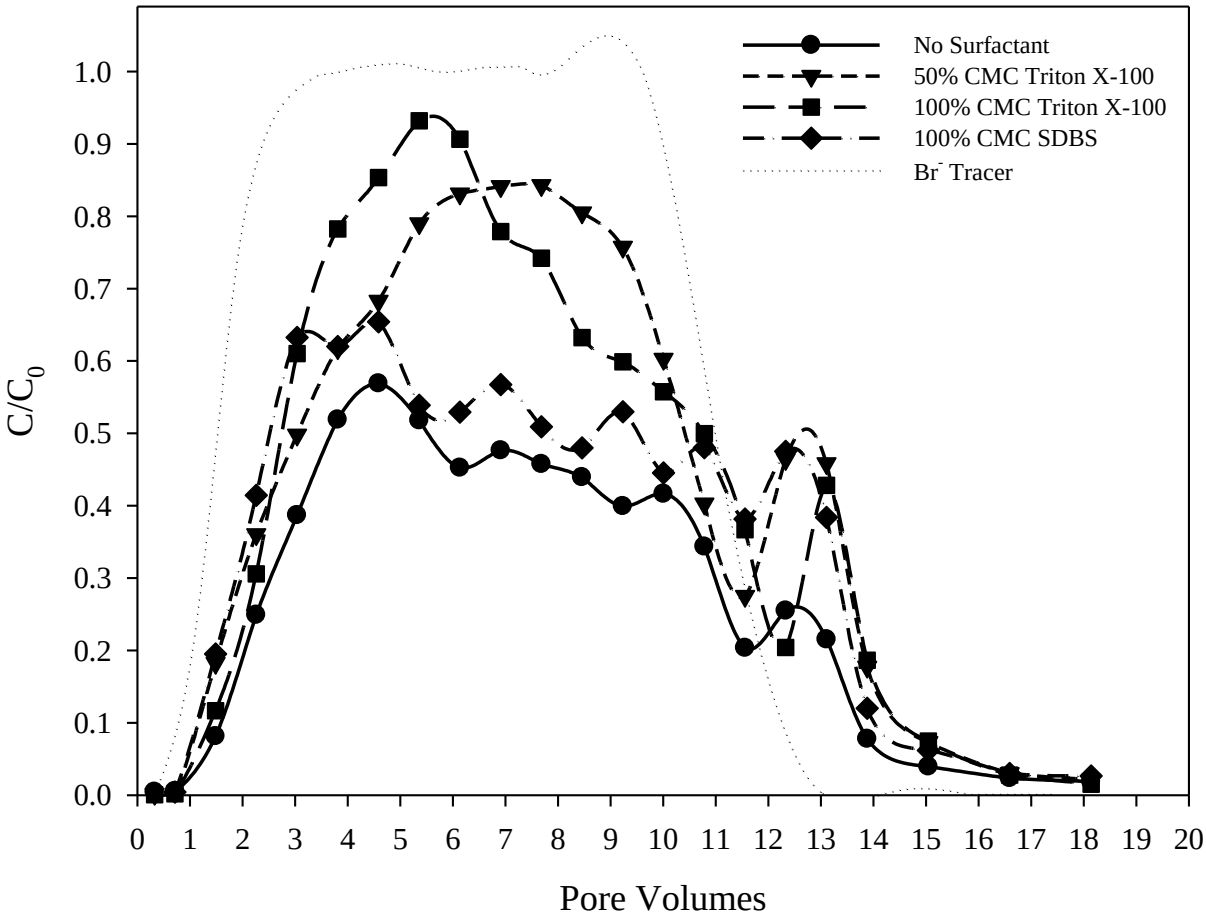

Fig. 6. Nano-TiO_2 BTCs without surfactant and with non-ionic surfactant (Triton X-100) and anionic surfactant (SDBS) at pH 9 and flow velocity of 0.0967 cm/s. BTC for a Br^- tracer is also included.

3.4.4. Influence of pH, flow velocity and non-ionic surfactant concentration on transport of nano-TiO_2

At pH 7, the addition of Triton X-100, a non-ionic surfactant, into aqueous dispersions in 50% and 100% CMC changed the average zeta potential of the nano-TiO_2 aggregates from 20.0 mV

for aqueous dispersion with no-surfactant to 13.6 and 21.2 mV, respectively (Table 2). The higher CMC permitted nano-TiO_2 at pH 7 to attain better stability in solution that resulted in higher transport of nano-TiO_2 through porous media (Table 5). As the pH increased from 7 to 9, the average zeta potential of the 50% and 100% CMC Triton X-100 dispersion systems became –17.9 and 17.6 mV, respectively. The stability of nano-TiO_2 at pH 9 was higher than at pH 7, allowing the nano-TiO_2 aggregates to repel one another for a longer period of time due to repulsive double layer interactions as also corroborated by the size of the nano-TiO_2 aggregates under different dispersion systems. The pH 9 provided better transport conditions for nano-TiO_2 than pH 7. At pH 9, the addition of non-ionic surfactant in different CMC did not affect the transport of nano-TiO_2 significantly.

Figures 3 to 6 provide a comparison of the BTCs of the 50% and 100% CMC Triton X-100 dispersion systems as a function of pH and varied flow velocity. The effect of flow velocity was investigated by interpreting the filtration theory with the experimental transport data. The computational analyses are presented in Tables 3 and 4. In the case of dispersion systems of 50% CMC Triton X-100 at pH 7 and pH 9 and 4.83×10^{-4} m/s, the single-collector contact efficiency, η_o, and the attachment efficiency, α, were 2.69×10^{-3}, 4.60 and 4.51×10^{-3}, 0.688, respectively. By doubling the flow velocity, η_o at pH 7 and pH 9 decreased by 63.4% and 63.7% whereas α increased by 112% at pH 7 and decreased by 62.6% at pH 9. At the lower flow velocity, the 100% CMC Triton X-100 dispersion system attained values of η_o and α of 3.53×10^{-3} and 2.94 at pH 7 while at pH 9 η_o and α were 4.33×10^{-3} and 0.899. The increase in flow velocity translated to an increase in the single-collector efficiency of approximately 63% for both pH values. The attachment efficiency did not change significantly at pH 7, but at pH 9 the increased

flow velocity induced a reduction in attachment efficiency of 115%. In terms of the percentage transport recovery of nano-TiO_2 through the porous medium, the change in pH had a positive effect in the 50% and 100% CMC Triton X-100 dispersion systems (Table 5). On the other hand, the increase in CMC from 50 to 100% had 45.2% and 83.3% increase in percentage transport recovery of nano-TiO_2 at pH 7 and 4.83×10^{-4} m/s and pH 7 and 9.67×10^{-4} m/s, respectively. The increase in CMC from 50 to 100% at pH 9 did not have significant impact at either flow velocity since the percentage transport recovery of nano-TiO_2 in the effluent for the 50% CMC Triton X-100 and 100% CMC Triton X-100 dispersion systems was very close at the corresponding flow velocities.

Table 3. Experimental parameters from BTC experiments calculated with filtration theory for a flow velocity of 0.0483 cm/s.

pH	Dispersion System	Particle Radius	Diffusion	Interception	Gravitational Sedimentation	Single-Collector Contact Efficiency	C/C_0	Attachment Efficiency	Maximum Transport Distance	Deposition Rate Coefficient
		a_p (nm)	η_D	η_I	η_G	$\eta_0 = \eta_D + \eta_I + \eta_G$		α	L_{max} (m)	k_d (h^{-1})
7	No Surfactant	253	1.84E-03	2.57E-04	4.98E-04	2.59E-03	2.59E-2	5.15	0.189	156
	50% CMC Triton X-100	223	2.07E-03	2.15E-04	4.00E-04	2.69E-03	3.41E-2	4.60	0.205	145
	100% CMC Triton X-100	122	3.32E-03	9.04E-05	1.18E-04	3.53E-03	5.89E-2	2.94	0.244	121
	100% CMC SDBS	103	3.69E-03	7.11E-05	8.18E-05	3.84E-03	6.03E-2	2.67	0.246	120
9	No Surfactant	102	3.79E-03	7.03E-05	8.24E-05	3.94E-03	0.431	0.782	0.820	36.1
	50% CMC Triton X-100	86.8	4.40E-03	5.59E-05	6.15E-05	4.51E-03	0.428	0.688	0.814	36.3
	100% CMC Triton X-100	90.4	4.21E-03	5.91E-05	6.55E-05	4.33E-03	0.345	0.899	0.649	45.5
	100% CMC SDBS	95.4	3.93E-03	6.35E-05	7.00E-05	4.06E-03	0.384	0.862	0.721	41.0

Table 4. Experimental parameters from BTC experiments calculated with filtration theory for a flow velocity of 0.0967 cm/s.

pH	Dispersion System	Particle Radius	Diffusion	Interception	Gravitational Sedimentation	Single-Collector Contact Efficiency	C/C_0	Attachment Efficiency	Maximum Transport Distance	Deposition Rate Coefficient
		a_p (nm)	η_D	η_I	η_G	$\eta_0 = \eta_D + \eta_I + \eta_G$		α	L_{max} (m)	k_d (h^{-1})
7	No Surfactant	253	1.12E-03	2.35E-04	2.31E-04	1.59E-03	3.79E-02	7.55	0.211	280
	50% CMC Triton X-100	223	1.26E-03	1.97E-04	1.85E-04	1.64E-03	9.51E-02	5.24	0.294	201
	100% CMC Triton X-100	122	2.02E-03	8.29E-05	5.47E-05	2.16E-03	1.95E-02	2.77	0.422	140
	100% CMC SDBS	103	2.25E-03	6.52E-05	3.79E-05	2.35E-03	2.53E-02	2.14	0.503	118
9	No Surfactant	102	2.31E-03	6.45E-05	3.82E-05	2.41E-03	0.463	1.17	0.898	65.9
	50% CMC Triton X-100	86.8	2.68E-03	5.13E-05	2.85E-05	2.76E-03	0.727	0.423	2.17	27.3
	100% CMC Triton X-100	90.4	2.56E-03	5.42E-05	3.04E-05	2.65E-03	0.739	0.417	2.29	25.8
	100% CMC SDBS	95.4	2.39E-03	5.83E-05	3.24E-05	2.49E-03	0.538	0.912	1.12	53.0

Table 5. Nano-TiO_2 transport recovery: total transport recovery and transport recovery from secondary energy minimum.

		Flow Velocity			
		4.83×10^{-4} m/s		9.67×10^{-4} m/s	
pH	**Dispersion System**	**Total Transport Recovery (%)**	**Transport Recovery from Secondary Energy Minimum (% of Total Transport Recovery)**	**Total Transport Recovery (%)**	**Transport Recovery from Secondary Energy Minimum (% of Total Transport Recovery)**
7	No Surfactant	3.80	28.0	4.98	18.8
	50% CMC Triton X-100	5.92	40.5	11. 6	16.4
	100% CMC Triton X-100	8.59	30.6	21.2	7.59
	100% CMC SDBS	7.72	22.5	29.6	6.79
9	No Surfactant	42.5	8.91	48.2	11.2
	50% CMC Triton X-100	45.9	17.8	76.2	13.6
	100% CMC Triton X-100	41.1	28.6	75.5	8.40
	100% CMC SDBS	45.4	17.4	63.4	15.2

3.4.5. Influence of pH, flow velocity and anionic surfactant on transport nano-TiO_2

The increase in flow velocity from $4.83x10^{-4}$ m/s (Figures 3 and 5) to $9.67x10^{-4}$ m/s (Figures 4 and 6) as well as the increase in pH from 7 to 9 in connection with the presence of anionic surfactant at 100% CMC enhanced the transport of nano-TiO_2 aggregates (Table 5). By doubling the flow velocity, the transport of nano-TiO_2 monitored in the effluent increased by 283% at pH 7 and only 39.7% at pH 9. The variation of pH from 7 to 9 had a greater impact in the mobility nano-TiO_2 through the porous medium than the increase of flow velocity. At a flow velocity of $4.83x10^{-4}$ m/s, the increase in pH resulted in 487% increase of nano-TiO_2 aggregates in the effluent as observed through the percentage transport recovery. At the higher flow velocity, the change in pH increased the percentage transport recovery of nano-TiO_2 by 114%. Therefore, the addition of anionic surfactant enhanced the effects of pH variation and flow velocity. According to filtration theory, at $4.83x10^{-4}$ m/s, the single-collector contact efficiency and attachment efficiency at pH 7 were $3.84x10^{-3}$ and 2.67 whereas at pH 9 these values were $4.06x10^{-3}$ and 0.862, respectively. The change in pH had a significant reduction in attachment efficiency while the single-collector contact efficiency increased slightly due to the reduction size of the nano-TiO_2 aggregates at pH 9. By doubling the flow velocity, the change in pH produced a reduction in attachment efficiency of 134% but the single-collector contact efficiency remained close. At pH 7, the increase in flow velocity decreased the attachment efficiency by 25.1% while at pH 9 the attachment efficiency did not have significant changes. In the case of the single-collector contact efficiency, the increase in flow velocity produced a decrease in single-collector contact efficiency of approximately 63% under both pH values.

3.4.6. Influence of non-ionic vs. anionic surfactant in the transport of nano-TiO_2

To investigate the effectiveness of the type of surfactant on the transport of nano-TiO_2 through saturated porous media, the BTCs for the 100% CMC Triton X-100 and SDBS where compared based on pH and flow velocity variation (Figures 3 – 6). At a flow velocity of $4.83x10^{-4}$ m/s, there is no significant difference in the BTCs of the non-ionic and anionic surfactant dispersion systems at pH 7. Based on the filtration theory, the maximum transport distance, L_{max}, of nano-TiO_2 through saturated porous media in the presence of 100% CMC Triton X-100 and SDBS at pH 7 was estimated to 0.244 and 0.246 m, respectively (Table 3 and 4). If the flow velocity was doubled, L_{max} for these systems under pH 7 was predicted to be 0.422 and 0.503 m, respectively. Under the later conditions, the 100% CMC SDBS system has a smaller attachment efficiency leading to an increase in the transport of nano-TiO_2 through the porous medium. As the pH of 100% CMC Triton X-100 and SDBS dispersion systems was increased to 9, the maximum transport distances for nano-TiO_2 at $4.83x10^{-4}$ m/s and $9.67x10^{-4}$ m/s were estimated to be 0.649, 0.721 m and 2.29, 1.12 m, respectively. At the higher flow velocity and pH 9, the 100% CMC Triton X-100 system had the smallest attachment efficiency allowing the nano-TiO_2 aggregates in this dispersion to transport the furthest (2.29 m) compared to all the other dispersion systems. The maximum transport distance for nano-TiO_2 was closely related to the single-collector contact efficiency and attachment efficiency that are a function of nano-TiO_2 aggregates size, flow velocity and pH.

3.5. Discussion

3.5.1. Nano-TiO_2 aggregation

The ability of nanoparticles to remain stable or dispersed is essential for the nano-TiO_2 to be mobile and transported in saturated porous media. The repulsive forces required to stabilize particles dispersion against van der Waals attractive forces are derived from the Coulombic repulsion forces deduced from electric particle surface charge or electrostatic double layer repulsions and the steric repulsion forces generated from the adsorption of long-chain-charged polymers on the surface of particles (Hirtzel and Rajagopalan, 1985). Steric repulsions between two particles result from volume restriction and osmotic effects. The former takes place from the configuration reduction in the zone between particle surfaces; the later arises from the high concentration of adsorbed charged macromolecules in the region between the particles as they come near (Hirtzel and Rajagopalan, 1985). Electrostatic and steric repulsion forces inhibit aggregation and attachment of particles to grain surfaces (Kretzschmar and Sticher 1997; Saleh et al., 2008). In Dispersion 1 and 2 systems consisting of nano-TiO_2 in aqueous solutions at pH 7 and pH 9, respectively, we observed that as the pH of the nano-TiO_2 dispersions came near the pHpzc nano-TiO_2 (6.7 -7.0), the nano-TiO_2 aggregates increased in size. At the pHpzc, the surface ionization of nanoparticles is suppressed, limiting the repulsive forces among nanoparticles allowing for aggregate formation. The increase in pH provided a better stability condition for nano-TiO_2 aggregates since it was two pH units apart from the nano-TiO_2 pH_{pzc}. The incorporation of Triton X-100, a non-ionic surfactant, and SDBS, an anionic surfactant, contributed to the steric repulsion forces and inhibited the uncontrollable aggregation of nano-TiO_2. In Dispersion 1 (pH 7) systems, the particle size of the nano-TiO_2 aggregates was directly related to the presence or absence of surfactants. The presence of non-ionic surfactant induced a

size reduction which was dependent on the CMC (Table 3 and 4). Nonionic surfactants adsorb on surfaces of particles in the form of micellar structures (Romero-Cano et al., 2002; Sharma et al., 2010) resulting from the initial adsorption of surfactant molecules on the surfaces, and their subsequent reorganization into micellar structures (Levitz et al., 1984). The stability of nanoparticles in nonionic surfactant solutions also depends on the extent of surface coverage by surfactant micelles and nanoparticle dispersions are stable as long as there is at least one layer of surfactant micelles that separates the nanoparticles according to Alexeev et al., 1996. As surfactant micelles adsorbed on the particle surface, these micelles provide a steric repulsion between the particles that stabilizes them against aggregation. The incorporation of anionic surfactant in 100% CMC produced the smallest nano-TiO_2 aggregates in Dispersion 1. The negatively charged SDBS molecules can easily react with positively charged metal ions by complexation effect, electron attraction and charge neutralization (Shao et al., 2010) leading to the generation of steric repulsion. Note that in this case nano-TiO_2 without surfactant attained a positive zeta potential of 20.0 mV. This facilitated the interaction between the anionic surfactant and the metal oxide nanoparticles. In Dispersion 2, the stability provided by the pH had a tremendous effect in the nano-TiO_2 aggregates size; the addition of surfactants did impact the hydrodynamic diameter of the nano-TiO_2 aggregates but in less significance compared to the systems in Dispersion 1. Figure 2 illustrates that at pH 9 very little sedimentation takes place in the No Surfactant system (less than 8% after 180 minutes of testing). Under the same conditions the 50% and 100% CMC Triton X-100 and 100% SDBS registered less than 29%, 23% and 15% sedimentation at the conclusion three-hour testing. The electrostatic and steric repulsion forces in connection to nano-TiO_2 aggregates diameter and flow velocity had a direct impact in the single-

collector efficiency and attachment efficiency which dictated the maximum transport distance of the Dispersion 1 and 2 systems.

3.5.2. Nano-TiO_2 mobility and transport

Electrostatic and steric repulsion forces generated by solution chemistry combined with favorable hydrodynamic conditions can further enhance the transport distances of nano-TiO_2. Doubling the flow velocity from $4.83x10^{-4}$ m/s to $9.67x10^{-4}$ m/s increased the transport of nano-TiO_2 aggregates without surfactant at pH 7 and pH 9. However, this increment in transport was not significant. If we combined the effect of increasing flow velocity with the presence of surfactants as well as increasing the pH from 7 to 9, i.e. 2 units away from pHpzc, a slight increase in transport was observed in some of the dispersion systems. From Table 4, we observe that by doubling the flow velocity at pH 9, the No Surfactant, 50% CMC Triton X-100, 100% CMC Triton X-100 and SDBS attained maximum transport of nano-TiO_2 distances of 0.898, 2.17, 2.29 and 1.12 m, respectively, among all experiments. The 18.9 nm nano-TiO_2 particle size produced nano-TiO_2 aggregates in aqueous solutions that were significantly larger than the original particle size. The hydrophobic characteristics and aggregation tendencies of some nanoparticles, such as nano-TiO_2, will either prevent their dispersal in natural environments or increase their deposition onto porous media thus limiting their transport. This factor in connection with pH variations and the presence of surfactants and NOM in subsurface environments may provide favorable conditions that can significantly reduce the attachment efficiency of the nanoaggregates thus increasing the transport of nano-TiO_2 through the soil matrix.

3.5.3. Nano-TiO_2 deposition and secondary energy minimum

Some authors have suggested that existing transport theory may not be adequate to predict the mobility and deposition behavior of nanoparticles or nanoaggregates (Tufenkji and Elimelech, 2004a; Tufenkji and Elimelech, 2005; Kuznar and Elimelech, 2007). Some of the discrepancies can be attributed to interaction energies between nanoparticles and collector surfaces, size difference between matrix pores and nanoaggregates, and shear forces (Guzman et al., 2006). Filtration theory assumes that the particle deposition rate k_d is constant. Nonetheless, changes in collector-particle interaction can lead to variations in the deposition rate. In the presence of the repulsive electrostatic double layer, particles in solution may demonstrate a dual deposition approach, that is, some portion of the particles experience a fast deposition rate whereas the rest of the particles experience a slow deposition rate (Tufenkji and Elimelech, 2004b). Favorable and unfavorable interactions between solution chemistry and colloids can be credited to the variation in deposition kinetics (Tufenkji and Elimelech, 2004b; Tufenkji and Elimelech, 2005). In the absence of repulsive interaction energies, particle deposition is favorable, i.e. increased deposition rates take place due to the occurrence of a deep secondary energy minimum well. In contrast, when repulsive colloidal interactions occur, unfavorable or slow rate deposition takes place because of the deep primary energy well (Tufenkji and Elimelech, 2004b; Tufenkji and Elimelech, 2005). Franchi and O'Melia (2003) and Hahn and O'Melia (2004) established the reversibility of particle deposition in the secondary energy minimum. In addition, particles deposited in the secondary energy minimum well may be released by vanquishing the energy barrier with electrolyte solution, that is, without colloids at a very low salt concentration (Franchi

and O'Melia, 2003; Hahn and O'Melia, 2004). In our study, nano-TiO_2 aggregates deposited onto surfaces of porous media due to secondary energy minimum were eventually released during the flushing period of the column with DI water. The reversible nano-TiO_2 deposition was depicted by the flushing peaks. It is our understanding, that this is the first time in which a research study reported the release of manufactured nanoaggregates due to the elimination of the secondary energy minimum well. At pH 7 and pH 9, the reversible deposition of nano-TiO_2 was more pronounced at the lower flow velocity of $4.83x10^{-4}$ m/s and was correlated to the presence and concentration of surfactants (Table 5), which may indicate that changes in solution chemistry may have more impact on the release of nano-TiO_2 from secondary energy minima than hydrodynamic forces. From the BTCs it is observed that the systems containing non-ionic surfactant were more effective in conducting reversible depositions upon the elimination of the secondary energy barrier. The deposition of nano-TiO_2 in primary and secondary energy minima, the reversibility of their deposition in secondary energy minima should be addressed when characterizing the fate and transport of nanoparticles in porous media when assessing the risk of nanoparticles to public health and the environment.

CHAPTER IV. DEPOSITION AND RELEASE KINETICS OF NANO-TIO_2 IN SATURATED POROUS MEDIA: EFFECTS OF SOLUTION IONIC STRENGTH AND SURFACTANTS

The chapter is a first-author manuscript published in the Environmental Pollution Journal in 2013.

4.1. Abstract

The aggregation, transport and deposition kinetics (i.e. attachment and release) of TiO_2 nanoparticles (nano-TiO_2) were investigated as a function of ionic strength and the presence of anionic (sodium dodecylbenzene sulfonate, SDBS) and non-ionic (Triton X-100) surfactants in 100% critical micelle concentration (CMC). The electrolyte concentration of the suspensions dictated the kinetic stability of nano-TiO_2 thus influencing the transport and retention of the nanoaggregates in the saturated porous medium. With increasing ionic strength, the interaction between approaching nano-TiO_2 and nano-TiO_2 already deposited onto collectors surfaces seemed to be more favorable than the interaction between approaching nano-TiO_2 and bare collectors surfaces. The abrupt and gradual reduction in electrolyte concentration during the flushing cycles of the column experiments induced the release of previously deposited nano-TiO_2 suggesting attachment of nano-TiO_2 through secondary energy minimum.

4.2. Introduction

Whether TiO_2 NPs resist attachment and travel long distances or accumulate onto porous media, part of the balance between free migration and deposition will be governed by the tendency of NPs to maintain dispersion stability without aggregating (Chen et al., 2011; Solovitch et al., 2010). Changes in solution chemistry may also induce the release (i.e. reversible deposition) of previously deposited NPs in secondary energy wells by vanquishing the energy barriers (Godinez and Darnault, 2011) thus affecting their overall distance traveled. Nonetheless, a limited number of studies have addressed this point which is critical to properly assess the risk that engineered TiO_2 NPs pose to aquifer systems. The objective of this chapter is to investigate the aggregation, transport and deposition kinetics (i.e. attachment and release) of titanium dioxide nanoparticles (nano-TiO_2) in saturated porous media as a function of ionic strength and the presence of anionic (sodium dodecylbenzene sulfonate, SDBS) and non-ionic (Triton X-100) surfactants in 100% critical micelle concentration (CMC). Several nanoparticles utilized in industrial processes have their surfaces modified, functionalized or coated (Wang et al., 2012; Labille et al., 2010; Tan et al., 2008; Wang et al., 2007). Hence, the nanomaterial residues released into the environment will probably consists of nanoparticles embedded in more or less altered matrixes. To emphasize this point, surface active agents were incorporated into some of the solutions suspensions.

4.3. Materials and Methods

4.3.1. Preparation of nano-TiO_2 suspensions and characterization of nano-TiO_2

Three sets of nano-TiO_2 suspensions were prepared. The electrolyte solutions of set one, two and three consisted of 0.001 M NaBr and 0.0001 M NaOH, 0.01 M NaBr and 0.001 M NaOH, and 0.1 M NaBr and 0.01 M NaOH, respectively. The NaOH solutions were added in the necessary amounts as to adjust the pH of the final solutions to a value of 9. This resulted in a final ionic strength of 0.0011 M for set one, 0.011 M for set two and 0.11 M for set three. Sodium bromide (ACS reagent, ≥99.0%) and sodium hydroxide (SigmaUltra, ≥98%) were purchased from Sigma-Aldrich Co. Once the desired pH was achieved, Aeroxide® TiO_2 P 25 provided by Evonik Degussa Corporation (Parsippany, NJ) was added to the solution to attain a final concentration of 25 mg/L in all suspensions. The Aeroxide® TiO_2 P 25 is composed of two crystalline phases (i.e. 80% anatase and 20% rutile) and its purity is in excess of 99.5%. The nano-TiO_2 suspensions were stored at 4 °C for a period of 24 hours prior to use.

All solution suspensions utilized in the experiments had a pH of 9. This value is two units apart from the pH_{pzc} of TiO_2 (e.g. 6.7 and 7.0) (Liu et al., 2008; Boncagni et al., 2009). The pH is in the alkaline region which takes place in natural settings associated with evaporative salt lakes and aquifer systems polluted by alkaline mine drainage (Naftz et al., 2011; Kelly et al., 2007). At alkaline conditions the surface of TiO_2 attains an important negative charge density due to the deprotonation of its hydroxyl groups (Svecova et al., 2008) thus providing good stability for the nanoaggregates in suspension. Multiple literature studies have also implemented this pH in their experiments (Chen et al., 2012; Godinez and Darnault, 2011; Thio et al., 2011; Fatisson et al., 2009).

Prior an experiment, the nano-TiO_2 suspensions were sonicated in an ultrasonic bath. The sonication period was 1 hr for the 0.0011 M and 0.011 M nano-TiO_2 suspensions and 1.5 hr for the 0.11 M nano-TiO_2 suspension. Upon this process, the suspensions were cooled to room temperature and stirred (20 minutes). These were then separated into two-100 mL volume parts which were utilized to conduct duplicates per experimental trial (e.g. column tests, particle size analysis, sedimentation and zeta potential experiments). Sufficient nano-TiO_2 suspensions were prepared to have three systems per set or ionic strength. Triton X-100 (nonionic surfactant, Sigma-Aldrich Co.) and SDBS (anionic surfactant, Sigma-Aldrich Co.) were added in 100% critical micelle concentration (CMC) to two of the systems. Each suspension set consisted of No Surfactant, 100% CMC Triton X-100 and 100% CMC SDBS. The CMC for Triton X-100 and SDBS were reported to be 0.22–0.24 mM (Sigma-Aldrich Co.) and 963 mg/L (Adak et al., 2005), respectively. Before performing an experiment, each 100 mL volume part was further sonicated for 40 minutes, cooled to room temperature and stirred. This was done to decrease spontaneous aggregation and unstable behavior of nano-TiO_2. Triton X-100 and SDBS are often utilized to modify or coat the surfaces of TiO_2 nanoparticles to enhance their industrial applications (Wang et al., 2012; Bettoni et al., 2012; Wang et al., 2007; Tkachenko et al., 2006). For example, Triton X-100 is used to control aggregation and promote dispersion stability of TiO_2 nanoparticles as well as to increase the hydrophilic properties of titania nanocomposite films to promote charge transfer at the electrode/electrolyte interface (Wang et al., 2012; Tkachenko et al., 2006). On the other hand, SDBS has been used as a surface-modified agent for TiO_2 nanoparticles to increase their wettability. Nanoparticles surface wettability plays a crucial role on the electrorheological effect (ER) that has applications for actuators, shock absorbers and active devices (Wang et al., 2007).

4.3.2. Group one column experiments

The porous medium utilized in this study consisted of ASTM graded sand (U.S. Silica Company, Ottawa, Illinois). The mean particle size of the sand (i.e. collector diameter, d_c) was approximately 0.307 mm. To remove the metal oxide coatings from the silica grains a series of acid and base washes were carried out as explained in Lenhart and Saiers (2002). A Spectra/Chrom® Aqueous column (Cole-Parmer Inc., Vernon Hills, Illinois) of 0.9 cm diameter and 15 cm length was utilized to conduct the column experiments. The original meshes of the column were removed and replaced by a Polypropylene Spectra/Mesh screen with pore size of 0.1 mm. The chemically treated sand was poured into the column following the procedure described in Godinez and Darnault (2011). The average porosity of the sand was 0.278; this value was determined according to the method of Danielson and Sutherland (1986) utilizing the measured bulk density and a specific solid density of 2.65 g/cm^3.

Upon packing the column with dry chemically treated sand, the porous medium was saturated with the electrolyte solution (i.e. no nano-TiO_2) corresponding to the feeding suspension of the system at hand. An L/S ® brushless digital drive (Cole-Parmer Vernon Hills, Illinois) connected to an L/S ® multi-channel pump head (Cole-Parmer Vernon Hills, Illinois) and Tygon® Autoanalysis Tubing (Cole-Parmer Vernon Hills, Illinois) were utilized to deliver the electrolyte solution into the column from the bottom. Twenty-five pore volumes (PVs) of electrolyte solution were passed through the porous medium to guarantee a homogenous compaction of the sand. At the end of the saturation process, 10 PVs of the corresponding nano-TiO_2 suspension

were loaded in the Pyrex beaker (i.e. supply tank see Fig. 1 in Godinez and Darnault, 2011). Both electrolyte solution and suspension were delivered into the column at a steady and almost pulse-free flow velocity (i.e. Darcy velocity) of 9.42 x 10^{-4} m/s. Once the feeding suspension entered the column, effluent samples were hand-collected in 5 mL BD Falcon round-bottom disposable polypropylene tubes (Fisher Scientific, Pittsburg, PA). To complete the transport experiments, 10 PVs of background electrolyte solution free of nano-TiO_2 were pumped followed by 10 PVs of DI water. Seventy-four effluent samples were collected per experiment. Each column test was conducted twice per system.

A Cary 300 Bio UV/Vis Spectrophotometer (Varian, Inc., Walnut Creek, CA) was used to measure the absorbance of the samples collected over a range of 220 to 500 nm. The scanning control parameters of the spectrophotometer were indicated in Godinez and Darnault (2011). For each system a most relevant wavelength absorbance value was selected (e.g. 320 nm for the systems at 0.0011 M and 0.011 M and 330 nm for the systems at 0.11 M). To create the breakthrough curves (BTCs), the ratio between the absorbance of the odd-numbered-collected effluent samples (C) and the actual absorbance of the starting feed-suspension (C_0) were plotted as a function of PV. The average of the C/C_0 duplicates per system is reported for all experiments. The hydraulic properties of the porous medium in the column were dictated by the tracer analysis. An IC25 and AS 50 Ion Chromatography System (Dionex Corporation) were used to determine the Br^- concentration (C) of the even-numbered-collected effluent samples. The tracer BTCs were formulated by plotting the ratio between concentration of Br^- in the effluent samples (C) and the actual Br^- concentration in the feeding suspension (C_0) as a function of PV.

4.3.3. Group two column experiments

Additional transport experiments were conducted to study the effect of ionic strength in the release of previously deposited nano-TiO_2 from the porous medium. For these tests, only the sets of nano-TiO_2 suspensions at 0.011 M and 0.11 M were utilized. The transport experiments consisted in delivering 10 PVs of nano-TiO_2 suspension through the column followed by a series of 10 PV flushing cycles of electrolyte solutions free of nanoaggregates. Upon completing the saturation process of the column experiments, the nano-TiO_2 delivery and flushing procedure for the 0.011 M nano-TiO_2 suspensions were conducted in the subsequent order: 10 PVs of nano-TiO_2 suspension, 10 PVs of background electrolyte solution free of nano-TiO_2, 10 PVs of electrolyte solution at 0.0011 M, and 10 PVs of DI water. For these experiments a total of 110 samples were collected. In the case of the suspensions at 0.11 M, 10 PVs of nano-TiO_2 suspension were first pumped through the column followed by 10 PVs of background electrolyte solution. To initiate the release of previously deposited nano-TiO_2 10 PVs of electrolyte solution at 0.011 M were then pumped through the porous medium followed by 10 PVs of 0.0011 M electrolytes solution and 10 PVs of DI water. A total of 140 samples were collected for these experiments. The BTCs of the column experiments were composed of the odd-numbered samples collected. All column tests were conducted in duplicates. The average of the C/C_0 duplicates is reported as a function of PV for all experiments.

For the first group (Fig. 5–7) and second group of column experiments at 0.011 M (Fig. 11) and 0.11 M (Fig. 12) the transport trends were equivalent for the first 20 PVs, that is, the

characteristics in experimental procedure overlapped. Based on the BTC results, it may be inferred that the consistency in experimental approach in both groups of transport tests was appropriate.

4.3.4. Batch experiments

Batch reactor experiments were performed in 20 mL glass vials to assess the attachment affinity of nano-TiO_2 aggregates to the surfaces of silica sand. Ten grams of dry sand were combined with 10 mL of each nano-TiO_2 suspension system (25 mg/L). The contents of the batch reactor were allowed to equilibrate for 140 min by slowly rotating the vial at 7 rpm using a vial rotator (Glas-Col®). The time frame corresponds to the time span of the longest transport experiment. The final concentration nano-TiO_2 in the supernatant was measured by UV/Vis spectrophotometer. The experiments were conducted 3 times per suspension system. The reported value of nano-TiO_2 adsorbed to the sand is the average of the 3 trials.

4.3.5. Dynamic Light Scattering

A DynaPro Titan Dynamic Light Scattering (DLS) probe from Wyatt Technology Corporation was utilized to determine the hydrodynamic radius of the nano-TiO_2 aggregates. The time-resolved hydrodynamic radius was measured as a function of ionic strength at pH 9. For each ionic strength, the extent of aggregation per system was measured every five minutes for a period of 145 min. Each DLS run collected 10 readings. The particle size of the nanoaggregates per time frame in each system was computed by taking the average value of three-DLS runs.

4.3.6. Sedimentation

Nano-TiO_2 sedimentation was determined via time-resolved optical absorbency. By monitoring the optical absorbance of nano-TiO_2 (Carry 300 Bio UV/Vis spectrophotometer) as a function of time, some characteristics of nano-TiO_2 stability in the different suspensions can be addressed. The absorbance of the systems was measured at the wavelengths indicated in section 3.3.2. Optical absorbency was monitored every 6 min for a period of three hours. All sedimentation tests were conducted in duplicates and the displayed C/C_0 vs. time plots represent the average value of the experiments.

4.3.7. Zeta potential measurements

A Zeta-Meter System 3.0+ (Zeta Meter, Inc., Staunton, VA) was utilized to take the measurements. It is important to mention that in our previous study (Godinez and Darnault, 2011) the apparatus was used without updating any of its parts. In the present study, the molybdenum anode of the electrophoresis cell was replaced and the apparatus was tested by a technician. Two suspensions per system were prepared to record the zeta potential of nano-TiO_2 as a function of time. Fifteen zeta potential readings were recorded per suspension every 10 minutes for one-hour. Refer to Godinez and Darnault (2011) for more information. The results presented are the average zeta potential per time frame of the duplicates per system.

To measure the zeta potential of the porous medium three sets of silica suspensions (i.e. 0.0011 M, 0.011 M and 0.11 M) at pH 9 were prepared. Each set consisted of the No surfactant, 100% CMC Triton X-100 and 100% CMC SDBS systems. The chemically treated sand was sieved and only the silica grains less than 150 µm were utilized in the preparation of the sand suspensions (250 mg/L); these were stored at 4 °C for a period of seven days prior to conducting the zeta potential measurements. The silica suspensions were sonicated for 1 hr then cooled to room temperature and stirred (20 min) prior to the analysis. Twenty zeta potential readings of the supernatant per sand system were measured and the average value is reported in the study.

4.3.8. Interaction energy profiles

The DLVO theory (Derjaguin and Landau, 1941; Verwey and Overbeek, 1948) is utilized to qualitatively comprehend the transport and retention tendencies of nano-TiO_2 in saturated porous media. The total interaction energy is expressed as the sum of the electrostatic double layer (EDL) and van der Waals (VDW) forces. The total interaction energy between nanoaggregates (i.e. nano-TiO_2–nano-TiO_2) is assumed to be created from a sphere-sphere interaction whereas that between nanoaggregates and sand grains (i.e. nano-TiO_2–Sand) is perceived from a point of view of a sphere-plate interaction.

The electrostatic double layer interaction energies for the nano-TiO_2–nano-TiO_2 and nano-TiO_2–Sand systems were computed by using equations 1 and 2, respectively (Hogg et al., 1966; Bhattacharjee and Elimelech, 1997):

$$\Phi_{EDLNano-TiO_2-Nano-TiO_2} = \frac{2\pi a_{p1} a_{p2} n_\infty k_B T}{\left(a_{p1}+a_{p2}\right)\kappa^2}\left[2\Psi_{p1}\Psi_{p2}\ln\left(\frac{1+e^{-\kappa y}}{1-e^{-\kappa y}}\right)+\left(\Psi_{p1}^2+\Psi_{p2}^2\right)\ln\left(1-e^{-2\kappa y}\right)\right] \quad (1)$$

$$\Phi_{EDLNano-TiO_2-Sand} = \pi\varepsilon_0\varepsilon_r a_p\left[2\xi_p\xi_c \ln\left(\frac{1+e^{-\kappa y}}{1-e^{-\kappa y}}\right)+\left(\xi_p^2+\xi_c^2\right)\ln\left(1-e^{-2\kappa y}\right)\right] \quad (2)$$

where a_{p1} and a_{p2} represent the radii of two interacting nano-TiO_2 aggregates and a_p denotes the radius of a nano-TiO_2 aggregate, n_∞ is the bulk number density of ions k_B is the Boltzmann constant, T is the absolute temperature, κ describes the inverse Debye-Hückel length, Ψ_{p1} and Ψ_{p2} are the reduced potentials ($\Psi = ze\zeta / k_BT$) of two interacting nano-TiO_2 aggregates, z is the ion valence, e is the electron charge, ε_0 refers to the permittivity of free space, ε_r represents the relative permittivity of water, ξ_p and ξ_c are the surface potentials of the sphere (i.e. nano-TiO_2) and the plate (i.e. collector), respectively, and y denotes the separation distance between two surfaces. Zeta potential measurements were used in place of surface potentials.

The retarded van der Waals interaction energies for the nano-TiO_2–nano-TiO_2 and the nano-TiO_2–Sand systems were calculated utilizing formulas 3 and 4, respectively (Gregory, 1981):

$$\Phi_{VDWNano-TiO_2-Nano-TiO_2} = -\frac{A_{121}a_{p1}a_{p2}}{6y\left(a_{p1}+a_{p2}\right)}\left[1-\frac{5.32y}{\lambda}\ln\left(1+\frac{\lambda}{5.32y}\right)\right] \quad (3)$$

$$\Phi_{VDWNano-TiO_2-Sand} = -\frac{A_{123}a_p}{6y}\left(\frac{1}{1+14\frac{y}{\lambda}}\right) \quad (4)$$

A_{121} and A_{123} denote the Hamaker constants for nano-TiO_2–water–nano-TiO_2 (3.5×10^{-20} J) and nano-TiO_2–water–Sand (1.4×10^{-20} J), respectively (Gomez-Merino et al., 2007; Hu et al., 1997; Jribi et al., 2009), and λ is the characteristic wavelength of the interaction (Gregory, 1981) and it is usually assumed to be 100 nm.

The total interaction energy profiles were only computed for the nano-TiO_2 suspensions in which the nanoaggregates did not significantly increase in size during the delivery of 10 PVs of nanoaggregate suspension into the column. The DLVO theory has a tendency to overestimate the electrostatic double layer and van der Waals interactions due to the Derjaguin approximation (Elimelech et al., 1995). Conversely, the theory also assumes the interaction between two perfectly spherical particles or the interaction of a perfectly spherical particle with a plate; this may not be the case of nano-TiO_2 aggregates since they are not perfect spheres. Thus, caution must be taken when interpreting the results derived from this theory.

4.3.9. Transport Theory

The attachment efficiency between suspended nano-TiO_2 and sand grains ($\alpha_{Nano\text{-}TiO2\text{–}Sand}$) is determined by the physicochemical conditions of the transport experiments and their corresponding column parameters. Tufenkji and Elimelech (2004) defined the expression for attachment efficiency as:

$$\alpha_{Nano-TiO2-Sand} = -\frac{2}{3}\frac{d_c}{(1-f)L\eta_0}\ln\left(\frac{C}{C_0}\right) \quad (5)$$

Here, *dc* represents the collector diameter (i.e. average sand grain diameter), *L* is the length of the filtering porous medium, C/C_0 denotes the ratio between particle effluent concentration and the particle influent concentration, *f* represents the porosity of the porous medium and η_0 is the single-collector contact efficiency given by the sum of the contributions of the individual transport mechanisms such as Brownian diffusion (η_D) interception (η_I) and gravitational sedimentation (η_G). The maximum distance (L_{max}) that particles may travel in saturated porous

media can be estimated as the distance where 99.9% of particles are removed from the pore solution. L_{max} is expressed as follows (Godinez and Darnault, 2011):

$$L_{\max} = -\frac{2}{3} \cdot \frac{d_c}{(1-f)\alpha_{Nano-TiO2-Sand}\eta_0} \ln\left(\frac{C}{C_0}\right) \quad (6)$$

where C/C_0 is 0.01. Table 1 describes the transport parameters for the nano-TiO_2 suspension systems in group one column experiments that maintained constant concentration and stable nanoaggregates size during the pumping of nano-TiO_2 (i.e. 10 PVs) into the porous medium (i.e. No surfactant and 100% CMC SDBS at 0.0011 M and 0.011 M and 100% CMC Triton X-100 at 0.011 M).

Table 1. Group one column experiments: Transport and deposition behavior of the nano-TiO_2 suspensions that adhere to the regulations of the physicochemical filtration theory (Tufenkji and Elimelech, 2004).

Ionic Strength	System	Nano-TiO_2 Diameter	Diffusion Coefficient				Single-Collector Contact Efficiency	Mean Plateau	Attachment Efficiency	Maximum Transport Distance
(M)		d_p (nm)	D_∞ (cm^2/s)	η_D	η_I	η_G	$\eta_0 = \eta_D + \eta_I + \eta_G$	C/C_0	$\alpha_{Nano\text{-}TiO2 - Sand}$	L_{max} (m)
0.0011	No Surfactant	384	1.09E-08	2.62E-03	3.84E-04	1.08E-04	3.11E-03	0.231	0.89	0.47
	100% CMC Triton X-100	355*						0.455		
	100% CMC SDBS	390	1.05E-08	2.54E-03	3.91E-04	1.08E-04	3.04E-03	0.815	0.13	3.37
0.011	No Surfactant	425	9.89E-09	2.42E-03	4.44E-04	1.32E-04	2.99E-03	0.347	0.67	0.65
	100% CMC Triton X-100	413	1.03E-08	2.49E-03	4.27E-04	1.26E-04	3.04E-03	0.537	0.39	1.11
	100% CMC SDBS	386	1.06E-08	2.56E-03	3.86E-04	1.06E-04	3.05E-03	0.421	0.54	0.80
0.11	No Surfactant	916*						0.013		
	100% CMC Triton X-100	765*						0.013		
	100% CMC SDBS	798*						0.031		

*Initial particle diameter (i.e. time = 0 min of aggregation kinetics experiments)

4.3.10. Nano-TiO_2 aggregation kinetics

Nano-TiO_2 aggregation kinetics are computed by recording the increase in hydrodynamic radius $a_h(t)$ with time t as measured by DLS. The rate of increase in hydrodynamic radius (i.e. the slope of the $a_h(t)$ versus time plot as t approaches zero) is linearly proportional to the product of the particle concentration N_0 and the initial aggregation rate constant k_{11} (Mylon et al., 2004; Chen and Elimelech, 2006). Based on this information, the inverse stability ratio ($1/W$) between nano-TiO_2 aggregates, also known as the attachment efficiency $\alpha_{\text{Nano-TiO2–Nano-TiO2}}$, at different ionic strengths and fixed N_0 can be determined from the slopes of plots of aggregation size as a function of time (Mylon et al., 2004; Chen and Elimelech, 2006):

$$\frac{1}{W} = \alpha_{Nano-TiO_2-Nano-TiO_2} = \frac{k_{11}}{(k_{11})_{fast}} = \frac{\left(\frac{da_h(t)}{dt}\right)_{t\to 0}}{\left(\frac{da_h(t)}{dt}\right)_{t\to 0,\, fast}} \qquad (7)$$

The term with the subscript "fast" denotes favorable aggregation conditions, that is, the ionic strength concentration is high enough to vanquish the energy barrier (no electrostatic repulsive interactions between nano-TiO_2 aggregates) resulting in diffusion-limited aggregation (Chen et al., 2006).

4.4. Results and discussion

4.4.1. Stability of nano-TiO_2 in suspension

The aggregation of nano-TiO_2 nanoparticles was studied over a range of ionic strength concentrations (i.e. 0.0011 M, 0.011 M and 0.11 M), pH 9 and the presence of non-ionic and

anionic surfactants (Fig. 1). Pristine TiO_2 nanoparticles (~19 nm, Godinez and Darnault, 2011) underwent aggregation in the different electrolyte solutions. However, upon attaining an initial kinetic stability, the No Surfactant and 100% CMC SDBS systems at 0.0011 M and 0.011 M demonstrated very little further aggregation over a period of 145 min. The aggregation rate measured for the 100% CMC Triton X-100 system at 0.11 M was the maximum for all suspensions utilized in the study. Considering this aggregation regime as diffusion-limited (favorable and fast due to no energy barrier), its corresponding maximum aggregation rate was utilized in equation 1 to determine the lower $\alpha_{Nano\text{-}TiO2–Nano\text{-}TiO2}$ for the remaining nano-TiO_2 suspensions (Table 2).

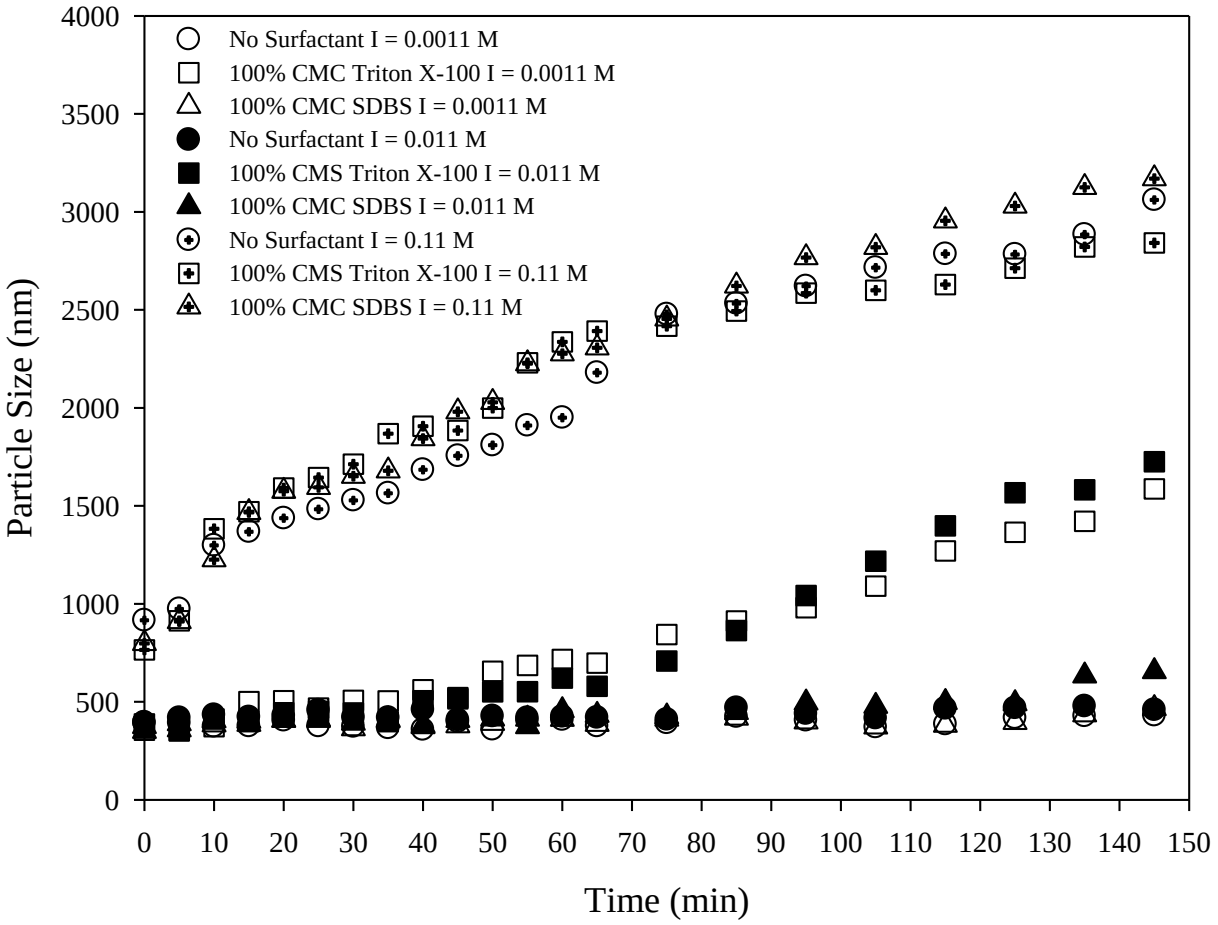

Fig. 1. Aggregation kinetics of nano-TiO_2 at pH 9 in suspension systems at 0.0011 M, 0.011 M and 0.11 M.

Table 2. Experimental parameters from group one column experiments for suspension systems that maintained kinetic stability during the injection of nano-TiO_2: Attachment efficiency between nano-TiO_2–nano-TiO_2 and nano-TiO_2–sand, maximum transport distance (L_{max}) and energy barriers estimated from total interaction energy profiles (flow velocity 9.42 x 10^{-4} m/s, Hamaker constant for nano-TiO_2-water-nano-TiO_2 3.5 x 10^{-20} J (Gomez-Merino et al., 2007) and nano-TiO_2-water-sand 1.4 x 10^{-20} J (Jribi et al., 2009)).

Ionic strength (M)	System	Attachment efficiency		Maximum transport distance	Nano-TiO_2–Sand energy barrier	Nano-TiO_2–Nano-TiO_2 energy barrier
		$\alpha_{Nano\text{-}TiO2–Nano\text{-}TiO2}$[a]	$\alpha_{Nano\text{-}TiO2–Sand}$[b]	L_{max} (m)[c]	(k_BT^f)[d]	(k_BT^f)[e]
0.0011	No Surfactant	0.0094	0.89	0.47	768	241
	100% CMC Triton X-100	0.06				
	100% CMC SDBS	0.0085	0.13	3.37	740	240
0.011	No Surfactant	0.01	0.67	0.65	552	145
	100% CMC Triton X-100	0.06	0.39	1.11	586	140
	100% CMC SDBS	0.03	0.54	0.80	593	150
0.11	No Surfactant	0.39				
	100% CMC Triton X-100	1.00				
	100% CMC SDBS	0.76				

[a] Calculated through Equation (7).
[b] Calculated through Equation (5).
[c] Calculated through Equation (6).
[d] Determined from the total interaction energy profiles for nano-TiO_2–Nano-TiO_2 interactions (Equations 1 and 3).
[e] Determined from the total interaction energy profiles for nano-TiO_2–Sand interactions (Equations 2 and 4).
[f] k_BT is a unit of energy (1 k_BT = 4.07 x 10^{-21} J).

Fig. 2 compares the time-resolved optical absorbency results (i.e. sedimentation) of the nine nano-TiO_2 suspensions. The No Surfactant and 100% CMC Triton X-100 systems at 0.0011 M and 0.11 M represent the upper and lower bounds of the sedimentation rates distribution, respectively. For the first 30 minutes, less than 1% of nano-TiO_2 underwent sedimentation in suspensions at 0.0011 M and 0.011 M. In the case of suspensions at 0.11 M, less than 4% sedimentation was recorded for the same time frame. A comparison between the aggregation kinetics and sedimentation rate patterns demonstrates that in a reaction-limited regime (unfavorable and slow due the presence of an energy barrier) an increase in ionic strength concentration shields the surface charge of the nanoaggregates, thus promoting faster aggregation and sedimentation (Chen et al., 2006; Chen and Elimelech, 2006). The transition from kinetic stability to rapid aggregation, commonly refer to as critical coagulation concentration (CCC), for the No Surfactant, 100% CMC Triton X-100 and 100% CMC SDBS systems take place in the ranges 0.011 M – 0.11 M, 0.0011 M – 0.011 M and 0.011 M – 0.11 M, respectively. The stability of nano-TiO_2 in the presence of Triton X-100 depends on the extent of surface coverage. In the present study it may be inferred that the non-ionic surfactant did not adsorb to the surfaces of the nanoaggregates in at least one layer of micelle structures which counteracted the long term kinetic stability of nano-TiO_2 in suspension at 0.0011 M and 0.011 M (Alexeev et al., 1996; Levitz et al., 1984).

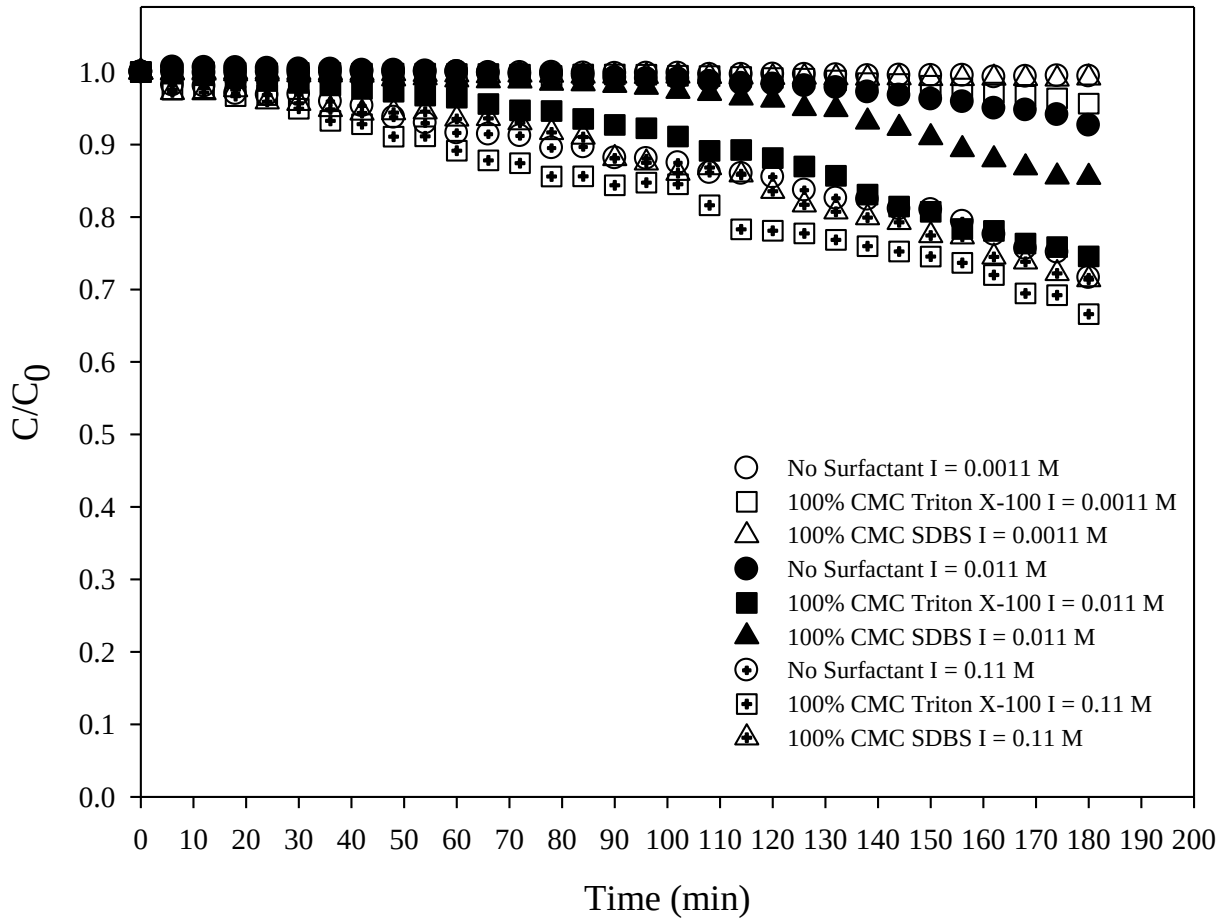

Fig. 2. Sedimentation of nano-TiO_2 at pH 9 in suspension systems at 0.0011 M, 0.011 M and 0.11 M.

Considering that the pumping (i.e. at 9.42 x 10^{-4} m/s) of 10 PVs of nano-TiO_2 into the porous medium took less than 30 min, we can corroborate that the nanoaggregates in the No Surfactant and 100% CMC SDBS systems at 0.0011 M and 0.011 M were delivered at a constant concentration and stable nano-TiO_2 aggregate size. This supports the application of the transport theory for these systems as presented by Tufenkji and Elimelech (2004).

4.4.2. Zeta potential of nano-TiO_2 and sand

The zeta potential measurements of nano-TiO_2 in the different suspensions are presented in Fig. 3 as a function of time. The starting zeta potential values for the suspensions without surfactants at the different ionic strengths are in accordance with experimental data previously published in literature (Liu et. al., 2008; Boncagni et al., 2009). The results illustrate that the zeta potential of nano-TiO_2 is slightly time-dependent, that is, a small reduction in the absolute value of the zeta potential is registered with the progression of time. As the ionic strength increases, this effect is a little more evident. The behavior is similar to that reported elsewhere for electrophoretic mobility (EPM) measurements of TiO_2 nanoparticles in seawater (Keller et al., 2010). An increase in salt concentration causes the compression of the nanoaggregate's diffuse layer, thus the repulsion between nanoaggregates is reduced and the zeta potential of nano-TiO_2 in suspension becomes less negative.

The sand grains' zeta potential values (Fig. 4) ranged from -64.2 to -67.7 mV at 0.0011 M, -55.8 to -62.2 mV at 0.011 M and -52.6 to -53.7 mV at 0.11 M. These readings are typical for SiO_2 particles under the present conditions (Litton and Olson, 1994).

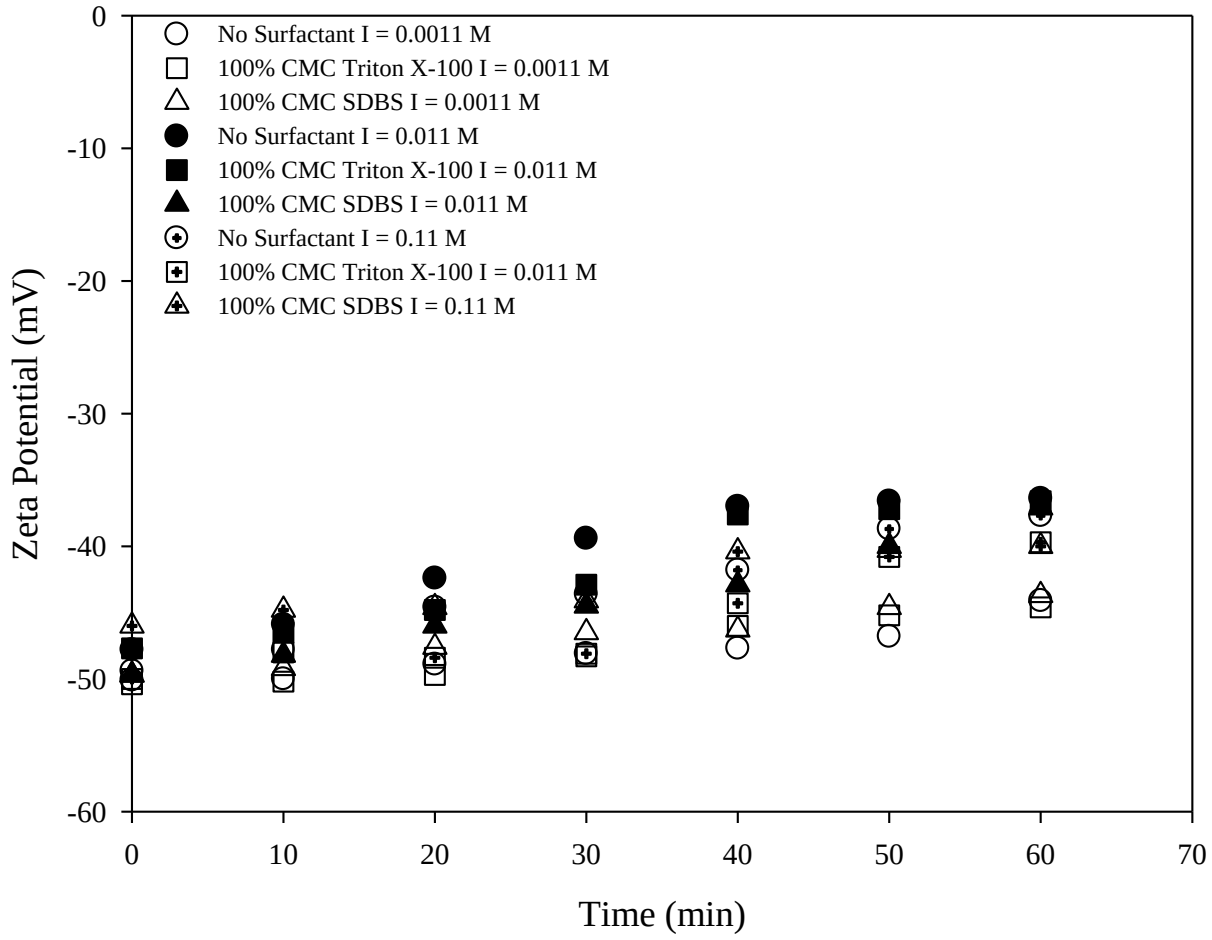

Fig. 3. Zeta potential of nano-TiO_2 at pH 9 in suspension systems at 0.0011 M, 0.011 M and 0.11 M.

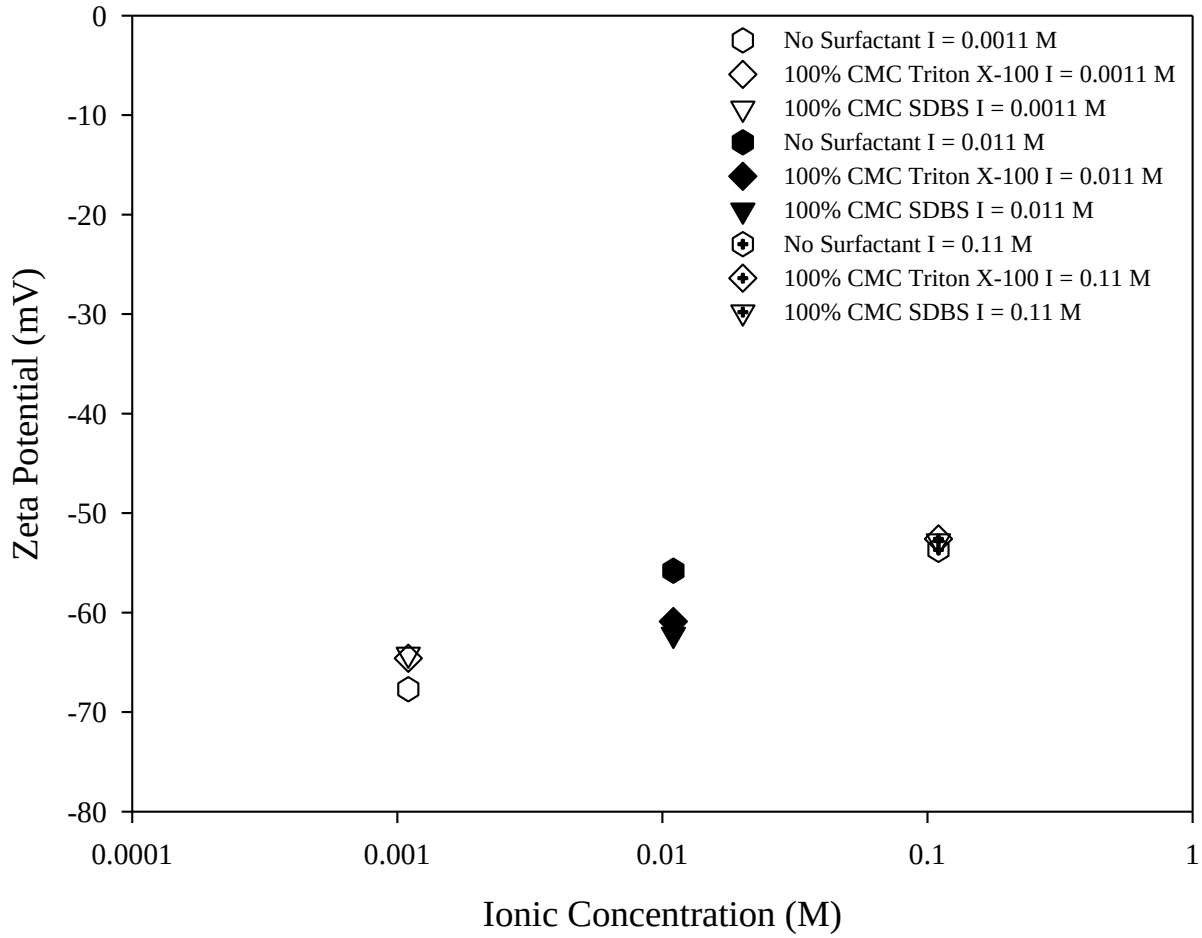

Fig. 4. Zeta potential of silica sand at pH 9 in suspension systems at 0.0011 M, 0.011 M and 0.11 M.

4.4.3. Influence of ionic strength and surfactants on nano-TiO_2 transport

The breakthrough curves (BTCs) of group one experiments are shown in Fig. 5–7. In these figures the normalized nano-TiO_2 concentration in the effluent, C/C_0, is plotted as a function of PV. Each figure includes a BTC for the inert Br^- tracer; it represents the mean of the tracer plots corresponding to the nano-TiO_2 experiments present in the respective figure. At zero PV, the

tracer registered a normalized Br^- concentration of 0.9 or higher. The latter denotes that during the saturation process the porous medium was equilibrated by the background electrolyte solution. The tracer BTCs attained a plateau of approximately 1; this indicates good permeability in the column system.

For the nano-TiO_2 suspensions that demonstrated long term kinetic stability (i.e. No Surfactant and 100% CMC SDBS at 0.0011 M and 0.011 M) the electrolyte-induced aggregation tests reveal that nano-TiO_2 aggregation in the column should be negligible due to low attachment efficiencies between nanoaggregates (Table 2). The deposition of nano-TiO_2 in the column, however, describes interactions between stable nano-TiO_2 and sand grains that are not necessarily in accordance with the DLVO theory. In the case of the No Surfactant system the increase in electrolyte concentration from 0.0011 M (Fig. 5) to 0.011 M (Fig. 6) registered a decrease in attachment efficiency (i.e. $\alpha_{Nano\text{-}TiO2\text{–}Sand}$ 0.89 to 0.67) between nano-TiO_2 and the porous medium. The deviations from the DLVO theory may be attributed to surface charge heterogeneities of sand grains. Previous studies have demonstrated that the surface charge heterogeneities between the collectors have the capacity to control particle deposition behavior under conditions classified as not ideal for retention (e.g. low ionic strength, repelling charge between nanoaggregates and collectors, and low attachment efficiency among nano-TiO_2) (Litton and Olson, 1993, 1994, 1996). Litton and Olson (1994) reported that the presence of neutrally charged and hydrophobic sites on the surfaces of collectors increased colloid deposition rates; these sites were properly concealed by using sodium dodecyl sulfate (SDS) in the electrolyte solutions thus yielding experimental results analogous to those predicted by the DLVO theory. Another possible source of surface charge heterogeneities may be the persistence

of metal oxides on collectors' surfaces, as it is unclear whether all metal oxides were completely eliminated by the washing technique (Litton and Olson, 1993, 1994; Lenhart and Saiers, 2002). Under the pH conditions maintained in the study, if impurities were still present on the surfaces of the collectors, metal oxides may have attained a near-neutral charge or carry a slightly positive charge (Litton and Olson, 1993). This environment is expected to furnish ideal sites for deposition on what in theory is supposed to be a not ideal site since silica at pH 9 is expected to possess a negative charge just as nano-TiO_2 (Litton and Olson, 1994; Boncagni et al., 2009). The 100% CMC SDBS suspensions at 0.0011 M and 0.011 M produced experimental results that are in agreement with the DLVO theory. SDBS is an anionic surfactant with negatively charged molecules that can react with positively charged metal oxide ions through electron attraction, charge neutralization and complexation (Tan et al., 2008; Shao et al., 2010). These properties provided SDBS molecules with the ability to masquerade surface charge heterogeneities of collectors at 0.0011 M. At the low ionic strength (0.0011 M) the affinity of nanoaggregates in 100% CMC SDBS to the collectors was the weakest with less than 18.5% retained in the column corresponding to a $\alpha_{Nano\text{-}TiO2\text{–}Sand}$ of approximately 0.13 and a predicted maximum transport distance through the porous medium of 3.37 m.

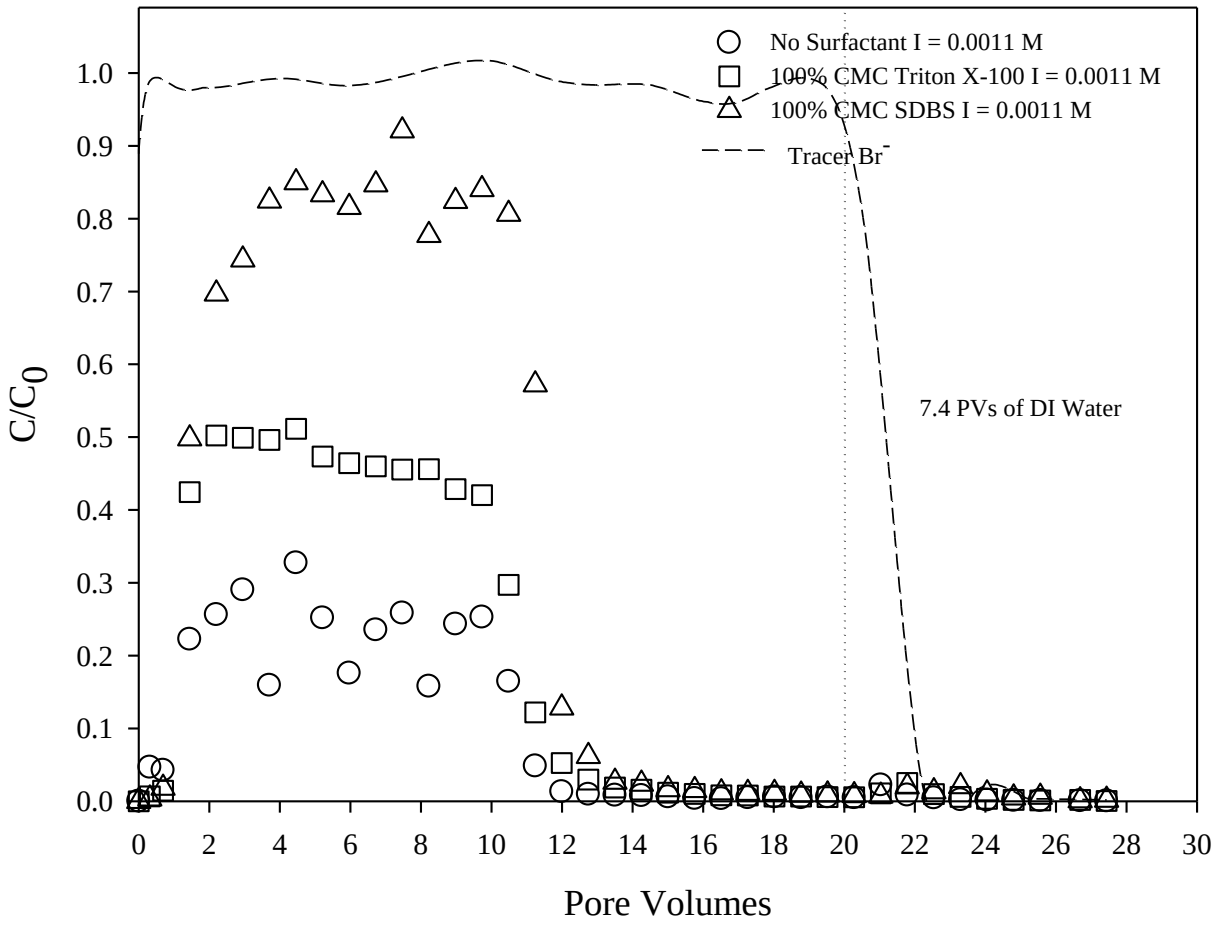

Fig. 5. Group one nano-TiO_2 breakthrough curve experiments at pH 9 and 0.0011 M.

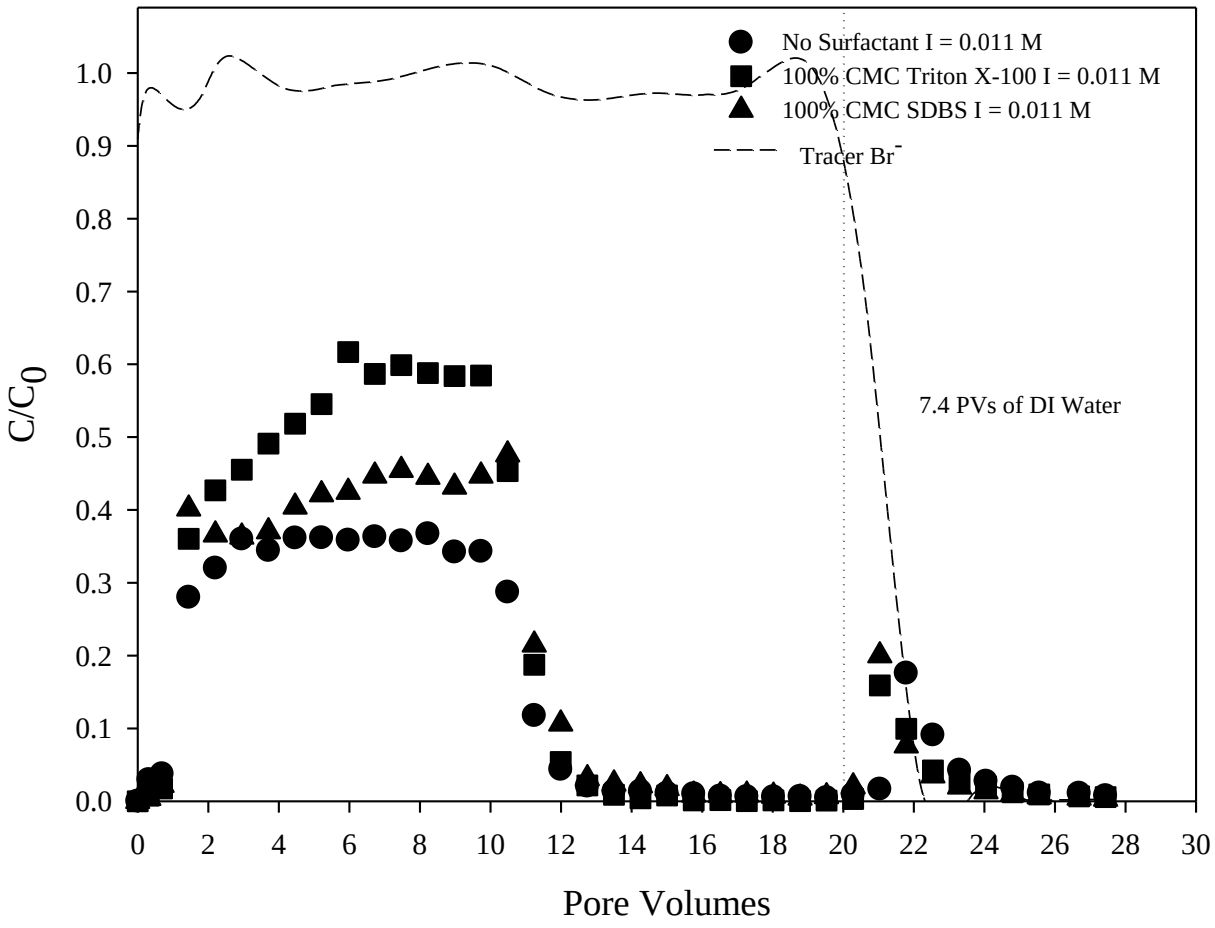

Fig. 6. Group one nano-TiO_2 breakthrough curve experiments at pH 9 and 0.011 M.

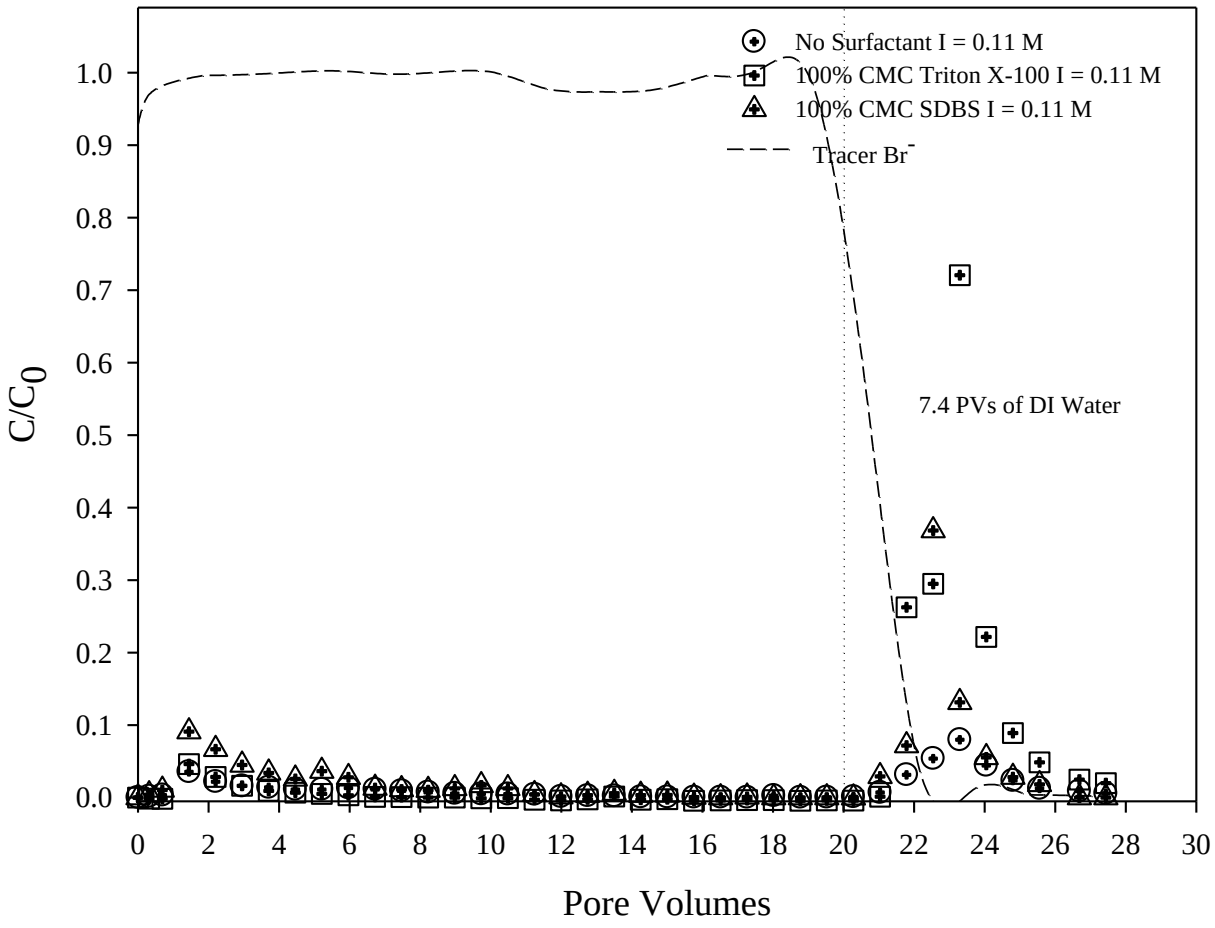

Fig. 7. Group one nano-TiO_2 breakthrough curve experiments at pH 9 and 0.11 M.

The ionic strength had a marked influence on the retention of nano-TiO_2 in the column. As the ionic strength increased from 0.0011 M to 0.11 M, the retention of nanoaggregates in the porous medium increased dramatically reaching more than 96% for all suspension systems at 0.11 M (Fig. 7). The BTC patterns for the suspensions at high ionic strength (0.11 M) are characterized by a gradual but extremely moderate increase in effluent nanoaggregate concentration that lasted for 1.5 PVs. At this point, the BTC patterns displayed a rapid decrease in the mobility of nano-TiO_2. This phenomenon has been observed in deep-bed filtration and colloid studies and is

commonly referred to as filter ripening (Elimelech and O'Melia, 1990; Darby and Lawler, 1990). The improvement in nano-TiO_2 retention in connection with the continuous aggregation of nano-TiO_2 at 0.11 M (i.e. attachment efficiencies between nanoaggregates greater than 0.39 (Table 2)) may indicate that previously deposited nano-TiO_2 served as additional collectors for approaching nanoaggregates.

A comparison between the BTCs for the 100% CMC Triton X-100 systems at low (i.e. 0.0011 M, Fig. 5) and medium (i.e. 0.011 M, Fig. 6) ionic strengths revealed a contrast in the nanoaggregate transport trends. At 0.0011 M this system registered a plateau with a continuous but modest decrease in C/C_0. At 0.011 M the systems depicted a continuous rise in C/C_0 until about the 6^{th} PV which is then followed by a plateau. The difference in BTC trends may rely in the almost instantaneous but moderate increase in aggregate size recorded for the suspension at 0.0011 M whereas the nanoaggregates in the suspension at 0.011 M maintained a kinetic stability for the first 40 min; this was sufficient time for the 10 PVs of nano-TiO_2 suspension to be transported through the column. The 100% CMC Triton X-100 system at 0.011 M may have exhibited a blocking retention mechanism (i.e. decline in deposition rate) as a consequence of reduced availability in attachment sites (e.g. previously deposited nano-TiO_2 or sand surfaces). This behavior is observed until reaching equilibrium between transport and retention of nanoaggregates and is illustrated by a plateau in the BTC. Similar transport and retention of TiO_2 nanoparticles in saturated porous media were found elsewhere at pH 5, variable ionic strength, nanoparticle concentration and flow rate (Chowdhury et al., 2011).

To explore the possible deposition mechanisms responsible for enhanced nano-TiO_2 removal with increasing ionic strength, the results derived from the batch experiments were compared and contrast to those from the column experiments. At low, medium and high ionic strengths the percentages of nano-TiO_2 adsorbed to the porous medium during the dynamic batch experiments (Fig. 8) were 3.21, 2.23, and 52.8 for the No Surfactant suspensions, 12.8, 45.9 and 46.9 for the 100% CMC Triton X-100 suspensions, and 1.64, 7.98 and 22.1 for the 100% CMC SDBS suspensions, respectively. On the contrary, the percentages of nano-TiO_2 retained by the porous medium at low, medium and high ionic strengths for group one column experiments were 76.9, 65.3 and 98.7 for the No Surfactant systems, 54.5, 46.3 and 98.7 for the 100% CMC Triton X-100 systems, and 18.5, 57.9 and 96.9 for the 100% CMC SDBS systems, respectively. The distinct sensitivity of nano-TiO_2 attachment to sand as a result of ionic strength between both types of experiments suggests that the interaction between approaching nano-TiO_2 and nano-TiO_2 that were already deposited onto sand was more favorable for deposition than the interaction between nano-TiO_2 and bare sand surfaces. This point is also supported by the DLVO profiles calculated for interactions between nano-TiO_2 aggregates and nano-TiO_2–Sand (Fig. 9 – 10). The former deposition mechanism was further magnified in column experiments involving nano-TiO_2 suspensions at 0.11 M.

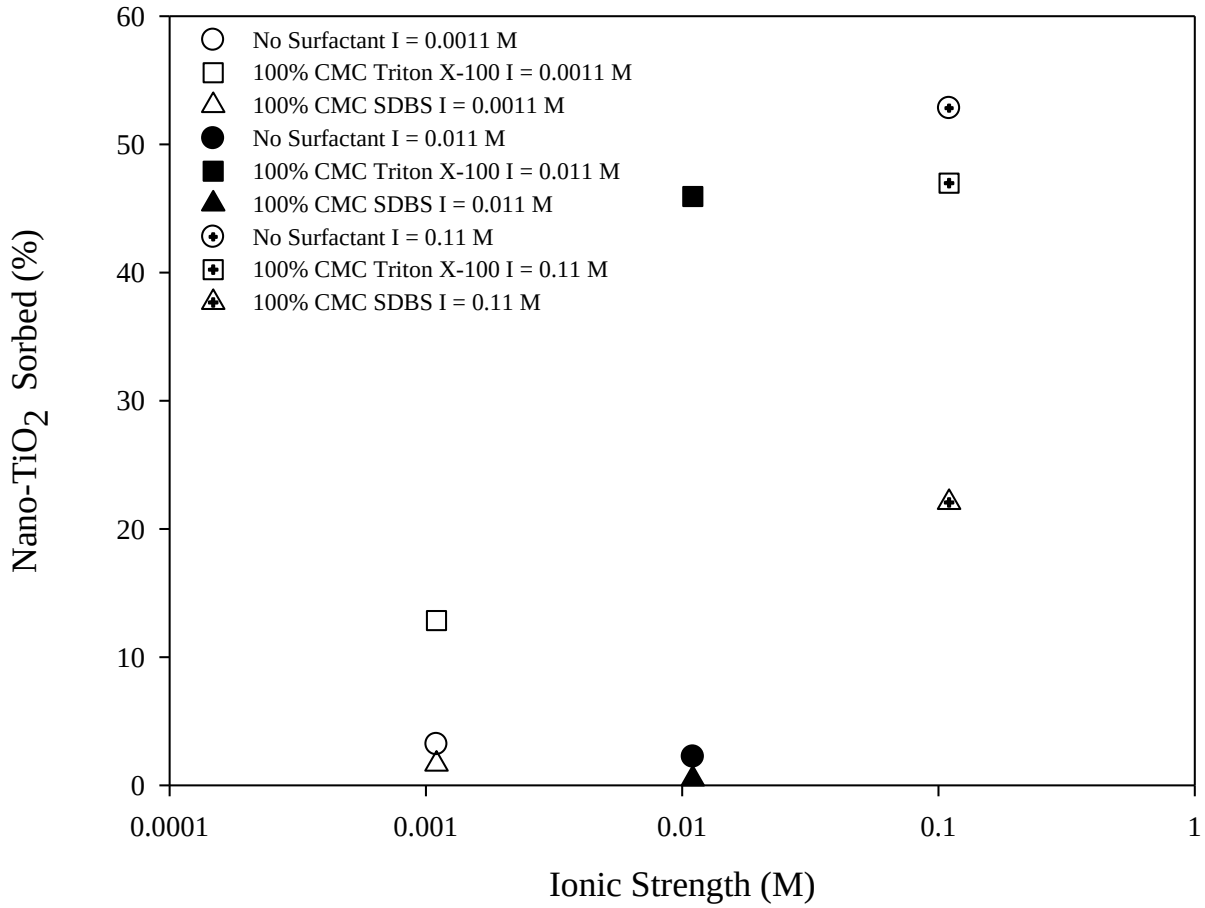

Fig. 8. Percentage of nano-TiO_2 adsorbed to the sand in batch experiments as a function of ionic strength and the presence of surfactants.

Fig. 9 and 10 show the nano-TiO_2–nano-TiO_2 and nano-TiO_2–Sand total interaction energy profiles, respectively. The DLVO profiles computed between nano-TiO_2 aggregates displayed smaller energy barriers than those between nano-TiO_2 and sand; this is a common feature of the mobility and retention of nano-TiO_2 in saturated porous media due to a greater Hamaker constant for nano-TiO_2–water–nano-TiO_2 (3.5×10^{-20} J; Gomez-Merino et al., 2007) compared to that of nano-TiO_2–water–sand (1.4×10^{-20} J; Jribi et al., 2009). Conversely, with increasing ionic strength, the energy barrier patterns for interactions between nanoaggregates decreased faster

than the energy barrier patterns for interactions between nano-TiO_2 and sand. The characteristics of the DLVO profiles in connection with the distinct sensibility of nano-TiO_2 deposition to the porous medium as a function of ionic strength in batch experiments and column experiments corroborate that the deposition of approaching nanoaggregates to nanoaggregates that were already deposited was more propitious. The theoretical and experimental results also suggest that the latter point became more relevant as the ionic strength increased.

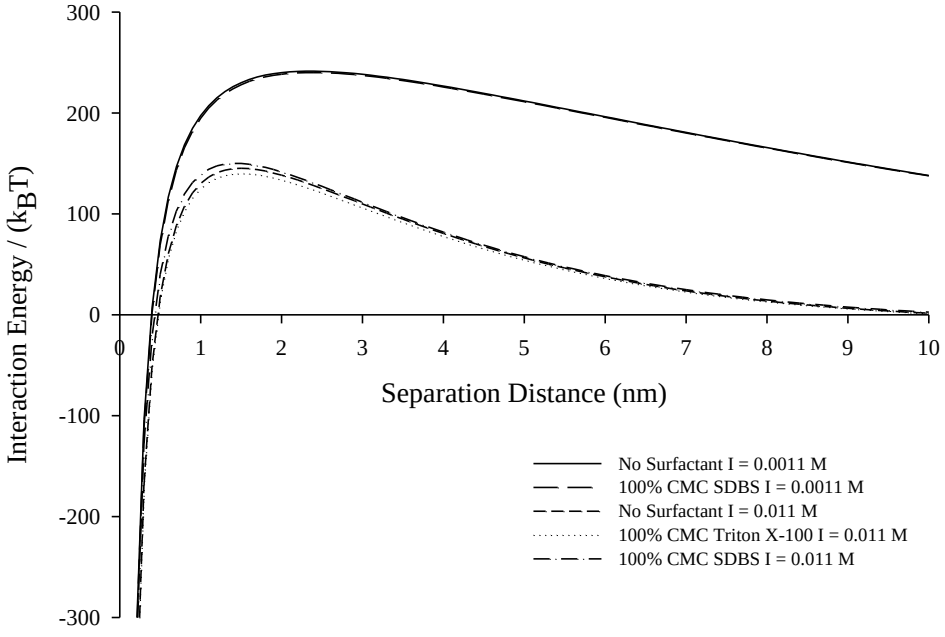

(a)

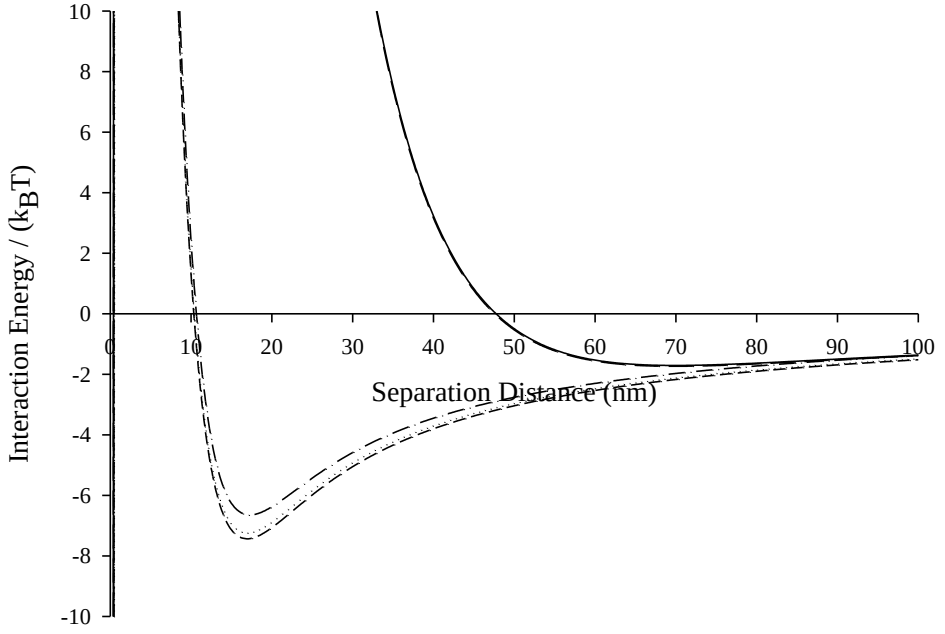

(b)

Fig. 9. Computed nano-TiO_2–nano-TiO_2 interaction energy profiles for suspension systems at ionic strengths 0.0011 M and 0.011 M and pH 9; (a) interaction energy barriers and (b) secondary energy minimum wells. Interaction energies were calculated by use of the starting zeta potentials and mean nanoaggregate diameters displayed in Fig. 3 and Table 1, respectively.

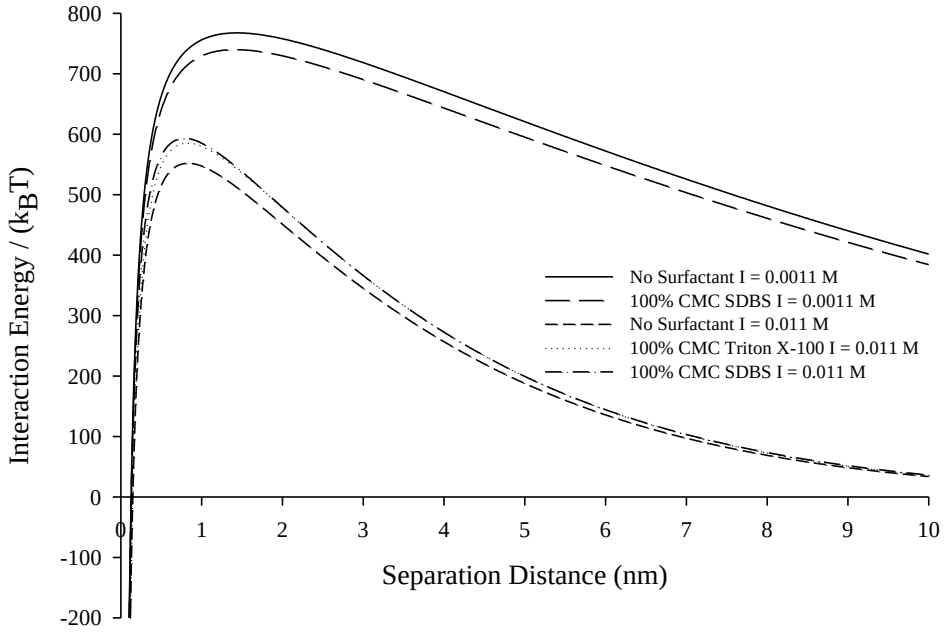

(a)

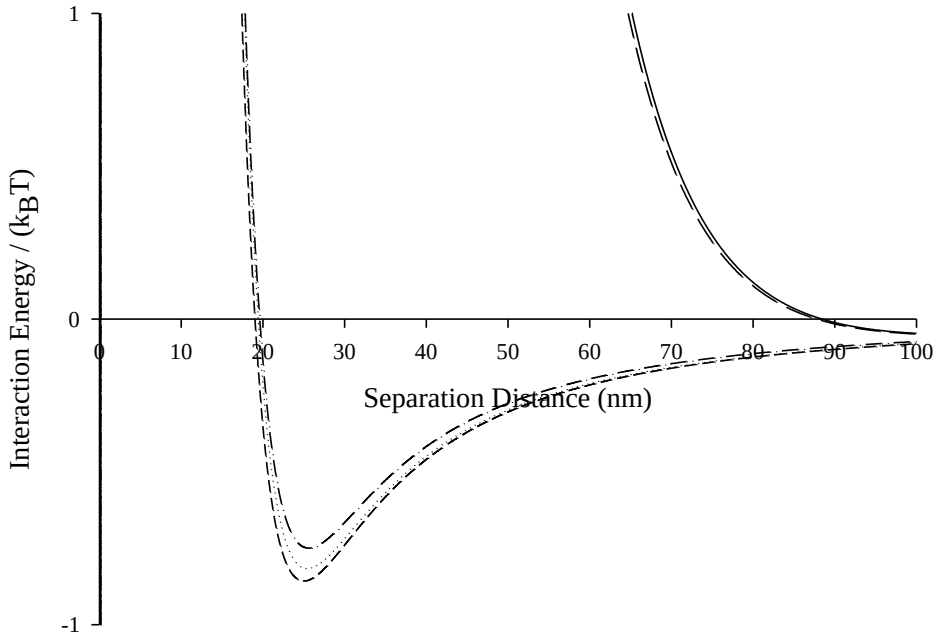

(b)

Fig. 10. Computed nano-TiO_2–Sand interaction energy profiles for suspension systems at ionic strengths 0.0011 M and 0.011 M and pH 9; (a) interaction energy barriers and (b) secondary energy minimum wells. Interaction energies were calculated by use of the starting zeta potentials and mean nanoaggregate diameters displayed in Fig. 3 – 4 and Table 1, respectively.

The repulsive forces (e.g. steric) required to stabilize nanoaggregates in suspension against van der Waals attractive interactions at high ionic strengths are derived from the adsorption of large molecular weight polyelectrolytes or naturally occurring organic macromolecules (Espinasse et al., 2007; Saleh et al., 2008). Triton X-100 (molecular weight 625 g/mole) and SDBS (molecular weight 348.48 g/mole) are classified as small molecules to render consequential electrosteric repulsion forces. In this study, it is believed that the adsorption of Triton X-100 onto nanoaggregates was not entirely successful due to the continuous aggregation of nano-TiO_2 in suspension (Alexeev et al., 1996; Levitz et al., 1984). The anionic surfactant, SDBS, was the only surface active agent capable of providing some degree of electrosteric repulsion to nano-TiO_2 as demonstrated by the enhanced stability of nanoaggregates in suspension at 0.0011 M and 0.011 M. The presence of Triton X-100 and SDBS did not counteract the effects of electrolyte concentration at 0.11 M.

4.4.4. Release of previously deposited nano-TiO_2

Group one column experiments displayed a "flushing peak" in the BTC patters for all nano-TiO_2 suspensions as the porous medium in the column was flushed with DI water. The total interaction energy profiles for interactions between nanoaggregates illustrate secondary energy wells for the suspension systems that demonstrated long term kinetic stability. At low and medium ionic strengths the depths of the wells are predicted to be 1.71 k_BT and 7.44 k_BT for the No Surfactant, and 1.74 k_BT and 6.65 k_BT for 100% CMC SDBS, respectively. The corresponding DLVO profile for the 100% CMC Triton X-100 at 0.011 M displayed a secondary energy well of 7.24 k_BT. The BTCs for these systems (Fig. 5–6) indicate that during the flushing cycle with DI water

nano-TiO_2 attached to nano-TiO_2 by the secondary energy minimum were released and reincorporated into the pore flow. Particles deposited in the secondary energy minimum may be released by vanquishing the energy barrier with electrolyte solution at a very low ion concentration (Franchi and O'Melia, 2003; Hahn and O'Melia 2004). For the nano-TiO_2 suspensions at 0.11 M, their aggregation kinetics and filter ripening during the column experiments may have created flocs of nano-TiO_2 aggregates at different points in the porous matrix; these were subsequently disturbed and reduced to smaller nanoaggregate flocs that were reintroduced into the hydrodynamic flow during the flushing with DI water.

The second group of column transport experiments at medium ionic strength (0.011 M, Fig. 11) demonstrated that by gradually decreasing the electrolyte concentration during the flushing cycles less nano-TiO_2 will be released into the hydrodynamic flow (see Table 4). During the third (i.e. 10 PVs of 0.0011 M electrolytes solution) and fourth (i.e. 10 PVs of DI water) flushing cycles of the No Surfactant transport experiment, 1.47% and 1.55% of nanoaggregates were released from the column (Table 4), respectively. This corresponds to about 8% of the total transport recovery for the No Surfactant system. Conversely, the third and fourth flushing cycles of the 100% CMC SDBS system yielded a transport recovery of 0.43% and 1.18%, respectively. This suggests that only 3.6% of the total transport recovery was the result of nano-TiO_2 detachment from the column system. During the flushing cycles, the release of nano-TiO_2 was not successful for the 100% CMC Triton X-100. Therefore, to release nano-TiO_2 previously deposited onto other nano-TiO_2 through the secondary energy minimum, sufficient reduction in electrolyte concentration must exist to eliminate the deep well and release the nanoaggregate. The nanoaggregates in suspensions at 0.011 M may not formulate vast nano-TiO_2 deposits in the

porous matrix because of good kinetic stability that renders small attachment efficiencies between nanoaggregates. In the case of the second group of column experiments at high ionic strength (0.11 M, Fig. 12), the gradual decrease in salt concentration recorded both a greater (No Surfactant) and a smaller (100% CMC Triton X-100 and 100% CMC SDBS) release of nano-TiO_2 compared to the first group of experiments (Fig. 7, Table 3 – 4). For the second group of column experiments at 0.11 M, the No Surfactant, 100% CMC Triton X-100 and 100% CMC SDBS released 16.1%, 6.2% and 3.9% nanoaggregates, respectively, as a result of the flushing cycles. This represents 96%, 91% and 55% of the total transport recovery for the No Surfactant, 100% CMC Triton X-100 and 100% CMC SDBS systems, respectively. In the absence of surfactants and at high ionic strength the release of nano-TiO_2 seems to have been more effective by gradually reducing the electrolyte concentration. This may be explained by a dual detachment process of nano-TiO_2 from the porous system, that is, nano-TiO_2 release from floc formations and nano-TiO_2 release from sand surfaces. The No Surfactant suspension registered the greatest nanoaggregates adsorption to silica sand in the batch experiments.

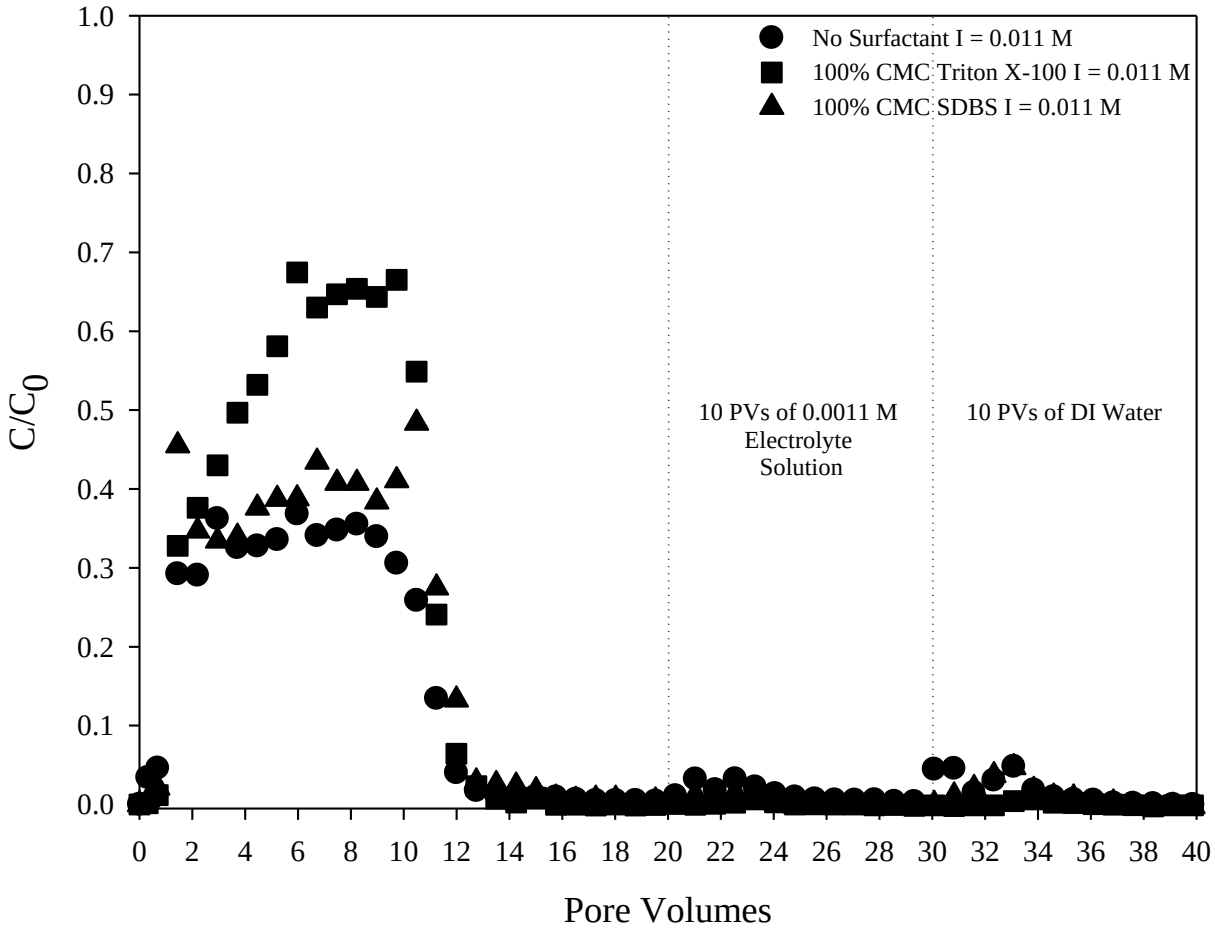

Fig. 11. Group two nano-TiO_2 breakthrough curve experiments at pH 9 and 0.011 M.

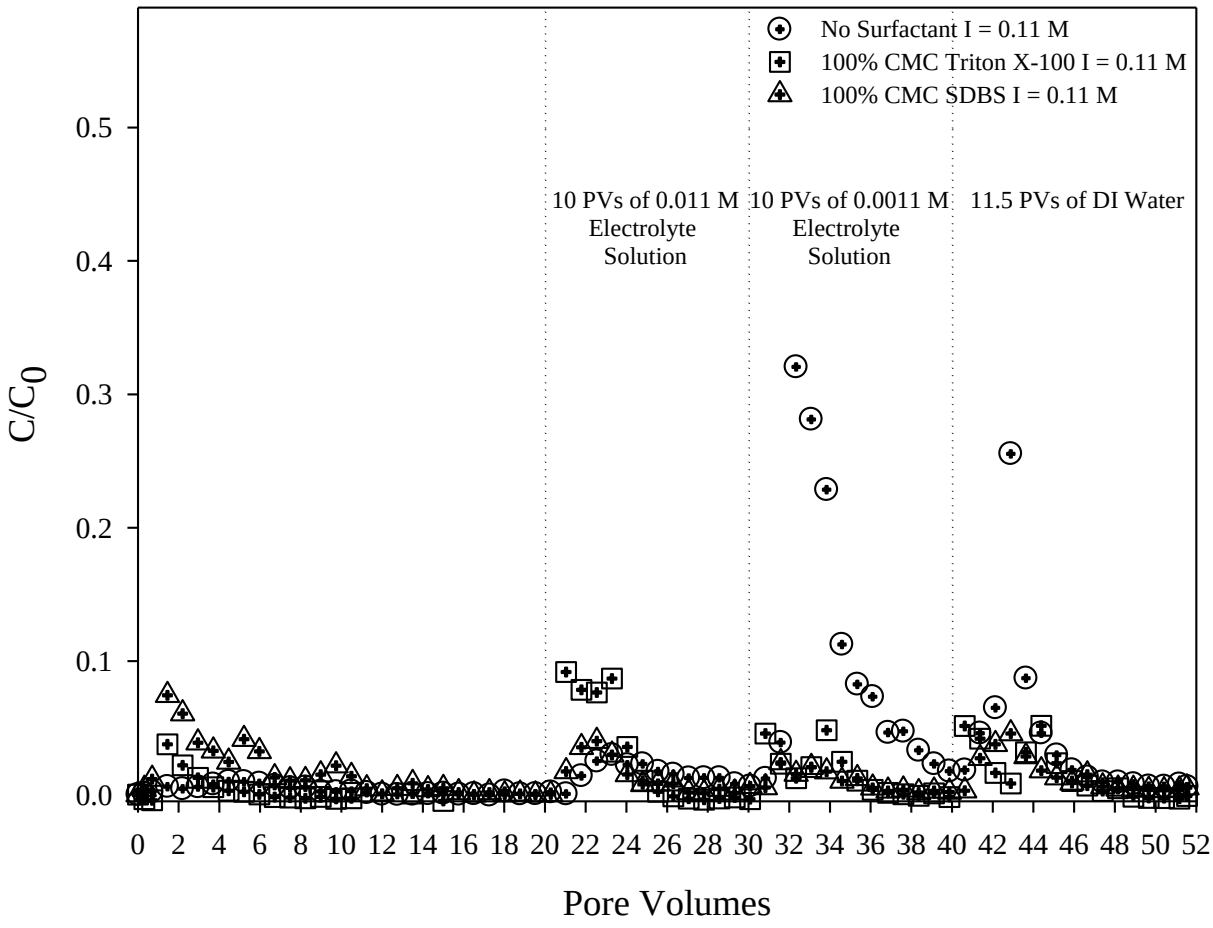

Fig. 12. Group two nano-TiO_2 breakthrough curve experiments at pH 9 and 0.11 M.

Table 3. Group one column experiments: Nano-TiO_2 transport recovery as a function of pore volume.

Location as a Function of PV	Transport Recovery (%)								
	I = 0.0011M			I = 0.011 M			I = 0.11M		
	No Surfactant	100% CMC Triton X-100	100% CMC SDBS	No Surfactant	100% CMC Triton X-100	100% CMC SDBS	No Surfactant	100% CMC Triton X-100	100% CMC SDBS
0 – 20	23.1	45.5	81.5	34.7	53.7	42.1	1.30	1.30	3.10
20 - 27.4	0.37	0.52	0.73	3.12	2.92	2.95	2.04	12.7	5.32
Total	23.5	46.0	82.2	37.8	56.6	45.1	3.3	14.0	8.4

Table 4. Group two column experiments: Nano-TiO_2 transport recovery as a function of pore volume.

Location as a Function of PV	Transport Recovery (%)					
	I = 0.011 M			I = 0.11M		
	No Surfactant	100% CMC Triton X-100	100% CMC SDBS	No Surfactant	100% CMC Triton X-100	100% CMC SDBS
0 – 20	34.4	57.0	43.0	0.64	0.63	3.24
20 – 30	1.47	0.10	0.43	1.49	2.88	1.30
30 – 40	1.55	0.12	1.18	10.0	1.63	0.95
40 - 51.5				4.64	1.68	1.65
Total	37.4	57.2	44.6	16.8	6.81	7.14

CHAPTER V. CONCLUSION

Whether titanium dioxide nanoparticles resist attachment and travel long distances or accumulate onto porous media, part of the balance between free aggregation and deposition will be governed by the tendency of nano-TiO_2 to maintain stable in suspension. The effects of solution chemistry demonstrated that as the pH of the suspension came near the point of zero charge (pH_{pzc}) of titanium dioxide (i.e. pH_{pzc} ~ 6.7 – 7.0) the size of nano-TiO_2 aggregates increased. As the pH of the suspensions came close to the pH_{pzc}, the surface ionization of the nanoparticles was suppressed, limiting the repulsive forces among nanoparticles and allowing for aggregate formation which induced an increase in the nanoparticles deposition rate coefficients. As the pH the suspensions increases, nano-TiO_2 attained better stability. The presence and concentration of surface active agents such as Triton X-100 (non-ionic) and SDBS (anionic) in suspensions under similar ionic strength and pH enhanced the overall mobility of nano-TiO_2 through the porous medium. The electrostatic and steric repulsion forces generated by solution chemistry in combination with an increase in hydrodynamic flow also favored the transport of nano-TiO_2 through the porous matrix.

The increase in electrolyte concentration induced an increase in nanoparticle aggregation that resulted in filter ripening of nano-TiO_2 in the porous medium. Under conditions in which the attachment efficiency between nanoaggregates prevailed (i.e. favorable) over the attachment efficiency between nanoaggregates and collectors, previously deposited nano-TiO_2 served as preferential sites for subsequent deposition. This had the potential to induce nano-TiO_2 to nano-TiO_2 deposition through secondary energy minimum at low and medium ionic strengths as well

as to create deposits of nanoaggregates at high ionic strength that were altered (i.e. part of the nanoaggregates detached and cleared out from the porous matrix) upon abrupt or gradual reductions in the electrolyte concentration of the solutions utilized to flush the saturated porous medium. These points must be properly addressed when assessing the fate and transport of engineered NPs in subsurface environments. In particular because the complexity of physicochemical parameters in aquifer systems (i.e. natural organic matter, monovalent and divalent ions, soil pH and hydrodynamic flow) may enhance the attachment-detachment process of nano-TiO_2 thus contributing to their mobility through the porous media.

CITED LITERATURE

Abu-Zreig, M., Rudra, R.P., Dickinson, W.T., 2003. Effect of application of surfactants on hydraulic properties of soils. Biosystems Engineering 84 (3), 363-372.

Adak, A., Bandyopadhyay, M., Pal, A., 2005. Removal of anionic surfactant from wastewater by alumina: A case study. Colloids and Surfaces A, Physicochemical and Engineering Aspects 254 (1-3), 165–171.

Adams, L.K., Lyon, D.Y., Alvarez, P.J.J., 2006. Comparative eco-toxicity of nanoscale TiO_2, SiO_2, and ZnO water suspensions. Water Research 40 (19), 3527-3532.

Akbour, R.A., Douch, J., Hamdani, M., Schmitz, P., 2002. Transport of kaolinite colloids through quartz sand: Influence of humic acid, Ca^{2+} and trace metals. Journal of Colloid and Interface Science 253(1), 1–8.

Alexeev, V.L., Ilekti, P., Persello, J., Lambard, J., Gulik, T., Cabane, B., 1996. Dispersions of silica particles in surfactant phases. Langmuir 12 (10), 2392–2401.

Amirbahman, A., Olson, T.M., 1995. Deposition kinetics of humic matter-coated hematite in porous-media in the presence of Ca^{2+}. Colloids and Surfaces. A, Physical and Engineering Aspects 99(1), 1–10.

Andrievski, R.A., Glezer, A.M., 2001. Size effects in properties of nanomaterials. Scripta Materialia 44 (8–9), 1621–1624.

Antoniou, M.G., Nicolaou, P.A., Shoemaker, J.A., de la Cruz, A.A., Dionysiou, D.D., 2009. Impact of the morphological properties of thin TiO_2 photocatalytic films on the detoxification of water contaminated with the cyanotoxin, microcystin-LR. Applied Catalysis B: Environmental 91 (1-2), 165-173.

Arbogast, J.W., Darmanyan, A.P., Foote, C.S., Rubin, Y., Diederich, F.N., Alvarez, M.M., Anz, S.J., Whetten, R.L., 1991. Photophysical properties of C60. Journal of Physical Chemistry 95 (1), 11–12.

Aruoja, V., Dubourguier, H.C., Kasemets, K., Kahru, A., 2009. Toxicity of nanoparticles of CuO, ZnO and TiO_2 to microalgae Pseudokirchneriella subcapitata. Science of the Total Environment 407 (4), 1461-1468.

ASTM Standard D 2434 – 68, 2006. "Standard Test Method for Permeability of Granular Soils (Constant Head)." ASTM International, West Conshohocken, PA, 2006, DOI: 10.1520/D2434-68R06, www.astm.org.

Bavykin, D.V., Friedrich, J.M., Walsh, F.C., 2006. Protonated titanates and TiO_2 nanostructured materials: Synthesis, properties, and applications. Advanced Materials 18 (21), 2807–2824.

Bettoni, M., Brinchi, L., Del Giacco, T., Germani, R., Meniconi, S., Rol, C., Sebastiani, G.V., 2012. Surfactant effect on titanium dioxide photosensitized oxidation of 4-dodedyloxybenzyl alcohol. Journal of Photochemistry and Photobiology A: Chemistry 229 (1), 53–59.

Bhattacharjee, S., Elimelech, M., 1997. Surface element integration: a novel technique for evaluation of DLVO interaction between a particle and a flat plate. Journal of Colloid and Interface Science 193 (2), 273–285.

Biju, V., Itoh, T., Anas, A., Sujith, A., Ishikawa, M., 2008. Semiconductor quantum dots and metal nanoparticles: Syntheses, optical properties, and biological applications. Analytical and Bioanalytical Chemistry 391 (7), 2469–2495.

Boiko, N., Zhu, X.M., Bobrovsky, A., Shibaev, V., 2001. First photosensitive liquid crystalline dendrimer: Synthesis, phase behavior, and photochemical properties. Chemistry of Materials 13 (5), 1447–1452.

Boncagni, N.T., Otaegui, J.M., Warner, E., Curran, T., Ren, J., Fidalgo de Cortalezzi, M.M., 2009. Exchange of TiO_2 nanoparticles between streams and streambeds. Environmental Science & Technology 43 (30), 7699–7705.

Bosman, A.W., Janssen, H.M., Meijer, E.W., 1999. About dendrimers: Structure, physical properties, and applications. Chemical Review 99 (7), 1665–1688.

Botta, C., Labille, J., Auffan, M., Borschneck, D., Miche, H., Cabie, M., Mason, A., Rose, J., Bottero, J.Y., 2011. TiO_2-based nanoparticles released in water from commercialized sunscreens in a life-cycle perspective: Structures and quantities. Environmental Pollution 159 (6), 1543–1550.

Bradford, S.A., Simunek, J., Bettahar, M., van Genuchten, M., Yates, S.R., 2003. Modeling colloid attachment, straining, and exclusion in saturated porous media. Environmental Science & Technology 37 (10), 2242–2250.

Bradford, S.A., Yates, S.R., Bettahar, M., Simunek, J., 2002. Physical factors affecting the transport and fate of colloids in saturated porous media. Water Resources Research 38 (12), 1327–1338.

Brant, J., Labille, J., Bottero, J.Y., Wiesner, M.R., 2007. Nanoparticle transport, aggregation, and deposition, in Environmental Nanotechnology, edited by Wiesner, M.R. and Bottero, J.Y. pp. 231-294, McGraw-Hill, New York, NY, USA.

Brown, D.G., Jaffe, P.R., 2001. Effects of nonionic surfactants on bacterial transport through porous media. Environmental Science & Technology 35 (19), 3877-3883.

Campbell, C.T., Parker, S.C., Starr, D.E., 2002. The effect of size-dependent nanoparticle energetics on catalyst sintering. Science 298 (5594), 811–814.

Chen, G., Liu, X., Su, C., 2011. Transport and retention of TiO_2 rutile nanoparticles in saturated porous media under low-ionic-strength conditions: Measurements and mechanisms. Langmuir 27 (9) 5393–5402.

Chen, G., Liu, X., Su, C., 2012. Distinct effects of humic acid on transport and retention of TiO_2 rutile nanoparticles in saturated sand columns. Environmental Science & Technology 46 (13), 7142–7150.

Chen, K.L., Elimelech, M., 2006. Aggregation and deposition kinetics of fullerene (C60) nanoparticles. Langmuir 22 (26), 10994–11001.

Chen, K.L., Elimelech, M., 2007. Influence of humic acid on the aggregation kinetics of fullerene (C_{60}) nanoparticles in monovalent and divalent electrolyte solutions. Journal of Colloid and Interface Science 309 (1), 126–134.

Chen, K.L., Mylon, S.E., Elimelech, M., 2006. Aggregation kinetics of alginate-coated hematite nanoparticles in monovalent and divalent electrolytes. Environmental Science & Technology 40(5), 1516–1523.

Chen, X., Mao, S.S., 2007. Titanium dioxide nanomaterials: Synthesis, properties, modifications, and applications. Chemical Review 107 (7), 2891–2959.

Cheng, X., Kan, A.T., Tomson, M.B., 2004. Naphthalene adsorption and desorption from aqueous C_{60} fullerene. Journal of Chemical and Engineering Data 49 (3), 675–683.

Cheng, X.K, Kan, A.T., Tomson, M.B., 2005. Study of C-60 transport in porous media and the effect of sorbed C-60 on naphthalene transport. Journal of Material Research 20 (12), 3244-3254.

Chowdhury, I., Hong, Y., Honda, R.J., Walker, S.L., 2011. Mechanisms of TiO_2 nanoparticle transport in porous media: Role of solution chemistry, nanoparticle concentration and flow rate. Journal of Colloid and Interface Science 360 (2), 548–555.

Comba, S., Di Molfetta, A., Sethi, R., 2011. A comparison between field applications of nano-, micro-, and millimetric zero-valent iron for the remediation of contaminated aquifers. Water Air and Soil Pollution 215 (1–4), 595–607.

Cullity, B.D., Stock, S.R., 2001. Elements of X-Ray Diffraction, third ed., Prentice Hall, New Jersey.

Dai, H.J., 2002. Carbon nanotubes: Synthesis, integration, and properties. Accounts of Chemical Research 35 (12), 1035–1044.

Danielson, R.E., Sutherland, P.L., 1986. Porosity, in: Klute, A. (ed.), Methods of soil analysis. Part 1. Physical and mineralogical methods 2nd ed. Agron. Monogr. 9. ASA and SSSA, Madison, WI, p. 443-461.

Darby, J.L., Lawler, D.F., 1990. Ripening in depth filtration: Effect of particle size on removal and head loss. Environmental Science and Technology 24 (7), 1069–1079.

Darlington, T.K., Neigh, A.M., Spencer, M.T., Nguyen, O.T., Oldenburg, S.J., 2009. Nanoparticle characteristics affecting environmental fate and transport through soil. Environmental Toxicology and Chemistry 28 (6), 1191-1199.

Davis, S.N., de Wiest, R.J.M., 1966. Hydrogeology, Wiley, New York.

Denison, A.B., Hope-Weeks, L.J., Meulenberg, R.W., Terminello, L.J., 2004. Quantum Dots. In *Introduction to Nanoscale Science and Technology* (De Ventra, M., Evoy, S. and Heflin, J.R., Eds.). Springer, New York, pp. 183–198.

Derjaguin, B.V., Landau, L.D., 1941. Theory of the stability of strongly charged lyophobic sols and of the adhesion of strongly charged particles in solutions of electrolytes. Acta Physicochim. URSS 14, 633–662.

Deshiikan, S.R., Eschenazi, E., Papadopoulos, K.D., 1998. Transport of colloids through porous beds in the presence of natural organic matter. Colloids and Surfaces. A, Physical and Engineering Aspects 145, 93–100.

Dorn, H.C., Duchamp, J.C., 2004. Fullerenes. In *Introduction to Nanoscale Science and Technology* (De Ventra, M., Evoy, S. and Heflin, J.R., Eds.). Springer, New York, pp. 119–135.

Elimelech, M., Gregory, J., Jia, X., Williams, R.A., 1995. Particle deposition and aggregation: Measurement, modeling and simulation. Butterworth–HeinemannLtd, Oxford.

Elimelech, M., O'Melia, C.R., 1990. Kinetics of deposition of colloidal particles in porous-media. Environmental Science and Technology 24 (10), 1528–1536.

Espinasse, B., Hotze, E.M., Wiesner, M.R., 2007. Transport and retention of colloidal aggregates of C_{60} in porous media: Effects of organic macromolecules, ionic composition, and preparation method. Environmental Science and Technology 41 (21), 7396–7402.

Fang, J., Shan, X.Q., Wen, B., Lin, J.M., Owens, G., 2009. Stability of titania nanoparticles in soil suspensions and transport in saturated homogeneous soil columns. Environmental Pollution 157 (4), 1101-1109.

Fatisson, J., Domingos, R.F., Wilkinson, K.J., Tufenkji, N., 2009. Deposition of TiO_2 nanoparticles onto silica measured using a quartz crystal microbalance with dissipation monitoring. Langmuir 25 (11), 6062–6069.

Feuston, B.P., Andreoni, W., Parrinello, M., Clementi, E., 1991. Electronic and vibrational properties of C60 at finite temperature from abinitio molecular-dynamics. Physical Review B 44 (8), 4056–4059.

Fiorino, D.J., 2010. PEN 19 – Voluntary initiatives, regulation, and nanotechnology oversight: Charting a path. Woodrow Wilson International Center for Scholars, *Project on Emerging Nanotechnologies.*

Fowler, P.W., Manolopoulos, D.E., 2006. An Atlas of Fullerenes. Dover Publications Inc., New York, USA.

Franchi, A., O'Melia, C.R., 2003. Effects of natural organic matter and solution chemistry on the deposition and reentrainment of colloids in porous media. Environmental Science & Technology 37 (6), 1122–1129.

French, R.A., Jacobson, A.R., Kim, B., Isley, S.L., Penn, R.L., Baveye, P.C., 2009. Influence of ionic strength, pH, and cation valence on aggregation kinetics of titanium dioxide nanoparticles. Environmental Science and Technology 43 (5), 1354-1359.

Fuchs, S., Kapp, T., Otto, H., Schoneberg, T., Franke, P., Gust, R., Schluter, A.D., 2004. A surface-modified dendrimer set for potential application as drug delivery vehicles: Synthesis, in vitro toxicity, and intracellular localization. Chemistry-A European Journal 10 (5), 1167–1192.

Godinez, I.G., Darnault, J.G.C., 2011. Aggregation and transport of nano-TiO_2 in saturated porous media: Effects of pH, surfactants and flow velocity. Water Research 45 (2), 839–851.

Gomez-Merino, A.I., Rubio-Hernandez, F.J., Velazquez-Navarro, J.F., Galindo-Rosales, F.J., Fortes-Quesada, P., 2007. The Hamaker constant of anatase aqueous suspensions. Journal of Colloid Interface Science 316 (2), 451–456.

Gregory, J. 1981. Approximate expressions for the retarded van der Waals interaction. Journal of Colloid and Interface Science 83 (1), 138–145.

Guzman, K.A.D., Finnegan, M.P., Banfield, J.F., 2006. Influence of surface potential on aggregation and transport of titania nanoparticles. Environmental Science and Technology 40 (24), 7688–7693.

Hahn, M.W., Abadzic, D., O'Melia, C.R., 2004. Aquasols: on the role of secondary minima. Environmental Science & Technology 38 (22), 5915–5924.

Hahn, M.W., O'Melia, C.R., 2004. Deposition and reentrainment of brownian particles in porous media under unfavorable chemical conditions: Some concepts and applications. Environmental Science & Technology 38 (1), 210–220.

He, F., Zhang, M., Qian, T.W., Zhao, D.Y., 2009. Transport of carboxymethyl cellulose stabilized iron nanoparticles in porous media: Column experiments and modeling. Journal of Colloids and Interface Science 334 (1), 96-102.

Hirtzel, C.S., Rajagopalan, R., 1985. Colloidal Phenomena: Advanced Topics, Noyes Publications, New Jersey.

Hoffmann, M.R., Martin, S.T., Choi, W.Y., Bahnemann, D.W., 1995. Environmental applications of semiconductor photocatalysis. Chemical Reviews 95 (1), 69-96.

Hogg, R., Healy, T.W., Fuerstenau, D.W., 1966. Mutual coagulation of colloidal dispersions. Transactions of Faraday Society 62, 1638–1651.

Holtz, R.D., Kovacs, W.D., 1981. An Introduction to Geotechnical Engineering, Prentice Hall, New Jersey.

Hong, R., Han, G., Fernandez, J.M., Kim, B.J., Forbes, N.S., Rotillo, V.M., 2006. Glutathione-mediated delivery and release using monolayer protected nanoparticle carriers. Journal of the American Chemical Society 128 (4), 1078–1079.

Hu, K., Fe-Ren, F., Bard, A.J., Hillier, A.C., 1997. Direct measurement of diffuse double-layer forces at the semiconductor/electrolyte interface using an atomic force microscope. Journal of Physical Chemistry B 101 (41), 8298–8303.

Hutchings, G.J., 2005. Catalysis by gold. Catalysis Today 100 (1–2), 55–61.

IARC Volume 93, 2006. International Agency for Research on Cancer (IARC). http://monographs.iarc.fr/ENG/Monographs/vol93/mono93.pdfhttp://monographs.iarc.fr/ENG/Monographs/vol93/mono93.pdf.

Jegatheesan, V., Vigneswaran, S., 1997. The effect of concentration on the early stages of deep bed filtration of submicron particles. Water Research 31 (11), 2910–2913.

Jegatheesan, V., Vigneswaran, S., 2000. Transient stage deposition of submicron particles in deep bed filtration under unfavorable conditions. Water Research 34 (7), 2119–2131.

Jeong, G.H., Lee, Y.W., Kim, M., Han, S.W., 2009. High-yield synthesis of multi-branched gold nanoparticles and their surface-enhanced Raman scattering properties. Journal of Colloid and Interface Science 329 (1), 97–102.

Jermann, D., Pronk, W., Meylan, S., Boller M., 2007. Interplay of different NOM fouling mechanisms during ultrafiltration for drinking water production. Water Research 41 (8), 1713–1722.

Johnson, W.P., Logan, B.E., 1996. Enhanced transport of bacteria in porous media by sediment-phase and aqueous-phase natural organic matter. Water Research 30 (4), 923–931.

Jolivet, J.P., Barron, A.R., 2007. Nanomaterials Fabrication. In *Environmental Nanotechnology* (Wiesner, M.R. and Bottero, J.-Y., Eds.). McGraw Hill, New York, pp. 29-103.

Jribi, R., Barthel, E., Bluhm, H., Grunze, M., Koelsch, P., Verreault, D., Sondergard, E., 2009. Ultraviolet irradiation suppresses adhesion on TiO_2. Journal of Physical Chemistry C 113 (19) 8273–8277.

Kanel, S.R., Greneche, J.M., Choi, H., 2006. Arsenic(V) removal from groundwater using nano scale zero-valent iron as a colloidal reactive barrier material. Environmental Science & Technology 40 (6), 2045–2050.

Keller, A.A., Wang, H., Zhou, D., Lenihan, H.S., Cherr, G., Cardinale, B.J., Miller, R., Ji, Z., 2010. Stability and aggregation of metal oxide nanoparticles in natural aqueous matrices. Environmental Science & Technology 44 (6), 1962–1967.

Kelly, J., Champagne, P., Michel, F., 2007. Assessment of metal attenuation in a natural wetland system impacted by alkaline mine tailings, Cobalt, Ontario, Canada. Mine Water and the Environment 26 (3), 181–190.

Kiser, M.A., Westerhoff, P., Benn, T., Wang, Y., Perez-Rivera, J., Hristovski, K., 2009. Titanium nanomaterial removal and release from wastewater treatment plants. Environmental Science & Technology 43 (17), 6757–6763.

Kretzschmar, R., Sticher, H., 1997. Transport of humic-coated iron oxide colloids in a sandy soil: Influence of Ca^{2+} and trace metals. Environmental Science & Technology 31 (12), 3497-3504.

Kuznar, Z.A., Elimelech, M., 2007. Direct microscopic observation of particle deposition in porous media: role of the secondary energy minimum. Colloids and Surfaces A: Physicochemical and Engineering Aspects 294 (1-3), 156–162.

Labille, J., Feng, J., Botta, C., Borschneck, D., Sammut, M., Cabie, M., Auffan, M., Rose, J., Bottero, J.Y., 2010. Aging of TiO_2 nanocomposites used in sunscreen. Dispersion and fate of the degradation products in aqueous environment. Environmental Pollution 158 (12), 3482–3489.

Lecoanet, H.F., Wiesner, M.R., 2004. Velocity effects on fullerene and oxide nanoparticles deposition in porous media. Environmental Science & Technology 38 (16), 4377-4382.

Lecoanet, H.F., Bottero, J.Y., Wiesner, M.R., 2004. Laboratory assessment of the mobility of nanomaterials in porous media. Environmental Science & Technology 38 (19), 5164-5169.

Lenhart, J.J., Saiers, J.E., 2002. Transport of silica colloids through unsaturated porous media: Experimental results and model comparisons. Environmental Science & Technology 36 (4), 769–777.

Leong, Y.K., Ong, B.C., 2003. Critical zeta potential and the Hamaker constant of oxides in water. Powder Technology 134 (3), 249–254.

Levitz, P., Damme, H.V., Keravis, D., 1984. Fluorescence decay study of the adsorption of nonionic surfactants at the solid-liquid interface. 1. Structure of the adsorption layer on a hydrophilic solid. Journal of Physical Chemistry 88 (11), 2228–2235.

Li, X.-Q., Elliott, D.W., Zhang, W.-X., 2006. Zero-valent iron nanoparticles for abatement of environmental pollutants: Materials and engineering aspects. Critical Reviews in Soil State and Materials Science 31 (4), 111–122.

Lin, D., Liu, N., Yang, K., Xing, B., Wu, F., 2010. Different stabilities of multiwalled carbon nanotubes in fresh surface water samples. Environmental Pollution 158, 1270-1274.

Litton, G.M., Olson, T.M., 1993. Colloid deposition rates on silica bed media and artifacts related to collector surface preparation methods. Environmental Science & Technology 27 (1), 185–193.

Litton, G.M., Olson, T.M., 1994. Colloid deposition kinetics with surface-active agents: Evidence for discrete surface charge effects. Journal of Colloid and Interface Science 165 (2), 522–525.

Litton, G.M., Olson, T.M., 1996. Particle size effects on colloid deposition kinetics: Evidence of secondary minimum deposition. Colloid and Surfaces A: Physicochemical and Engineering Aspects 107, 273–283.

Liu, G.J., Zhang, X.R., McWilliams, L., Talley, J.W., Neal, C.R., 2008. Influence of ionic strength, electrolyte type, and NOM on As(V) adsorption onto TiO_2. Journal of Environmental Science and Health Part A 43 (4), 430–436.

Liu, H.T., Ma, L.L., Zhao, J.F., Liu, J., Yan, J.Y., Ruan, J., Hong, F.S., 2009. Biochemical toxicity of nano-anatase TiO_2 particles in mice. Biological Trace Element Research 129 (1-3), 170-180.

Liu, S.W., Yu, J.G., Jaroniec, M., 2011. Anatase TiO_2 with dominant high-energy {001} facets: Synthesis, properties and applications. Chemistry of Materials 23 (18), 4085–4093.

Luo, S., Yang, S.G., Wang, X.D., Sun, C., 2010. Reductive degradation of tetrabromobisphenol A over iron-silver bimetallic nanoparticles under ultrasound radiation. Chemosphere 79 (6), 672–678.

Mansoori, G.A., 2005. Principles of Nanotechnology Molecular-Based Study of Condensed Matter in Small Systems. World Scientific Publishing Co, Singapore.

McDowell-Boyer, L.M., Hunt, J.R., Sitar, N., 1986. Particle transport through porous media. Water Resources Research 22 (13), 1901-1921.

Michalet, X., Pinaud, F.F., Bentalila, L.A., Tsay, J.M., Doose, S., Li, J.J., Sundaresan, G., Wu, A.M., Gambhir, S. S., Weiss, S., 2005. Quantum dots for live cells, in vivo imaging, and diagnostics. Science 307 (5709), 538–544.

Mingorance, M.D., Fernandez Galvez, J.F., Pena, A., Barahona, E. 2007. Laboratory methodology to approach soil water transport in the presence of surfactants. Colloids and Surfaces A: Physicochemical and Engineering Aspects. 302, 75-82.

Murray, C.B., Norris, D.J., Bawendi, M.G., 1993. Synthesis and characterization of nearly monodisperse CdE (E = S, Se, Te) semiconductor nanocrystallites. Journal of the American Chemical Society 115 (19), 8706–8715.

Mylon, S.E., Chen, K.L., Elimelech, M., 2004. Influence of natural organic matter and ionic composition on the kinetics and structure of hematite colloid aggregation: Implications to iron depletion in estuaries. Langmuir 20(21), 9000–9006.

Naftz, D.L., Cederberg, J.R., Krabbenhoft, D.P., Beisner, K.R., Whitehead, J., Gardberg, J., 2011. Diurnal trends in methylmercury concentration in a wetland adjacent to Great Salt Lake, Utah, USA. Chemical Geology 283 (1-2), 78–86.

Navarro, E., Baun, A., Behra, R., Hartmann, N.B., Filser, J., Miao, A.J., Quigg, A., Santschi, P.H., Sigg, L., 2008. Environmental behavior and ecotoxicity of engineered nanoparticles to algae, plants and fungi. Ecotoxicology 17 (5), 372–386.

Nowack, B., Bucheli, T.D., 2007. Occurrence, behavior and effects of nanoparticles in the environment. Environmental Pollution 150 (1), 5-22.

Nurmi, J.T., Tratnyek, P.G., Sarathy, V., Baer, D.R., Amonette, J.E., Pecher, K., Wang, C., Linehan, J.C., Matson, D.W., Penn, R.L., Driessen, M.D., 2005. Characterization and properties of metallic iron nanoparticles: Spectroscopy, electrochemistry, and kinetics. Environmental Science & Technology 39 (5), 1221–1230.

Obare, S.O., Meyer, G.J., 2004. Nanostructured materials for environmental remediation of organic contaminants in water. Journal of Environmental Science and Health Part A: Toxic/Hazardous Substances & Environmental Engineering 39 (10), 2549–2582.

Pelley, A.J., Tufenkji, N., 2008. Effect of particle size and natural organic matter on the migration of nano- and microscale latex particles in saturated porous media. Journal of Colloids and Interface Science 321 (1), 74–83.

Pelton, R., Geng, X.L., Brook, M., 2006. Photocatalytic paper from colloidal TiO_2–fact or fantasy. Advances in Colloid and Interface Science 127 (1), 43–53.

Phenrat, T., Saleh, N., Sirk, K., Tilton, R.D., Lowry, G.V., 2007. Aggregation and sedimentation of aqueous nanoscale zerovalent iron dispersions. Environmental Science & Technology 41 (1), 284-290.

Puzder, A., Williamson, A.J., Reboredo, F.A., Galli, G., 2003. Structural stability and optical properties of nanomaterials with reconstructed surfaces. Physical Review Letters 91 (15), 1574051–1574054.

Quan, X., Zhao, X., Chen, S., Zhao, H.M., Chen, J.W., Zhao, Y.Z., 2005. Enhancement of p,p'-DDT photodegradation on soil surfaces using TiO_2 induced by UV-light. Chemosphere 60 (2), 266–273.

Rajagopalan, R., Tien, C., 1976. Trajectory analysis of deep-bed filtration with the sphere-in-cell porous media model. American Institute of Chemical Engineers 22 (3), 523-533.

Ramirez, A.P., 2005. Carbon nanotubes for science and technology. Bell Labs Technical Journal 10 (3), 171–185.

Redman, J.A., Walker, S.L., Elimelech, M., 2004. Bacteria adhesion and transport in porous media: role of the secondary energy minimum. Environmental Science & Technology 38 (6), 1777–1785.

Robichaud, C.O., Tanzil, D., Weilenmann, U., Wiesner, M.R., 2005. Relative risk analysis of several manufactured nanomaterials: An insurance industry context. Environmental Science & Technology 39 (22), 8985–8994.

Robichaud, C.O., Uyar, A.E., Darby, M.R., Zucker, L.G., Wiesner, M.R., 2009. Estimates of upper bounds and trends in nano-TiO_2 production as a basis for exposure assessment. Environmental Science & Technology 43 (12), 4227–4233.

Romero-Cano, M.S, Martinez-Rodriguez, A., de las Nieves, F.J., 2002. Electrokinetic behavior of polymer colloids with adsorbed Triton X-100. Colloid Polymer Science 280, 526-532.

Ryan, J.N., Elimelech, M., 1996. Colloid mobilization and transport in groundwater. Colloids and Surfaces. A, Physical and Engineering Aspects 107, 1–56.

Saleh, N., Kim, H.J., Phenrat, T., Matyjaszewski, K., Tilton, R.D., Lowry, G.V., 2008. Ionic strength and composition affect the mobility of surface-modified Fe^0 nanoparticles in water-saturated sand columns. Environmental Science & Technology 42 (9), 3349–3355.

Schrick, B., Blough, J.L., Jones, A.D., Mallouk, T.E., 2002. Hydrodechlorination of trichloroethylene on hydrocarbons using bimetallic nickel-iron nanoparticles. Chemistry of Materials 14 (12), 5140–5147.

Scott, R.W.J., Wilson, O.M., Crooks, R.M., 2005. Synthesis, characterization, and applications of dendrimer-encapsulated nanoparticles. Journal of Physical Chemistry B 109 (2), 692–704.

Shan, J., Tenhu, H., 2007. Recent advances in polymer protected gold nanoparticles: Synthesis, properties and applications. Chemical Communications 44, 4580–4598.

Shao, D., Jiang, Z., Wang, X., 2010. SDBS modified XC-72 carbon for the removal of Pb(II) from aqueous solutions. Plasma Processes and Polymers 7 (7), 552–560.

Sharma, K.P., Aswal, V.K., Kumaraswamy, G., 2010. Adsorption of nonionic surfactants on silica nanoparticles: Structure and resultant interparticle interactions. Journal of Physical Chemistry B 114, 10986-10994.

Smith, B.W., Luzzi, D.E., 2004. Carbon Nanotubes. In *Introduction to Nanoscale Science and Technology* (De Ventra, M., Evoy, S. and Heflin, J.R., Eds.). Springer, New York, pp. 137–182.

Solovitch, N., Labille, J., Rose, J., Chaurand, P., Borschneck, D., Wiesner, M.R., Bottero, J.Y., 2010. Concurrent aggregation and deposition of TiO_2 nanoparticles in a sandy porous media. Environmental Science & Technology 44 (13), 4897–4902.

Stewart, S.J., Fernandez-Garcia, M., Belver, C., Mun, B.S., Requejo, F.G., 2006. Influence of N-Doping on the structure and electronic properties of titania nanoparticle photocatalysts. Journal of Physical Chemistry B 110 (33), 16482–16486.

Svecova, L., Cremel, S., Sirguey, C., Simonnot, M.O., Sardin, M., Dossot, M., Mercier-Bion, F., 2008. Comparison between batch and column experiments to determine the surface charge properties of rutile TiO_2 powder. Journal of Colloid and Interface Science 325 (2), 363–370.

Tan, X., Fang, M., Chen, C., Yu, S., Wang, X., 2008. Counterion effects of nickel and sodium dodecylbenzene sulfonate adsorption to multiwalled carbon nanotubes in aqueous solution. Carbon 46 (13), 1741–1750.

Thio, B.J.R., Zhou, D., Keller, A.A., 2011. Influence of natural organic matter on the aggregation and deposition of titanium dioxide nanoparticles. Journal of Hazardous Materials 189 (1–2), 556–563.

Tian, Y., Gao, B., Silvera-Batista, C., Ziegler, K.J., 2010. Transport of engineered nanoparticles in saturated porous media. Journal of Nanoparticle Research 12, 2371-2380.

Tiraferri, A., Sethi, R., 2009. Enhanced transport of zerovalent iron nanoparticles in saturated porous media by guar gum. Journal of Nanoparticle Research 11, 635-645.

Tkachenko, N.H., Yaremko, Z.M., Bellmann, C., Soltys, M.M, 2006. The influence of ionic and nonionic surfactants on aggregative stability and electrical surface properties of aqueous suspensions of titanium dioxide. Journal of Colloid and Interface Science 299 (2), 686–695.

Tufenkji, N., Elimelech, M., 2004a. Correlation equation for predicting single-collector efficiency in physicochemical filtration in saturated porous media. Environmental Science & Technology 38 (2), 529-536.

Tufenkji, N., Elimelech, M., 2004. Deviation from the classical colloid filtration theory in the presence of repulsive DLVO interactions. Langmuir 20 (25), 10818–10828.

Tufenkji, N., Elimelech, M., 2005. Breakdown of colloid filtration theory: Role of the secondary energy minimum and surface charge heterogeneities. Langmuir 21 (3), 841-852.

USEPA, 2007. Nanotechnology White Paper. Prepared for the U.S. Environmental Protection Agency by Members of the Nanotechnology Workgroup, a Group of EPA's Science Policy Council. U.S. Environmental Protection Agency, Washington, DC. http://www.epa.gov/osa/pdfs/nanotech/epa-nanotechnology-whitepaper-0207.pdf pp. 20460 (April 25, 2010).

Verwey, E.J.W., Overbeek, J.Th.G., 1948. Theory of the Stability of Lyophobic Colloids. Elsevier, Amsterdam.

Wang, B.X., Zhao, Y., Zhao, X.P., 2007. The wettability, size effect and electrorheological activity of modified titanium oxide nanoparticles. Colloids and Surfaces A – Physicochemical and Engineering Aspects 295 (1-3), 27–33.

Wang, C.T., Yen, C.F., 2012. Titania nanocomposite films derived by modified sol-gel process for photovoltaic application. Journal of Sol-Gel Science and Technology 61 (1), 83–89.

Wang, C.X., Yin, L.W., Zhang, L.Y., Qi, Y.X., Lun, N., Liu, N.N., 2010. Large scale synthesis and gas-sensing properties of anatase TiO_2 three-dimensional hierarchical nanostructures. Langmuir 26 (15), 12841–12848.

Wang, X.Y., Chen, C., Chang, Y., Liu, H.L., 2009. Dechlorination of chlorinated methanes by Pd/Fe bimetallic nanoparticles. Journal of Hazardous Materials 161 (2–3), 815–823.

Warheit, D.B., Webb, T.R., Reed, K.L., Frerichs, S., Sayes, C.M., 2007. Pulmonary toxicity study in rats with three forms of ultrafine-TiO_2 particles: Differential responses related to surface properties. Toxicology 230 (1), 90–104.

Wiel-Shafran, A., Ronen, Z., Weisbrod, N., Adar, E., Gross, A., 2006. Potential changes in soil properties following irrigation with surfactant-rich greywater. Ecological Engineering 26 (4), 348-354.

Wiesner, M.R., Lowry, G.V., Alvarez, P., Dionysiou, D., Biswas, P., 2006. Assessing the risks of manufactured nanomaterials. Environmental Science & Technology 40 (14), 4336–4345.

Xu, X.X., Zhuang, J., Wang, X., 2008. SnO_2 quantum dots and quantum wires: Controllable synthesis, self-assembled 2D architectures, and gas-sensing properties. Journal of the American Chemical Society 130 (37), 12527–12535.

Yao, K.M., Habibian, M.T., O'Melia, C.R., 1971. Water and waste water filtration: Concepts and applications. Environmental Science & Technology 5 (11), 1105-1112.

Zhang, J.Z., 1997. Ultrafast studies of electron dynamics in semiconductor and metal colloidal nanoparticles: Effects of size and surface. Account of Chemical Research 30 (10), 423–429.

Zhou, W.Y., Bai, X.D., Wang, E.G., Xie, S.S., 2009. Synthesis, structure, and properties of single-walled carbon nanotubes. Advanced Materials 21 (45), 4565–4583.

Zhu, X., Zhou, J., Cai, Z., 2011. TiO_2 nanoparticles in the marine environment: Impact on the toxicity of tributyltin to abalone (haliotis diversicolor supertexta) embryos. Environmental Science & Technology 45 (8), 3753–3758.

VITA

ITZEL GUADALUPE GODINEZ
iggodinez@gmail.com

SUMMARY OF QUALIIFCATIONS

I have more than six years' research experience evaluating the mechanisms controlling the deposition, mobility and stability of engineered nanosized particles in subsurface environments. I developed a comprehensive graduate studies course curriculum in Water Resources Engineering, Geoenvironmental and Environmental Engineering integrated with atomic and molecular concepts of nanotechnology and nanomaterials. I am an articulate person with a goal-oriented mind, quite capable of working independently or as a team member. I am a proponent of life-long learning and I am eager to acquire more technical knowledge on concepts related to Civil and Environmental Engineering from a cadre of scientists/engineers who are experts in their subject matter.

EDUCATION

Doctorate in Philosophy in Civil Engineering, May 2013, University of Illinois at Chicago
Master of Science in Civil Engineering, December 2008, University of Illinois at Chicago
Bachelor of Science in Civil Engineering, May 2006, University of Illinois at Chicago

RESEARCH EXPERIENCE

Department of Civil and Materials Engineering – University of Illinois at Chicago
Research and/or Teaching Assistant: Chicago, Illinois, August 2006 – December 2012

- Managed a Doctoral thesis project to investigate the aggregation kinetics, transport and retention mechanisms of titanium dioxide nanoparticles (nano-TiO_2) in order to assess the environmental consequences of the release and accumulation of these engineered nanoparticles in saturated-subsurface and estuarine environments.
- Involved in all aspects of project management including preparing budgets, proposal and article writing as well as personnel management.
- Dedicated 50 to 60 hours a week to my project and received a monthly stipend of $1795.
- Skillfully supervised a Water Resources Laboratory and instituted hands-on laboratory experiments to bridge the gap between theoretical concepts and engineering applications for the students enrolled in Water Resource Engineering, Hydraulic Design and/or Engineering Hydrology.
- Managed to participate on side projects such as the NATO Advanced Study Institute on Overexploitation and Contamination of Shared Groundwater Resources which took place in 2006 in Varna, Bulgaria; I collaborated in the composition of a chapter on coastal aquifers and saltwater intrusion as well as executed crucial administrative and logistic tasks for the institute.

Institute of Refrigeration and Cryogenics – Shanghai Jiao Tong University
Research Assistant: Shanghai, China, May – August 2010

- One of fifty selected participants who received the 2010 NSF International Research and Education in Engineering (IREE) Program Fellowship to conduct 12 weeks of frontier engineering research in China.
- Compiled a comprehensive report on the latest breakthroughs in thermal energy storage systems.
- Effectively handled the overall writing and editing processes of a research study that proposed a unique solar assisted heat pump in-store drying system for grains (e.g. corn).
- Published the study in the Applied Thermal Engineering Journal in 2011.
- Worked 40 hours per week and was granted a stipend of $8500 to cover for travel, housing and meal expenses.

Summer Research Opportunities Program (SROP) – University of Michigan
Undergraduate Research Assistant: Ann Arbor, Michigan, June – August 2004

- One of forty selected-participants who earned the opportunity to enhance academic and research skills by working one-on-one with a faculty member at the University of Michigan.
- Collaborated in the research of the Wavelet Analysis which studies digitized pictures of soil strata to identify the particle size of homogeneous soil—the pictures are collected by an in-situ testing device called the Vision Cone Penetrometer (VisCPT).
- Tested the Wavelet Analysis to check its ability to identify particle sizes of non-homogeneous soil masses.
- Prepared laboratory specimens of heterogeneous soils and their corresponding images.
- Derived results provided important information that could result in proper modifications to the code of the analysis to allow it to estimate particle sizes in heterogeneous soil.
- Devoted 40 hours per week to my assigned projects and was provided with a $4000 stipend to cover expenses.

LEADERSHIP EXPERIENCE

American Geophysical Union (AGU) Joint Assembly
Session Co-Chair: Acapulco, Mexico, May 2007

- Invited to serve as a moderator and co-chair for a session in the Hydrology Division called *Coastal Aquifer: Saltwater Intrusion and Submarine Groundwater Discharge*.

Center for the Advancement of Hispanics in Science and Engineering Education (CAHSEE)
Instructor: Washington, D.C. & Boston, Massachusetts, June – August of 2001, 2002 & 2005

- Instructed college-level courses in Physics and Vector Mechanics to talented students enrolled in Junior and Secondary school.
- Coach-mentored students to develop their intellectual abilities as well as to commit to academic excellence to pursue a degree in the fields of science, mathematics and/or engineering.

- Developed a thorough report to evaluate the academic progress of the students; the analysis of the results was included in a major proposal submitted to the program's main sponsor, NASA.
- Invested 40 to 50 hours a week to prepare/teach the courses; I was given a $2500 stipend.

Minority Engineering Retention and Recruitment Program (MERRP) – University of Illinois at Chicago

Instructor: Chicago, Illinois, August 2001 – May 2005

- Facilitated a workshop for engineering students in Differential and Integral Calculus.
- Successfully engaged the students into the habit of breaking down the problems into steps to illustrate an objective path to apply the mathematical concepts that permitted the students to arrive to the correct solutions.
- Dedicated 10 hour per week to the workshop and was paid $7 per hour.

PROFESSIONAL AFFILIATIONS

- American Geophysical Union, American Society of Civil Engineers, Society of Women Engineers, Society of Hispanic Professional Engineers, Society for Advancement of Chicanos/Latinos and Native Americans in Science.

MAJOR AWARDS & HONORS

- UIC Water Research Forum, 2nd Place Graduate Student Poster Presentation in Water Pollution Research and Technology, 2012
- Illinois LSAMP Spring Symposium and Student Research Conference in STEM, 2nd Place Graduate Student Poster Presentation in Engineering, 2012
- Emerging Researchers National Conference in STEM, 1st Place Graduate Student Poster Presentation in Ecology, Environmental and Earth Sciences, 2012
- NSF International Research and Education in Engineering Program Fellowship, 2010
- UIC Abraham Lincoln Fellowship, 2009
- NSF Fellowship for the Summer Institute on Nano-mechanics, Nano-materials and Micro/Nanomanufacturing, 2007
- NSF-UIC Bridge to the Doctorate Fellowship, 2006
- NATO Advanced Study Institute on Overexploitation and Contamination of Shared Groundwater Resources Travel Student Award, 2006
- NACME Academic and Leadership Scholarship, December 2003 – Spring 2005
- HSF/SHPE, Inc. Scholarship Program, 2001-2002, 2002-2003 & 2003-2004
- MERRP Extra Effort Award, 2002 - 2005

PUBLICATIONS

- **Godinez, I.G.**, Darnault, C.J.G., Khodadoust, A.P., Bogdan, D., 2013. Deposition and release kinetics of nano-TiO_2 in saturated porous media: Effects of solutions ionic strength and surfactants. Environmental Pollution 174, 106–113.

- **Godinez, I.G.**, Darnault, C.J.G., 2011. Aggregation and transport of nano-TiO_2 in saturated porous media: Effects of pH, surfactants and flow velocity. Water Research 45 (2), 839–851.

- Li, Y., Li, H.F., Dai, Y.J., Gao, S.F., Wei, L., Li, Z.L., **Godinez, I.G.**, Wang, R.Z., 2011. Experimental investigation on a solar assisted heat pump in-store drying system. Applied Thermal Engineering 31 (10), 1718–1724.

- Darnault, C., **Godinez, I.G.**, 2008. Fate of environmental pollutants. Water Environment Research 80 (10), 1844–1857.

- Darnault, C.J.G., **Godinez, I.**, 2008. Costal Aquifers and Saltwater Intrusion. In: Darnault, C.J.G., Baveye, P. (Eds.), NATO Sciences Series Overexploitation and Contamination of Shared Groundwater Resources: Management, (Bio)Technological, and Political Approaches to Avoid Conflicts. Springer, Netherlands, pp. 185–201.

- Darnault, C.J.G., **Godinez, I.G.**, 2007. Fate of environmental pollutants. Water Environment Research 79 (10), 2049–2070.

- Darnault, C., **Godinez, I.**, 2006. Fate of environmental pollutants. Water Environment Research 78 (10), 1975–1993.

LANGUAGE SKILLS

- Fluent in Spanish and English (oral and written).

APPENDIX A

ELSEVIER LICENSE AGREEMENT TO USE THE ARTICLE CALLED "AGGREGATION AND TRANSPORT OF NANO-TIO_2 IN SATURATED POROUS MEDIA: EFFECTS OF PH, SURFACTANTS AND FLOW VELOCTY"

ELSEVIER LICENSE
TERMS AND CONDITIONS

Mar 06, 2013

This is a License Agreement between Itzel G Godinez ("You") and Elsevier ("Elsevier") provided by Copyright Clearance Center ("CCC"). The license consists of your order details, the terms and conditions provided by Elsevier, and the payment terms and conditions.

All payments must be made in full to CCC. For payment instructions, please see information listed at the bottom of this form.

Supplier	Elsevier Limited The Boulevard,Langford Lane Kidlington,Oxford,OX5 1GB,UK
Registered Company Number	1982084
Customer name	Itzel G Godinez
Customer address	2600 Moss Lane Aurora, IL 60504
License number	3103240453445
License date	Mar 06, 2013
Licensed content publisher	Elsevier
Licensed content publication	Water Research
Licensed content title	Aggregation and transport of nano-TiO2in saturated porous media: Effects of pH, surfactants and flow velocity
Licensed content author	Itzel G. Godinez,Christophe J.G. Darnault
Licensed content date	January 2011
Licensed content volume number	45
Licensed content issue number	2
Number of pages	13
Start Page	839
End Page	851
Type of Use	reuse in a thesis/dissertation
Portion	full article
Format	both print and electronic
Are you the author of this Elsevier article?	Yes
Will you be translating?	No
Order reference number	

Title of your thesis/dissertation	Transport, Deposition and Release Kinetics of Nano-TiO2 in Saturated Porous Media
Expected completion date	Mar 2013
Estimated size (number of pages)	115
Elsevier VAT number	GB 494 6272 12
Permissions price	0.00 USD
VAT/Local Sales Tax	0.0 USD / 0.0 GBP
Total	0.00 USD
Terms and Conditions	

INTRODUCTION

1. The publisher for this copyrighted material is Elsevier. By clicking "accept" in connection with completing this licensing transaction, you agree that the following terms and conditions apply to this transaction (along with the Billing and Payment terms and conditions established by Copyright Clearance Center, Inc. ("CCC"), at the time that you opened your Rightslink account and that are available at any time at http://myaccount.copyright.com).

GENERAL TERMS

2. Elsevier hereby grants you permission to reproduce the aforementioned material subject to the terms and conditions indicated.

3. Acknowledgement: If any part of the material to be used (for example, figures) has appeared in our publication with credit or acknowledgement to another source, permission must also be sought from that source. If such permission is not obtained then that material may not be included in your publication/copies. Suitable acknowledgement to the source must be made, either as a footnote or in a reference list at the end of your publication, as follows:

"Reprinted from Publication title, Vol /edition number, Author(s), Title of article / title of chapter, Pages No., Copyright (Year), with permission from Elsevier [OR APPLICABLE SOCIETY COPYRIGHT OWNER]." Also Lancet special credit - "Reprinted from The Lancet, Vol. number, Author(s), Title of article, Pages No., Copyright (Year), with permission from Elsevier."

4. Reproduction of this material is confined to the purpose and/or media for which permission is hereby given.

5. Altering/Modifying Material: Not Permitted. However figures and illustrations may be altered/adapted minimally to serve your work. Any other abbreviations, additions, deletions and/or any other alterations shall be made only with prior written authorization of Elsevier Ltd. (Please contact Elsevier at permissions@elsevier.com)

6. If the permission fee for the requested use of our material is waived in this instance, please be advised that your future requests for Elsevier materials may attract a fee.

7. Reservation of Rights: Publisher reserves all rights not specifically granted in the combination of (i) the license details provided by you and accepted in the course of this licensing transaction, (ii) these terms and conditions and (iii) CCC's Billing and Payment terms and conditions.

8. License Contingent Upon Payment: While you may exercise the rights licensed immediately upon issuance of the license at the end of the licensing process for the transaction, provided that you have disclosed complete and accurate details of your proposed use, no license is finally effective unless and until full payment is received from you (either by publisher or by CCC) as provided in CCC's Billing and Payment terms and conditions. If full payment is not received on a timely basis, then any license preliminarily granted shall be deemed automatically revoked and shall be void as if never granted. Further, in the event that you breach any of these terms and conditions or any of CCC's Billing and Payment terms and conditions, the license is automatically revoked and shall be void as if never granted. Use of materials as described in a revoked license, as well as any use of the materials beyond the scope of an unrevoked license, may constitute copyright infringement and publisher reserves the right to take any and all action to protect its copyright in the materials.

9. Warranties: Publisher makes no representations or warranties with respect to the licensed material.

10. Indemnity: You hereby indemnify and agree to hold harmless publisher and CCC, and their respective officers, directors, employees and agents, from and against any and all claims arising out of your use of the licensed material other than as specifically authorized pursuant to this license.

11. No Transfer of License: This license is personal to you and may not be sublicensed, assigned, or transferred by you to any other person without publisher's written permission.

12. No Amendment Except in Writing: This license may not be amended except in a writing signed by both parties (or, in the case of publisher, by CCC on publisher's behalf).

13. Objection to Contrary Terms: Publisher hereby objects to any terms contained in any purchase order, acknowledgment, check endorsement or other writing prepared by you, which terms are inconsistent with these terms and conditions or CCC's Billing and Payment terms and conditions. These terms and conditions, together with CCC's Billing and Payment terms and conditions (which are incorporated herein), comprise the entire agreement between you and publisher (and CCC) concerning this licensing transaction. In the event of any conflict between your obligations established by these terms and conditions and those established by CCC's Billing and Payment terms and conditions, these terms and conditions shall control.

14. Revocation: Elsevier or Copyright Clearance Center may deny the permissions described in this License at their sole discretion, for any reason or no reason, with a full refund payable to you. Notice of such denial will be made using the contact information provided by you. Failure to receive such notice will not alter or invalidate the denial. In no event will Elsevier or Copyright Clearance Center be responsible or liable for any costs, expenses or damage incurred by you as a result of a denial of your permission request, other than a refund of the amount(s) paid by you to Elsevier and/or Copyright Clearance Center for denied permissions.

LIMITED LICENSE

The following terms and conditions apply only to specific license types:

15. **Translation**: This permission is granted for non-exclusive world **English** rights only unless your license was granted for translation rights. If you licensed translation rights you may only translate this content into the languages you requested. A professional translator must perform all translations and reproduce the content word for word preserving the integrity of the article. If this license is to re-use 1 or 2 figures then permission is granted for non-exclusive world rights in all languages.

16. **Website**: The following terms and conditions apply to electronic reserve and author websites:
Electronic reserve: If licensed material is to be posted to website, the web site is to be password-protected and made available only to bona fide students registered on a relevant course if:
This license was made in connection with a course,
This permission is granted for 1 year only. You may obtain a license for future website posting,
All content posted to the web site must maintain the copyright information line on the bottom of each image,
A hyper-text must be included to the Homepage of the journal from which you are licensing at http://www.sciencedirect.com/science/journal/xxxxx or the Elsevier homepage for books at http://www.elsevier.com , and
Central Storage: This license does not include permission for a scanned version of the material to be stored in a central repository such as that provided by Heron/XanEdu.

17. **Author website** for journals with the following additional clauses:

All content posted to the web site must maintain the copyright information line on the bottom of each image, and the permission granted is limited to the personal version of your paper. You are not allowed to download and post the published electronic version of your article (whether PDF or HTML, proof or final version), nor may you scan the printed edition to create an electronic version.
A hyper-text must be included to the Homepage of the journal from which you are licensing at http://www.sciencedirect.com/science/journal/xxxxx . As part of our normal production process, you will receive an e-mail notice when your article appears on Elsevier's online service ScienceDirect (www.sciencedirect.com). That e-mail will include the article's Digital Object Identifier (DOI). This number provides the electronic link to the published article and should be included in the posting of your personal version. We ask that you wait until you receive this e-mail and have the DOI to do any posting.

Central Storage: This license does not include permission for a scanned version of the material to be stored in a central repository such as that provided by Heron/XanEdu.

18. **Author website** for books with the following additional clauses:
Authors are permitted to place a brief summary of their work online only.
A hyper-text must be included to the Elsevier homepage at http://www.elsevier.com . All content posted to the web site must maintain the copyright information line on the bottom of each image.
You are not allowed to download and post the published electronic version of your chapter, nor may you scan the printed edition to create an electronic version.

Central Storage: This license does not include permission for a scanned version of the material to be stored in a central repository such as that provided by Heron/XanEdu.

19. **Website** (regular and for author): A hyper-text must be included to the Homepage of the journal from which you are licensing at http://www.sciencedirect.com/science/journal/xxxxx. or for books to the Elsevier homepage at http://www.elsevier.com

20. **Thesis/Dissertation**: If your license is for use in a thesis/dissertation your thesis may be submitted to your institution in either print or electronic form. Should your thesis be published commercially, please reapply for permission. These requirements include permission for the Library and Archives of Canada to supply single copies, on demand, of the complete thesis and include permission for UMI to supply single copies, on demand, of the complete thesis. Should your thesis be published commercially, please reapply for permission.

21. **Other Conditions**:

v1.6

If you would like to pay for this license now, please remit this license along with your payment made payable to "COPYRIGHT CLEARANCE CENTER" otherwise you will be invoiced within 48 hours of the license date. Payment should be in the form of a check or money order referencing your account number and this invoice number RLNK500971851. Once you receive your invoice for this order, you may pay your invoice by credit card. Please follow instructions provided at that time.

Make Payment To:
Copyright Clearance Center
Dept 001
P.O. Box 843006
Boston, MA 02284-3006

For suggestions or comments regarding this order, contact RightsLink Customer Support: customercare@copyright.com or +1-877-622-5543 (toll free in the US) or +1-978-646-2777.

Gratis licenses (referencing $0 in the Total field) are free. Please retain this printable license for your reference. No payment is required.

APPENDIX B

ELSEVIER LICENSE AGREEMENT TO USE THE ARTICLE CALLED "DEPOSITION AND RELEASE KINETICS OF NANO-TiO_2 IN SATURATED POROUS MEDIA: EFFECTS OF SOLUTION IONIC STRENGTH AND SURFACTANTS"

ELSEVIER LICENSE
TERMS AND CONDITIONS

Mar 06, 2013

This is a License Agreement between Itzel G Godinez ("You") and Elsevier ("Elsevier") provided by Copyright Clearance Center ("CCC"). The license consists of your order details, the terms and conditions provided by Elsevier, and the payment terms and conditions.

All payments must be made in full to CCC. For payment instructions, please see information listed at the bottom of this form.

Supplier	Elsevier Limited The Boulevard,Langford Lane Kidlington,Oxford,OX5 1GB,UK
Registered Company Number	1982084
Customer name	Itzel G Godinez
Customer address	2600 Moss Lane Aurora, IL 60504
License number	3103241410860
License date	Mar 06, 2013
Licensed content publisher	Elsevier
Licensed content publication	Environmental Pollution
Licensed content title	Deposition and release kinetics of nano-TiO2in saturated porous media: Effects of solution ionic strength and surfactants
Licensed content author	Itzel G. Godinez,Christophe J.G. Darnault,Amid P. Khodadoust,Dorin Bogdan
Licensed content date	March 2013
Licensed content volume number	174
Licensed content issue number	
Number of pages	8
Start Page	106
End Page	113
Type of Use	reuse in a thesis/dissertation
Portion	full article
Format	both print and electronic
Are you the author of this Elsevier article?	Yes
Will you be translating?	No

Order reference number	
Title of your thesis/dissertation	Transport, Deposition and Release Kinetics of Nano-TiO2 in Saturated Porous Media
Expected completion date	Mar 2013
Estimated size (number of pages)	115
Elsevier VAT number	GB 494 6272 12
Permissions price	0.00 USD
VAT/Local Sales Tax	0.0 USD / 0.0 GBP
Total	0.00 USD
Terms and Conditions	

INTRODUCTION

1. The publisher for this copyrighted material is Elsevier. By clicking "accept" in connection with completing this licensing transaction, you agree that the following terms and conditions apply to this transaction (along with the Billing and Payment terms and conditions established by Copyright Clearance Center, Inc. ("CCC"), at the time that you opened your Rightslink account and that are available at any time at http://myaccount.copyright.com).

GENERAL TERMS

2. Elsevier hereby grants you permission to reproduce the aforementioned material subject to the terms and conditions indicated.

3. Acknowledgement: If any part of the material to be used (for example, figures) has appeared in our publication with credit or acknowledgement to another source, permission must also be sought from that source. If such permission is not obtained then that material may not be included in your publication/copies. Suitable acknowledgement to the source must be made, either as a footnote or in a reference list at the end of your publication, as follows:

"Reprinted from Publication title, Vol /edition number, Author(s), Title of article / title of chapter, Pages No., Copyright (Year), with permission from Elsevier [OR APPLICABLE SOCIETY COPYRIGHT OWNER]." Also Lancet special credit - "Reprinted from The Lancet, Vol. number, Author(s), Title of article, Pages No., Copyright (Year), with permission from Elsevier."

4. Reproduction of this material is confined to the purpose and/or media for which permission is hereby given.

5. Altering/Modifying Material: Not Permitted. However figures and illustrations may be altered/adapted minimally to serve your work. Any other abbreviations, additions, deletions and/or any other alterations shall be made only with prior written authorization of Elsevier Ltd. (Please contact Elsevier at permissions@elsevier.com)

6. If the permission fee for the requested use of our material is waived in this instance, please be advised that your future requests for Elsevier materials may attract a fee.

7. Reservation of Rights: Publisher reserves all rights not specifically granted in the combination of (i) the license details provided by you and accepted in the course of this licensing transaction, (ii) these terms and conditions and (iii) CCC's Billing and Payment terms and conditions.

8. License Contingent Upon Payment: While you may exercise the rights licensed immediately upon issuance of the license at the end of the licensing process for the transaction, provided that you have disclosed complete and accurate details of your proposed use, no license is finally effective unless and until full payment is received from you (either by publisher or by CCC) as provided in CCC's Billing and Payment terms and conditions. If full payment is not received on a timely basis, then any license preliminarily granted shall be deemed automatically revoked and shall be void as if never granted. Further, in the event that you breach any of these terms and conditions or any of CCC's Billing and Payment terms and conditions, the license is automatically revoked and shall be void as if never granted. Use of materials as described in a revoked license, as well as any use of the materials beyond the scope of an unrevoked license, may constitute copyright infringement and publisher reserves the right to take any and all action to protect its copyright in the materials.

9. Warranties: Publisher makes no representations or warranties with respect to the licensed material.

10. Indemnity: You hereby indemnify and agree to hold harmless publisher and CCC, and their respective officers, directors, employees and agents, from and against any and all claims arising out of your use of the licensed material other than as specifically authorized pursuant to this license.

11. No Transfer of License: This license is personal to you and may not be sublicensed, assigned, or transferred by you to any other person without publisher's written permission.

12. No Amendment Except in Writing: This license may not be amended except in a writing signed by both parties (or, in the case of publisher, by CCC on publisher's behalf).

13. Objection to Contrary Terms: Publisher hereby objects to any terms contained in any purchase order, acknowledgment, check endorsement or other writing prepared by you, which terms are inconsistent with these terms and conditions or CCC's Billing and Payment terms and conditions. These terms and conditions, together with CCC's Billing and Payment terms and conditions (which are incorporated herein), comprise the entire agreement between you and publisher (and CCC) concerning this licensing transaction. In the event of any conflict between your obligations established by these terms and conditions and those established by CCC's Billing and Payment terms and conditions, these terms and conditions shall control.

14. Revocation: Elsevier or Copyright Clearance Center may deny the permissions described in this License at their sole discretion, for any reason or no reason, with a full refund payable to you. Notice of such denial will be made using the contact information provided by you. Failure to receive such notice will not alter or invalidate the denial. In no event will Elsevier or Copyright Clearance Center be responsible or liable for any costs, expenses or damage incurred by you as a result of a denial of your permission request, other than a refund of the amount(s) paid by you to Elsevier and/or Copyright Clearance Center for denied permissions.

LIMITED LICENSE

The following terms and conditions apply only to specific license types:

15. **Translation**: This permission is granted for non-exclusive world **English** rights only unless your license was granted for translation rights. If you licensed translation rights you may only translate this content into the languages you requested. A professional translator must perform all translations and reproduce the content word for word preserving the integrity of the article. If this license is to re-use 1 or 2 figures then permission is granted for non-exclusive world rights in all languages.

16. **Website**: The following terms and conditions apply to electronic reserve and author websites:
Electronic reserve: If licensed material is to be posted to website, the web site is to be password-protected and made available only to bona fide students registered on a relevant course if:
This license was made in connection with a course,
This permission is granted for 1 year only. You may obtain a license for future website posting,
All content posted to the web site must maintain the copyright information line on the bottom of each image,
A hyper-text must be included to the Homepage of the journal from which you are licensing at http://www.sciencedirect.com/science/journal/xxxxx or the Elsevier homepage for books at http://www.elsevier.com , and
Central Storage: This license does not include permission for a scanned version of the material to be stored in a central repository such as that provided by Heron/XanEdu.

17. **Author website** for journals with the following additional clauses:

All content posted to the web site must maintain the copyright information line on the bottom of each image, and the permission granted is limited to the personal version of your paper. You are not allowed to download and post the published electronic version of your article (whether PDF or HTML, proof or final version), nor may you scan the printed edition to create an electronic version.
A hyper-text must be included to the Homepage of the journal from which you are licensing at http://www.sciencedirect.com/science/journal/xxxxx . As part of our normal production process, you will receive an e-mail notice when your article appears on Elsevier's online service ScienceDirect (www.sciencedirect.com). That e-mail will include the article's Digital Object Identifier (DOI). This number provides the electronic link to the published article and should be included in the posting of your personal version. We ask that you wait until you receive this e-mail and have the DOI to do any posting.

Central Storage: This license does not include permission for a scanned version of the material to be stored in a central repository such as that provided by Heron/XanEdu.

18. **Author website** for books with the following additional clauses:
Authors are permitted to place a brief summary of their work online only.
A hyper-text must be included to the Elsevier homepage at http://www.elsevier.com . All content posted to the web site must maintain the copyright information line on the bottom of each image.
You are not allowed to download and post the published electronic version of your chapter, nor may you scan the printed edition to create an electronic version.

Central Storage: This license does not include permission for a scanned version of the material to be stored in a central repository such as that provided by Heron/XanEdu.

19. **Website** (regular and for author): A hyper-text must be included to the Homepage of the journal from which you are licensing at http://www.sciencedirect.com/science/journal/xxxxx. or for books to the Elsevier homepage at http://www.elsevier.com

20. **Thesis/Dissertation**: If your license is for use in a thesis/dissertation your thesis may be submitted to your institution in either print or electronic form. Should your thesis be published commercially, please reapply for permission. These requirements include permission for the Library and Archives of Canada to supply single copies, on demand, of the complete thesis and include permission for UMI to supply single copies, on demand, of the complete thesis. Should your thesis be published commercially, please reapply for permission.

21. **Other Conditions**:

v1.6

If you would like to pay for this license now, please remit this license along with your payment made payable to "COPYRIGHT CLEARANCE CENTER" otherwise you will be invoiced within 48 hours of the license date. Payment should be in the form of a check or money order referencing your account number and this invoice number RLNK500971864. Once you receive your invoice for this order, you may pay your invoice by credit card. Please follow instructions provided at that time.

Make Payment To:
Copyright Clearance Center
Dept 001
P.O. Box 843006
Boston, MA 02284-3006

For suggestions or comments regarding this order, contact RightsLink Customer Support: customercare@copyright.com or +1-877-622-5543 (toll free in the US) or +1-978-646-2777.

Gratis licenses (referencing $0 in the Total field) are free. Please retain this printable license for your reference. No payment is required.